

# **Development of Universal Curve for Damping and Framework for Tension Estimation in Stay Cable with Damper**

(ダンパーを有する斜張橋ケーブルの減衰評価ユニバーサル曲  
線と張力推定法の構築)

**By**

**Le Xuan Luu**

**Dissertation**

Submitted in partial fulfillment of requirements  
for the degree of Doctor of Philosophy in Engineering  
at the Graduate School of Urban Innovation of  
Yokohama National University, 2022.

## Contents

Contents .....	i
List of Figures .....	iv
List of Tables .....	ix
Notations .....	xi
Abstract .....	xv
Acknowledgements .....	xvii
CHAPTER 1: INTRODUCTION.....	1
1.1. Background .....	1
1.1.1. Damping of stay cables with dampers .....	4
1.1.2. Vibration-based tension estimation of stay cables.....	11
1.2. Problem statement .....	14
1.3. Aims and methodology .....	15
1.4. Structure of the dissertation.....	16
1.5. Publications .....	16
CHAPTER 2. REDUCTION OF DAMPING IN STAY CABLE WITH DAMPER UNDER ROTATIONAL RESTRAINT BETWEEN DAMPER AND CABLE.....	18
2.1. Introduction .....	18
2.2. Schematic diagram, equation of motion and eigenvalue analysis .....	19
2.3. Attainable cable damping.....	22
2.4. Effect of damper support stiffness and damper stiffness on damping .....	27
2.5. Extend results to cable with High Damping Rubber Damper (HDR damper)...	30
2.6. Full-scale experimental for validation.....	35
2.7. Summary .....	35
Appendix: Formulas in from Eq. (2.11) to (2.13) .....	37
CHAPTER 3. DEVELOPMENT OF UNIVERSAL DAMPING CURVE FOR DESIGN OF CABLE DAMPING WITH DAMPER .....	38
3.1. Introduction .....	38
3.2. Cable model.....	40

3.3. Governing equation and eigenfrequency analysis.....	41
3.4. Attainable cable damping.....	43
3.5. Propose universal damping curve for design of cable damping .....	46
3.5.1. Universal damping curve for cable with HDR damper .....	46
3.5.2. Universal damping curve for cable with viscous damper.....	52
3.6. Design example .....	54
3.6.1. Single-mode vibration control .....	54
3.6.2. Multi-Mode Vibration Control .....	57
3.7. Summary .....	59
Appendix: Formulas in Eqs. (3.10a-h).....	61
CHAPTER 4. DAMPING ANALYSIS OF FULL-SCALE CABLES FROM FIELD MEASUREMENT DATA.....	62
4.1. Target bridge and measurement .....	62
4.1.1. Bridge information.....	62
4.1.2. Measurement data .....	63
4.2. Damping analysis of full-scale stay cables from field measurement.....	65
4.3.1. Damping analysis procedure.....	65
4.3.2. Results of measured damping and measured frequencies .....	66
4.3. Theoretical damping and damper effectiveness.....	69
4.4. Discussion on the amplitude dependency of measured damping .....	73
4.5. Summary .....	75
Appendix: Finite Difference Method .....	76
CHAPTER 5. FRAMEWORK FOR ESTIMATION OF CABLE TENSION UNDER LIMITED INFORMATION OF CABLE PROPERTIES BY APPLICATION OF ARTIFICIAL NEURAL NETWORKS (ANNS).....	79
5.1. Introduction .....	79
5.2. Methodology and modeling of the stay cable .....	82
5.2.1. Cable model .....	82

5.2.2. Case 1: Equation of motion and eigenvalue analysis of cable without lateral attachments .....	83
5.2.3. Case 2: Equation of motion and eigenvalue analysis of cable with lateral attachments .....	86
5.3. Application of ANNs for cable tension estimation with unknown cable parameters .....	89
5.4. Numerical verifications .....	93
5.4.1. Verification 1: Cable without lateral attachments .....	94
5.4.2. Verification 2: Cable with lateral attachments .....	100
5.5. Discussion on the ranges of unknown parameters for training, validation and testing in ANNs .....	104
5.5.1. Range of cable tension .....	104
5.5.2. Range of cable bending stiffness, axial stiffness and cable inclination angle .....	104
5.5.3. Range of rotational restraint stiffness at cable ends .....	105
5.5.4. Range of the parameters of lateral attachments .....	107
5.6. Application of the proposed framework for the estimation of tensions in stay cables of Tatara Bridge .....	108
5.7. Summary .....	112
Appendix: Derivation of stiffness matrix .....	114
CHAPTER 6. CONCLUSIONS AND FUTURE STUDY .....	116
6.1. Conclusions .....	116
6.2. Future study .....	117
REFERENCES .....	118



## List of Figures

### CHAPTER 1

<b>FIGURE 1.1.</b> Tataru Bridge (currently 8 <sup>th</sup> longest cable stay bridge in the world). .....	1
<b>FIGURE 1.2.</b> Inherent damping in logarithmic decrement versus natural frequency. ..	2
<b>FIGURE 1.3.</b> Dampers of stay cables <sup>9</sup> . a) Viscous dampers in Sakitama Bridge; and b) High Damping Rubber (HDR) damper in Shonan Ginza Bridge.....	3
<b>FIGURE 1.4.</b> Taut-string cable with viscous damper. ....	4
<b>FIGURE 1.5.</b> Universal damping curve proposed by Pacheco et al. <sup>12</sup> (Noted: $\omega_{01} = (\pi/l)Hm$ ). ....	5
<b>FIGURE 1.6.</b> Maximum damping ratio versus sag parameter $\lambda^2$ . ....	7
<b>FIGURE 1.7.</b> Cable model accounting for cable bending stiffness EI and sag effect. ..	8

### CHAPTER 2

<b>FIGURE 2. 1.</b> Cable with a viscous damper. ....	20
<b>FIGURE 2. 2.</b> Damping curve of cable with viscous damper under rotational restraint. ....	25
<b>FIGURE 2. 3.</b> a) Reduction factor $R_r$ of the maximum modal damping; and b) modification factor $\alpha$ of the optimal damper coefficient with different cable bending stiffness ( $a/l = 0.02$ ).....	25
<b>FIGURE 2. 4.</b> Modal damping in a cable with a viscous damper accounting for the rotational restraint between the damper and cable: a) small bending stiffness; and b) large bending stiffness. ....	26
<b>FIGURE 2. 5.</b> Modal damping Mode 1 and Mode 3: a) without rotational restraint ( $kr = 0$ ); and, b) with rotational restraint ( $kr = 0.01$ ). ....	27
<b>FIGURE 2. 6.</b> Cable with a viscous damper accounting for: a) Damper support stiffness; and b) damper stiffness.....	27

<b>FIGURE 2. 7.</b> Demonstration of damping curve of cable with viscous damper considering for: a) damper support stiffness; and b) damper stiffness. ....	29
<b>FIGURE 2. 8.</b> Reduction factors of damping: a) $R_{vs}$ ; and b) $R_{vp}$ .....	30
<b>FIGURE 2. 9.</b> Damping curve: a) different values of damper support stiffness $K_{vs}$ ; and b) different values of damper stiffness $K_{vp}$ .....	30
<b>FIGURE 2. 10.</b> Model of cable with HDR damper.....	31
<b>FIGURE 2. 11.</b> Damping curve of cable with HDR damper under rotational restraint. ....	32
<b>FIGURE 2. 12.</b> (a) Reduction factor $R_{rd}$ of damping ratio; and b) Modification factor damper coefficient. ....	33
<b>FIGURE 2. 13.</b> Damping ratio in a cable with an HDR damper accounting for the rotational restraint between the damper and cable: a) small bending stiffness; and b) large bending stiffness. ....	34
<b>FIGURE 2. 14.</b> Damping ratio with different vibration modes: a) small bending stiffness; and b) large bending stiffness. ....	34

### CHAPTER 3

<b>FIGURE 3. 1.</b> Schematic diagram of a stay cable with a damper.....	40
<b>FIGURE 3. 2.</b> HDR damper types: a) conventional HDR damper; b) HDR damper with damper support stiffness; c) negative stiffness HDR damper; and d) negative stiffness HDR damper with damper support stiffness. ....	41
<b>FIGURE 3. 3.</b> Viscous damper types: a) conventional viscous damper; b) viscous damper with damper support stiffness; c) viscous damper with damper stiffness; and d) viscous damper with both damper stiffness and damper support stiffness. ....	41
<b>FIGURE 3. 4.</b> Modification factor of damping due to restraint at cable ends ( $a/l = 0.02$ ). ....	49
<b>FIGURE 3. 5.</b> Modification factor of damping due to damper support stiffness $R_2$ , and due to negative stiffness damper $R_3$ .....	49
<b>FIGURE 3. 6.</b> Variations in modal damping ratio of HDR damper versus different factors: a) material loss factor $\phi$ ( $Kr = \infty; Kvs = \infty; KNS = 0; \eta = 1 \times 10^{-6}; a/l =$	

0.02) ; b) cable bending stiffness parameter  $\eta$  ( $Kr = \infty; Kvs = \infty; KNS = 0; \phi = 0.25; a/l = 0.02$ ); c) damper location  $a/l$  ( $Kr = \infty; Kvs = \infty; KNS = 0; \phi = 0.25; \eta = 1 \times 10^{-6}$ ); d) restraints at cable ends  $Kr$  ( $Kvs = \infty; KNS = 0; \eta = 1 \times 10^{-4}; \phi = 0.25; a/l = 0.02$ ); e) damper support stiffness  $Kvs$  ( $Kr = \infty; KNS = 0; \eta = 1 \times 10^{-6}; \phi = 0.25; a/l = 0.02$ ); and, f) negative stiffness  $KNS$  ( $Kr = \infty; Kvs = \infty; \eta = 1 \times 10^{-6}; \phi = 0.25; a/l = 0.02$ ). ..... 50

**FIGURE 3. 7.** Damping curve: a) by Eq. (3.37); and b) by the proposed universal curve. .... 52

**FIGURE 3. 8.** Universal damping curve for viscous damper types. .... 54

**FIGURE 3. 9.** Design HDR damper using the proposed universal damping curve. .... 55

**FIGURE 3. 10.** Damping of multi-mode control: a) locations of modes on the universal damping curve; and b) added damping ratio for each mode. .... 58

**FIGURE 3. 11.** Damping of the five controlled modes: a) locations of modes on the universal damping curve; and b) added damping ratio for each mode. .... 59

## CHAPTER 4

**FIGURE 4. 1.** Layout of the bridge. .... 62

**FIGURE 4. 2.** The measurement setup and data acquisition. .... 63

**FIGURE 4. 3.** Raw acceleration data of cables C17E, C17W, 18W. .... 65

**FIGURE 4. 4.** Four-step procedures for identifying cable damping ratio  $\xi$ . .... 66

**FIGURE 4. 5.** Fourier spectrum analysis. .... 67

**FIGURE 4. 6.** Filtered acceleration of free-decay responses. .... 68

**FIGURE 4. 7.** Comparison between theoretical damping ratios and measured values. .... 72

**FIGURE 4. 8.** Amplitude dependency of damping ratios and frequencies of cable C17E. .... 73

**FIGURE 4. 9.** Amplitude dependency of damping ratios and frequencies of cable C17W. .... 74

<b>FIGURE 4. 10.</b> Amplitude dependency of damping ratios and frequencies of cable C18W.....	74
<b>FIGURE 4. 11.</b> Discretized cable with an HDR damper. ....	76

## CHAPTER 5

<b>FIGURE 5. 1.</b> Schematic diagram: a) cable without lateral components; and b) cable with lateral components (Note: lateral components are dampers and/or cross ties). ....	82
<b>FIGURE 5. 2.</b> Finite difference scheme for discretized cable. ....	84
<b>FIGURE 5. 3.</b> Viscous damper and HDR damper. ....	87
<b>FIGURE 5. 4.</b> Distributed damper coefficient over cable length.....	88
<b>FIGURE 5. 5.</b> Framework of vibration-based cable tension estimation with ANNs... ..	92
<b>FIGURE 5. 6.</b> Convergence of cable fundamental frequency versus the number of interior nodes. ....	94
<b>FIGURE 5. 7.</b> Fundamental frequencies of cable C04 against cable properties.....	96
<b>FIGURE 5. 8.</b> Performance of training in ANNs versus number of neurons. ....	97
<b>FIGURE 5. 9.</b> R, MAPE and RMSE of training, validation and testing in ANNs for cables without lateral attachments.....	97
<b>FIGURE 5. 10.</b> Scatters between estimated and targeted tensions with different input scenarios: a) scenario 1 ( $l, m, f_1$ ); b) scenario 2 ( $l, m, f_1, f_2$ ); and, c) scenario 3 ( $l, m, f_1, f_2, f_3$ ). ....	98
<b>FIGURE 5. 11.</b> Normalized mode shapes of cables with lateral attachments. ....	103
<b>FIGURE 5. 12.</b> R, MAPE and RMSE of training, validation and testing in ANNs for cables with lateral attachments.....	103
<b>FIGURE 5. 13.</b> Normalized fundamental frequency of 19 cables over a wide range of $K_r$ .....	106
<b>FIGURE 5. 14.</b> Tatara Bridge: a) general view; b) selected cables for the identification of tensions; c) span arrangement, and d) stay cables vibration measurement by LDV. ....	108

**FIGURE 5. 15.** Ambient vibration of Tatara Bridge stay cables and their frequency spectra measured by LDV: a) cable C1; b) cable C2; c) cable C3; and d) cable C4. . 109

**FIGURE 5. 16.** R, MAPE and RMSE of training in ANNs of Tatara Bridge cables (cable C1, cable C2, cable C3, cable C4)..... 111

**FIGURE 5. 17.** Scatters between estimated and targeted tensions with five known features ( $l, m, f_1, f_2, f_3$ )..... 112

## List of Tables

### CHAPTER 1

TABLE 1.1. Characteristics of rain-wind vibration .....	3
TABLE 1.2. Cable model and optimal damping ratio .....	10

### CHAPTER 2

TABLE 2. 1. Cable properties in the experimental validation .....	35
TABLE 2. 2. Improvement of damping estimation .....	35

### CHAPTER 3

TABLE 3. 1. Damper force component $F_a$ of the dampers .....	45
TABLE 3. 2. Factors of the modal damping ratio and optimal damper coefficient for HDR damper .....	48
TABLE 3. 3. Factors of the modal damping ratio and optimal damper coefficient for viscous damper types .....	54

### CHAPTER 4

TABLE 4. 1. Measured frequencies and damping ratios $\xi$ .....	69
TABLE 4. 2. Cable properties and damper parameters .....	69
TABLE 4. 3. Theoretical damping ratios .....	70
TABLE 4. 4. Reduction factors of damping due to cable sag for Mode 1 .....	71
TABLE 4. 5. Reduction factors of damping due to cable sag for Mode 2 .....	72
TABLE 4. 6. Reduction factors of damping due to cable sag for Mode 3 .....	72

### CHAPTER 5

TABLE 5. 1. Cable properties .....	94
TABLE 5. 2. Natural frequencies of the cables without lateral supports .....	95
TABLE 5. 3. Ranges of cable parameters used in generating datasets .....	95

<b>TABLE 5. 4.</b> Estimated tension by ANNs for cables without lateral attachments.....	99
<b>TABLE 5. 5.</b> Estimated cable tension based on taut-string theory Eq. (5.33) .....	100
<b>TABLE 5. 6.</b> Information of lateral attachments .....	101
<b>TABLE 5. 7.</b> Analytically derived natural frequencies of cables with lateral supports .....	101
<b>TABLE 5. 8.</b> Estimated tensions by ANNs with unknown information of lateral attachments .....	102
<b>TABLE 5. 9.</b> Cable properties used in parametric analysis.....	106
<b>TABLE 5. 10.</b> Known parameters of cable properties and measured frequencies.....	109
<b>TABLE 5. 11.</b> Unknown cable properties .....	110
<b>TABLE 5. 12.</b> Unknown damper parameters .....	110
<b>TABLE 5. 13.</b> Estimated tension and the comparison with designed value. ....	112

## Notations

*The following symbols are used in this dissertation*

### CHAPTER 2

$a$	Damper location $x = a$
$C_i$	Constants in the mode shape function
$c$	Viscous coefficient
$EI$	Cable bending stiffness
$F_a$	Damper force
$i$	Imaginary number
$K$	Spring factor of the HDR damper
$\bar{K}$	Nondimensional stiffness of $K$ ( $\bar{K} = Ka/H$ )
$K_r$	Rotational restraint stiffness at damper location
$\bar{k}_r$	Nondimensional rotational restraint stiffness $\bar{k}_r = K_r/(Ha)$
$K_{vp}$	Damper stiffness
$\bar{k}_{vp}$	Nondimensional damper stiffness $\bar{k}_{vp} = K_{vp}a/H$
$K_{vs}$	Damper support stiffness
$\bar{k}_{vs}$	Nondimensional damper support stiffness $\bar{k}_{vs} = K_{vs}a/H$
$l$	Cable length
$M_r$	Moment contributed by rotational restraint
$m$	Mass per unit length of cable
$r$	Nondimensional damper location $r = a/(l\sqrt{\eta})$



$q$	Intermediate parameter of cable bending stiffness $q = (1 - e^{-r})/r$
$H$	Cable tension
$R_f$	Reduction of damping due to cable bending stiffness
$R_r$	Reduction of damping due to rotational restraint at damper location for viscous damper
$R_{rd}$	Reduction of damping due to rotational restraint at damper location for HDR damper
$R_{vs}$	Reduction of damping due to damper support stiffness
$R_{vp}$	Reduction of damping due to damper stiffness
$t$	Time coordinate
$v(x,t)$	Cable transverse displacement
$x$	Coordinate along cable length
$\tilde{v}_a$	Amplitudes of cable displacement at damper location $x = a$
$\tilde{v}(x)$	Mode shape of cable
$\alpha$	Modification factor of the optimal damper coefficient due to the rotational restraint at the damper location
$\beta_n$	$n^{\text{th}}$ wave number of a cable with a damper
$\beta_m$	$n^{\text{th}}$ wave number of a taut string without a damper
$\delta_{1,2}$	parameters of cable mode shape
$\eta$	Nondimensional cable bending stiffness $EI/Hl^2$
$\eta_f$	Modification of damper coefficient due to cable bending stiffness
$\eta_r$	Modification of damping due to rotational restraint at damper location
$\eta_{vs}$	Modification factor for damping due to damper support stiffness

$\eta_{vp}$	Modification factor for damping due to damper stiffness
$\xi_n$	Damping ratio of cable
$\omega_n$	$n^{\text{th}}$ complex natural frequency of cable
$\phi$	Loss factor of rubber material of HDR damper

### CHAPTER 3

$K_r$	Rotational stiffness at cable ends
$\bar{K}_r$	Nondimensional stiffness $\bar{K}_r = K_r/(Ha)$
$K_{vp}$	Damper stiffness
$\bar{K}_{vp}$	Nondimensional damper stiffness $\bar{K}_{vp} = K_{vp}a/H$
$K_{vs}$	Damper support stiffness
$\bar{K}_{vs}$	Nondimensional damper support stiffness $\bar{K}_{vs} = K_{vs}a/H$
$K_{NS}$	Negative stiffness
$\bar{K}_{NS}$	Nondimensional negative stiffness of $\bar{K}_{NS} = K_{NS}a/H$
$R_1, \eta_1$	Modification factors of the damping ratio due to rotational restraints at cable ends
$R_2, \eta_2$	Modification factors of the damping ratio due to damper support stiffness
$R_3, \eta_3$	Modification factors of the damping ratio due to negative stiffness
$R_3', \eta_3'$	Modification factors due to damper stiffness
$X$	X-axis of universal damping curve
$Y$	Y-axis of universal damping curve
$\varphi$	Cable inclination

## CHAPTER 5

RMSE	Root Mean Square Error
MAPE	Mean Absolute Percentage Error
R	Correlation coefficient
$H_{pred,i}$	Predicted tension of the $i^{th}$ data point
$H_{targ,i}$	Targeted tensions of the $i^{th}$ data point
$\lambda$	Sag parameter
$\zeta$	Nondimensional parameter of cable bending stiffness
$p$	Complex number
$\delta$	Dirac delta function

## Abstract

In the family of bridge system, cable-stayed bridges are a focus of interest for bridge engineers worldwide owing to their ability to reach large spans. The recorded span length jumped remarkably from around 250 meters in 1950s to more than 1000 meters in 2010s. Cables are the distinctive element in cable-stayed bridges which play an undoubtedly central role in supporting bridge decks. Stay cables, in fact, are slender structures and have low inherent damping (0.01–0.2%). This characteristic of cable makes it extremely vulnerable to vibration sources, especially rain-wind induced excitation. Providing added damping ( $> 0.5\%$ ) by means of mounting dampers to cables would be needed to suppress extreme vibrations.

For stay cables with dampers, damping and tension are two engineering values. This study covers a wide range of problems related to damping and tension estimation of stay cables from theoretical development, practical proposal, field measurement, damping analysis, and applications to existing bridges. Chapter 2 analytically analyzes several factors which trigger low performance of dampers including rotational restraint between cable and damper, damper stiffness, damper support stiffness, and cable bending stiffness. Chapter 3 theoretically develops the universal damping curve for the design of cable damping and damper, which is as a tool for engineers to design dampers effortlessly. Chapter 4 shows the verification between the theoretical development of universal damping curve and measured damping from full-scale measurement of cable vibration; the comparison between theoretical damping and measured damping is carried out to check the damper effectiveness. Chapter 5 proposes a framework for tension estimation of cables with and without dampers, using some available parameters and regardless of many unknown cable-damper properties. Finally, the conclusions and recommendation for future study are summarized in Chapter 6.

The main results showed that in the presence of restraints between cable and damper, damper stiffness, and damper support stiffness, attainable damping is lower than its value of non-restraint cases. The modification factors of damping due to restraints, which are proposed in this study, can be used to reidentify of cable damping. Also, by adjusting supports at cable ends with finite rotational restraint stiffness, the damper works more effectively. Negative stiffness damper provides superior damping to cable compared to conventional damper. The universal damping curve is proposed in this study, which is a single curve and independent of any cable-damper parameter. The

universal curve of damping groups all cable-damper parameters into X and Y axis that facilitates the design of cable damping, especially for multi-mode vibration control. Damper effectiveness determined by full-scale measurement of cable vibration in this study was around 70% on average; amplitude dependency of measured damping was also observed. Finally, the framework for vibration-based cable tension estimation under limited information of cable parameters is proposed. Cable tension was successfully estimated using just three known parameters including cable length, mass per unit length and measured frequencies, and regardless of other unknown factors like cable bending stiffness, axial stiffness, cable inclination, restrained conditions at cable ends and lateral attachments.

## Acknowledgements

First and foremost, I would like to acknowledge Prof. Hiroshi Katsuchi for guiding me throughout this research. There have been a lot of difficulties on doing this topic, but we have successfully solved a couple of problems and published our contribution. I profoundly appreciate the motivation and discussion of Prof. Hiroshi Katsuchi. His research perspective “*I cannot do good research in a short time. Also, good results require discussion*” is keeping me on the right track.

Next, I would like to express the appreciation to Prof. Hitoshi Yamada for his discussion on my research. I am grateful to his efforts to give me and many other Vietnamese students a study abroad opportunity.

I would like to thank Assoc Prof. Dionysius Siringoringo and Prof. Yozo Fujino for advising me about the estimation of cable tension in Chapter 5.

I would also like to thank Assoc Prof. Hiroshi Tamura and all members in the Bridge and Structural Laboratory of Yokohama National University for their support and comments on my Lab’s presentations.

Words cannot express my appreciation to Assoc Prof. Ho Lan Huong from University of Transport and Communications, Vietnam for introducing me to Prof. Hitoshi Yamada. Her introduction opened my dream of studying in Japan.

Additionally, I would like acknowledge Honda Foundation, Honda Y-E-S Award 2015 and Honda Y-E-S Plus 2017 for indirectly offering me a chance to study in Japan.

And I would like to thank Japanese government for providing me with scholarship under the Monbukagakusho (MEXT) program.

I would like to thank University of Transport and Communications (UTC), Vietnam for allowing me to study in Japan. I also acknowledge my colleagues in Mechanics of Materials Section of UTC for their encouragement and helps.

Finally, I could not have completed this dissertation without the constant support of my parents. I want to spend special thanks to my wife for taking care of my kids and motivating me when I faced obstacles.

## CHAPTER 1: INTRODUCTION

This chapter provides a general picture of this study including the background of cable vibration with dampers, problem statement, aims, objectives, methodology and the structure of this dissertation. The brief remarks on the main contributions as well as related publications of the Ph.D candidate are also summarized.

### 1.1. Background

In the second half of the 20st century, cable-stayed bridges were dominantly constructed, especially for moderate to long span bridges due to its economic advantages, loading capacities and aesthetic aspects<sup>1</sup>. Cables play an undoubtedly essential role in supporting bridge decks<sup>2,3</sup>. Tension and damping in cables must be properly measured or estimated during the construction, regular assessments, and long-term health monitoring<sup>4,5</sup>. These parameters of cables provide owners with useful information about bridge safety, possible damages, structural changes, and deterioration<sup>6-8</sup>. Figure 1.1 shows an example of cable stay bridge (Tatara Bridge) used in this study.

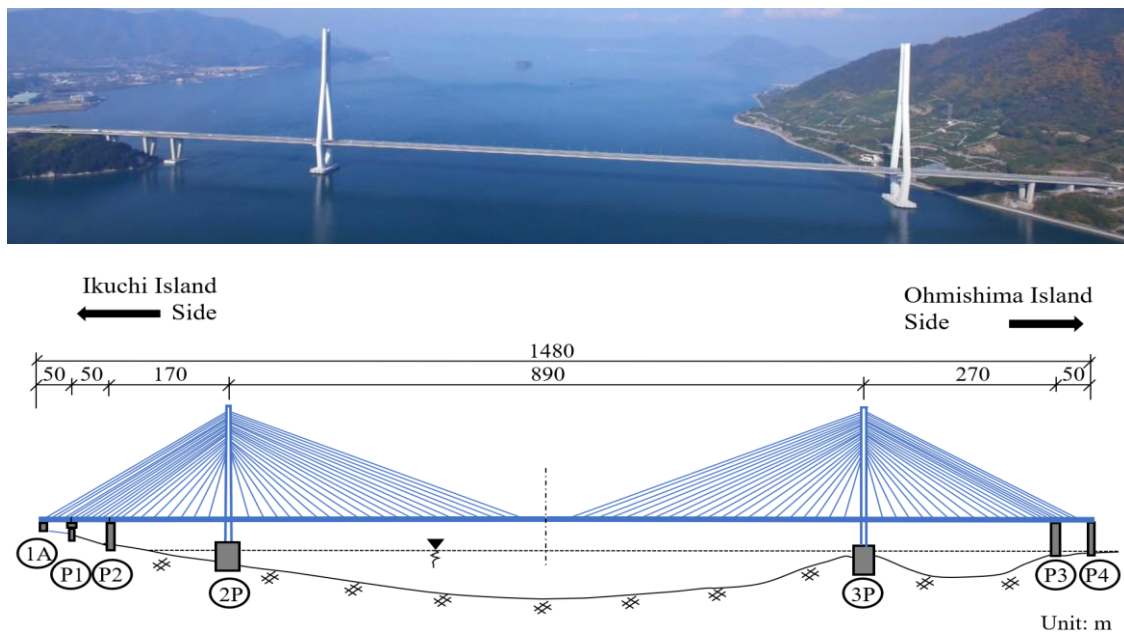


**FIGURE 1.1.** Tatara Bridge (currently 8<sup>th</sup> longest cable stay bridge in the world).

Stay cables, however, are prone to vibration under wind or traffic loads because of its low intrinsic damping. Gimsing and Georgakis<sup>2</sup> pointed out that the inherent damping ratio  $\xi_0$  of cables is in the order of 0.01% – 0.2% (log-decrement = 0.00063 – 0.013). Also, Fujino et al.<sup>9</sup> summarized inherent damping in term of logarithmic decrement ( $\delta_0 \approx 2\pi\xi_0$ ) of 50 cables of cable-stayed bridges based on field observations as shown in Figure 1.2. Overall, the inherent damping ratio of stay cables  $\xi_0$  is significantly small, which has an equivalent logarithmic decrement  $\delta_0$  is less than 0.005 ( $\xi_0 \approx 0.08\%$ ).

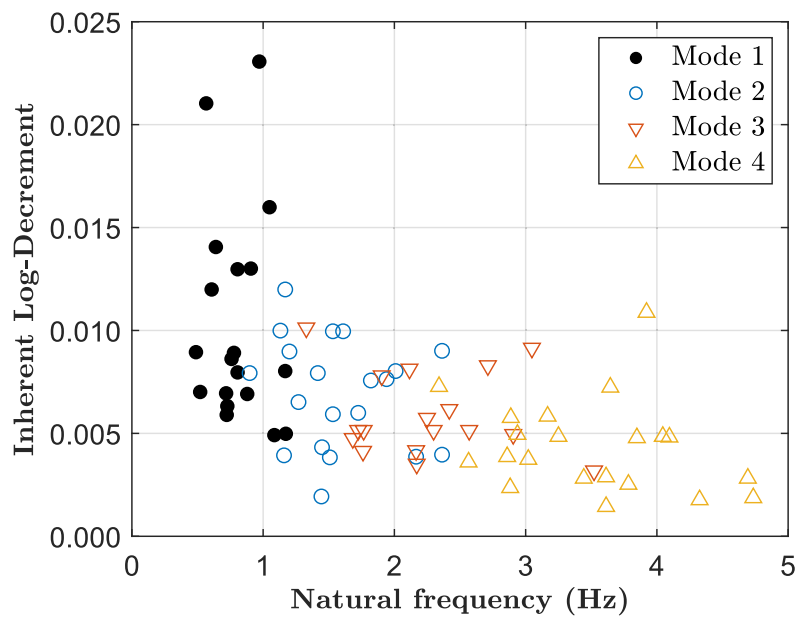


**FIGURE 1.2.** Inherent damping in logarithmic decrement versus natural frequency.

Because of low inherent damping, stay cables are vulnerable to vibration sources. There are several vibration incidents have been documented like galloping with snow, vortex excitation, rain-wind excitation, parametric excitation, etc.; among them, most of the known cable vibrations were triggered by the rain-wind excitation. According to according to U.S. Department of Transportation, Federal Highway Administration (FHA)<sup>10</sup>, the rain-wind induced vibration of a cable are usually occurred with the features and conditions as listed in Table 1.1.

Meanwhile, PTI Guide Specification<sup>11</sup> suggested that a cable damping ratio of  $\xi$  equal to 0.5 % to 1.0 %, which is equivalent to a Scruton number of at least 10 is often required to suppress rain-wind induced vibrations. To achieve this amount of required damping, dampers are often mounted to cables to provide additional



damping. Although several dampers have been introduced, viscous dampers (VD) and High Damping Rubber (HDR) dampers are commonly adopted in many cable-stayed bridges, especially in Japan. For instance, in the book “Wind resistant design of bridges in Japan: developments and practices”, Fujino et al.<sup>9</sup> introduced Japanese experiences on the countermeasures of cable vibrations (e.g., dampers, cross ties, spacer, and aerodynamic treatments) in 47 cable-stayed bridges, in which 20/47 and 13/47 of bridges adopting HDR dampers and viscous dampers, respectively. Figure 1.2 shows engineering applications of viscous damper and HDR damper to cables of cable-stayed bridge. Again, damping and tension are two main engineering values of cable with damper, hence the reference studies about damping and tension of cables with dampers will be reviewed in the following sub-sections.

**TABLE 1.1.** Characteristics of rain-wind vibration

<b>Features</b>	<b>Conditions</b>
Rain level	Moderate
Wind speeds	8–15 m/s
Wind directions to the cable plane	20° to 60°.
Frequency ranges	3 Hz
Peak amplitudes	0.25 to 1.0 m.

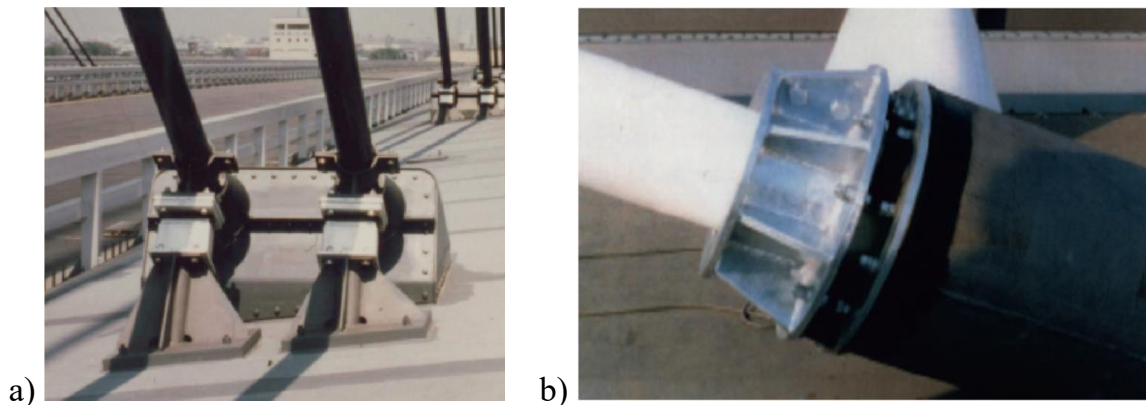


**FIGURE 1.3.** Dampers of stay cables<sup>9</sup>. a) Viscous dampers in Sakitama Bridge; and b) High Damping Rubber (HDR) damper in Shonan Ginza Bridge.

### 1.1.1. Damping of stay cables with dampers

#### 🚧 Cable model without sag effect and bending stiffness (taut-string cables)

Vibration of cables with external dampers have been studied over the years, in which the sharp focus has been put on the derivation of damping formulation. Cable based on taut-string theory is the simplest model. The term “taut” means the cable sag is ignored while “string” implies that cable bending stiffness is also not considered. Pacheco et al.<sup>12</sup> used numerical complex-eigenvalue analysis to establish damping curve of with a viscous damper, and a universal damping curve was also introduced accordingly by grouping parameters into nondimensional components. Figure 1.4 shows a model of a taut-string cable with a viscous damper. Cable has length  $l$ , tension  $H$ , mass per unit length  $m$ . A viscous damper is installed at location  $x = a$ . The coordinate with  $x$  is along cable length.

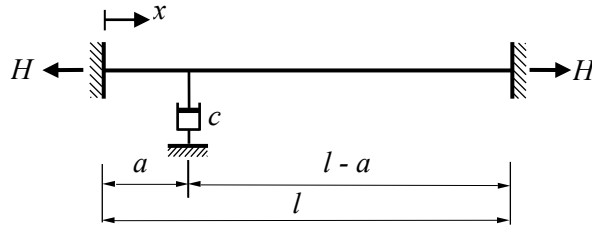


**FIGURE 1.4.** Taut-string cable with viscous damper.

Equation of motion

$$H \frac{\partial^2 v(x,t)}{\partial x^2} = m \frac{\partial^2 v(x,t)}{\partial t^2} + c \frac{\partial v(x,t)}{\partial t} \delta(x-a) \quad (1.1)$$

where  $\delta$  is the Dirac's delta function; and  $v(x, t)$  is the transverse displacement. The displacement of the cable  $v(x, t)$  is approximated by a finite series

$$v(x,t) = \sum_{n=1}^N b_n(t) \phi_{on}(x) \quad (1.2)$$

where  $b_n(t)$  is the  $n^{\text{th}}$  generalized displacement;  $\phi_{on}(x)$  denotes generalized coordinate; and  $N$  is the number of degrees of freedom. Referencing to Pacheco et al.<sup>12</sup> for the detailed solution. The result was a universal damping curve as plotted in Figure 1.5.

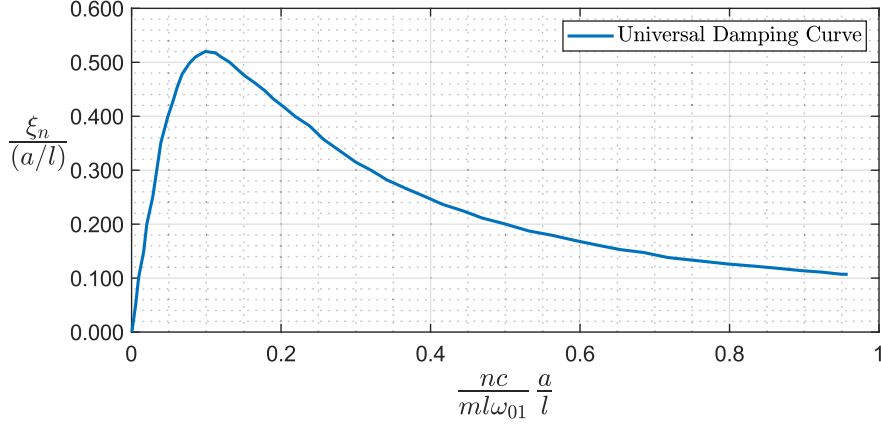


**FIGURE 1.5.** Universal damping curve proposed by Pacheco et al.<sup>12</sup> (Noted:  $\omega_{01} = (\pi/l)\sqrt{H/m}$ ).

The maximum added damping  $\xi_{\max}$  and its optimal damper coefficient  $c_{opt}$

$$\xi_{\max} = 0.52 \frac{a}{l} \text{ at } c_{opt} = 0.1ml \frac{\omega_{01}}{(na/l)} \quad (1.3)$$

The universal damping curve proposed by Pacheco et al.<sup>12</sup> is obviously useful in the design of cable damping because the damping curve is independent of cable-damper parameters. The universal damping curve, however, was presented through numerical result instead of an explicit form. To alleviate this difficulty, Krenk<sup>13</sup> introduced asymptotic solution to solve Eq. (1.1). An explicit presentation of damping ratio as

$$\frac{\xi_n}{(a/l)} = \frac{n\pi ac/l\sqrt{Hm}}{1 + (n\pi ac/l\sqrt{Hm})^2} \quad (1.4)$$

It is worth mentioning that the maximum added damping ratio of Eq. (1.4) by Krenk<sup>13</sup> is  $\xi_{\max} = 0.5a/l$  while this value by Pacheco et al.<sup>12</sup> is higher  $\xi_{\max} = 0.52a/l$ . Although taut-string cable approach yielded an explicit solution of damping as in Eq. (1.4), it oversimplified cable vibration by ignoring cable sag and cable bending stiffness. This oversimplification could pose unaccepted errors in estimation of damping in cables with unignorable bending or sag.

### 🚧 Cable model with sag effect but ignore cable bending stiffness

Krenk and Nielsen<sup>14</sup> extended the asymptotic solution by Krenk<sup>13</sup> and applied to a shallow cable. Shallow simply means cable with sag effect. They pointed out that cable sag caused the reduction of added damping. In other words, damper works ineffectively under sag effect. The sag or so-called static profile of cable is expressed by a parabolic formula as

$$y(x) = 4d \left(1 - \frac{x}{l}\right) \frac{x}{l} \quad (1.5)$$

where  $d$  = sag of cable at mid length; and  $y(x)$  = cable sag profile.

Damping ratio

$$\frac{\xi_n}{(a/l)} = \frac{\frac{ac}{\sqrt{Hm}} \beta_n^0}{1 + \left(\frac{ac}{\sqrt{Hm}} \beta_n^0\right)^2} \frac{\left(\tan\left(\frac{1}{2} \beta_n^0 l\right) - \frac{1}{2} \beta_n^0 a\right)^2}{\tan^2\left(\frac{1}{2} \beta_n^0 l\right) + (12/\lambda^2) \left(\frac{1}{2} \beta_n^0 l\right)^2} \quad (1.6)$$

where  $\beta_n^0$  = the wavenumber of sag cable without damper, and it is determined by solving the following equation given by Irvine & Caughey<sup>15</sup>

$$\tan\left(\frac{1}{2} \beta_n^0 l\right) = \frac{\beta_n^0 l}{2} - \frac{4}{\lambda^2} \left(\frac{\beta_n^0 l}{2}\right)^3 \quad (1.7)$$

here the well-known parameters  $\lambda^2$  is Irvine parameters (Irvine & Caughey<sup>15</sup>), which represents for cable sag effect. Large  $\lambda^2$  means large sag effect, and vice versa.

$$\lambda^2 = \left(\frac{mgl}{H}\right)^2 \frac{l}{HL_e / EA}; \quad L_e \approx l \left[1 + \frac{1}{8} \left(\frac{mgl}{H}\right)^2\right] \quad (1.8)$$

in which,  $EA$  = cable axial stiffness.

The comparison about damping of cable between considering sag effect and not considering sag effect can be made as followings: For cable without sag, the damping ratio is written in form of Eq. (1.4) and has maximum damping at  $\xi_{\max} = 0.5a/l$ . For cable with sag effect, damping ratio is defined by Eq. (1.6), and maximum damping ratio  $\xi_{\max}$  is lower than its damping of cable without sag. This reduction of maximum damping ratio  $\xi_{\max}$  due to sag effect is plotted in Figure 1.6.

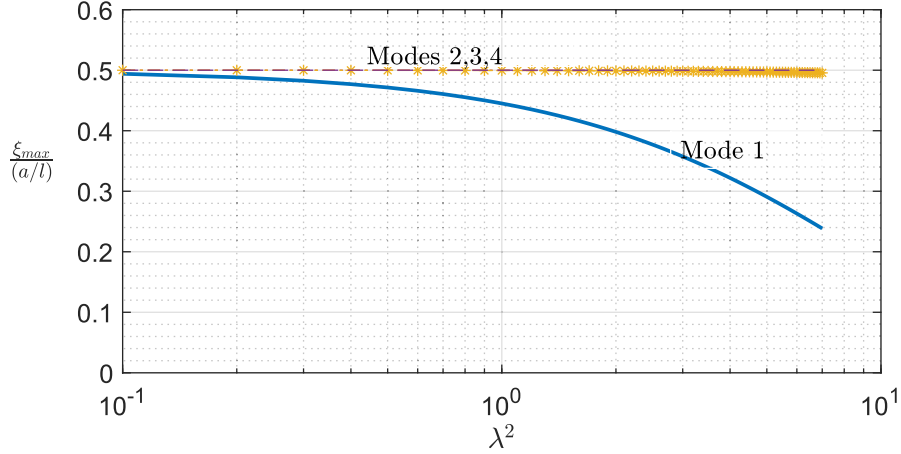


**FIGURE 1.6.** Maximum damping ratio versus sag parameter  $\lambda^2$ .

For stay cables, Mehrabi & Tabatabai<sup>16</sup> stated that the sag parameter with  $\lambda^2 < 3.1$  covers 95% of cables in cable-stayed bridges around the world. Within that range of  $\lambda^2$ , only the damping of the first vibration mode (Mode 1) is affected by cable sag as displayed in Figure 1.6. In details, increase in  $\lambda^2$  (more sag effect) leads to decrease in added damping in Mode 1 while damping in higher modes stay nearly unchanged.

#### **✚ Cable model with bending stiffness and sag effect**

Hoang and Fujino<sup>17</sup> proposed a taut cable with a viscous damper, in which cable bending stiffness  $EI$  is included whereas cable sag is neglected. They found that bending stiffness in cable caused the reduction of added damping compared to taut cable approach. Without bending stiffness, the maximum added damping ratio is  $\xi_{\max} = 0.5a/l$ . This value of maximum damping is reduced by a factor  $R_f$  due to cable bending stiffness.

$$\xi_{\max} = R_f \times \left( 0.5 \frac{a}{l} \right) \quad (1.9)$$

and

$$R_f = \frac{(1-q)^2}{1-q-0.5rq^2} \quad (1.10)$$

where  $\eta = EI/(Hl^2)$ ;  $r = a/(l\sqrt{\eta})$ ; and,  $q = (1 - e^{-r})/r$ .

A year later, Fujino and Hoang<sup>18</sup> expanded their previous work by incorporating cable bending stiffness, cable sag and damper support stiffness into a cable model,

providing a deeper insight into damper effectiveness. Figure 1.7 depicts their cable model<sup>18</sup>. The coordinates are  $x$  axis along the chord length of cable and  $y$  axis in perpendicular direction to  $x$ . Cable parameters consists of mass per unit length  $m$ , cable length  $l$ , chord tension  $H$ , cable's inclination angle  $\varphi$ , bending stiffness  $EI$ , axial stiffness  $EA$ , cable sag at mid span  $d$ . A viscous damper with viscous coefficient  $c$  is mounted to cable at location  $x = a$ . It is assumed that the damper is installed after installing cable, so the static shape of the cable is unaffected by damper.

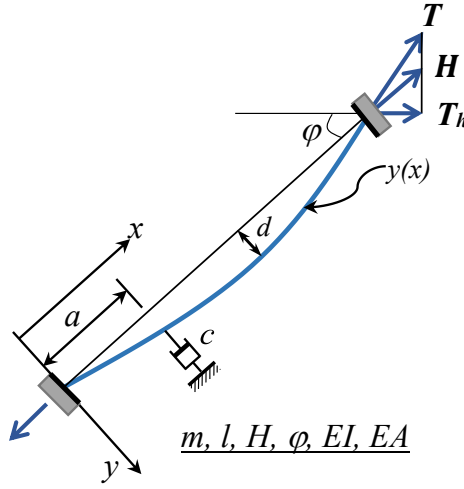


**FIGURE 1.7.** Cable model accounting for cable bending stiffness  $EI$  and sag effect.

Equation of motion

$$H \frac{\partial^2 v(x,t)}{\partial x^2} - m \frac{\partial^2 v(x,t)}{\partial t^2} + h(t) \frac{d^2 y(x)}{dx^2} - EI \frac{\partial^4 v(x,t)}{\partial x^4} = f_c(t) \delta(x-a) \quad (1.11)$$

where  $f_c(t)$  = the concentrated damping force;  $\delta$  = the Dirac's delta function;  $v(x,t)$  = the cable transverse displacement;  $y(x)$  = the cable static profile; and  $h(t)$  = the time-dependent additional chord tension due to vibration. Referencing to Fujino and Hoang<sup>18</sup> for the detailed solution. The authors employed asymptotic solution to derive the analytical damping ratio. The damping ratio is given as below.

$$\frac{\xi_n}{(a/l)} = R_f R_{sn} \frac{\eta_f \eta_{sn} \eta_n}{1 + (\eta_f \eta_{sn} \eta_n)^2} \quad \text{where } \eta_n = n\pi(a/l)c / \sqrt{Hm} \quad (1.12)$$

where  $R_f < 1$  and  $\eta_f$  are the modification factors of damping due to cable bending stiffness; and  $R_{sn} < 1$  and  $\eta_{sn}$  are the modification factors of damping due to sag

effect. For taut-string cable (no bending stiffness, no sag effect), these modification factors are unity ( $R_f = \eta_f = R_{sn} = \eta_{sn} = 1$ ).

Maximum damping ratio and its optimal coefficient

$$\xi_{\max} = 0.5R_f R_{sn} \frac{a}{l} \text{ at } \eta_n^{opt} = \frac{1}{\eta_f \eta_{sn}} \quad (1.13)$$

Without bending stiffness and sag, the maximum added damping ratio is  $\xi_{\max} = 0.5a/l$ . This value of maximum damping is reduced by factors  $R_f$  and  $R_{sn}$  due to cable bending stiffness and sag effect, respectively.

By considering stiffness  $K_{vs}$  of damper support, Eq. (1.12) becomes

$$\frac{\xi_n}{(a/l)} = R_k R_f R_{sn} \frac{\eta_k \eta_{sn} \eta_n}{1 + (\eta_k \eta_{sn} \eta_n)^2} \quad (1.14)$$

and maximum damping ratio

$$\xi_{\max} = 0.5R_k R_f R_{sn} \frac{a}{l} \text{ at } \eta_n^{opt} = \frac{1}{\eta_k \eta_{sn}} \quad (1.15)$$

where  $R_k < 1$  and  $\eta_k$  are the modification factors of damping owing to the effect of damper support stiffness. Table 1.2 summarizes cable model, maximum damping ratio and its optimal value.

Hoang and Fujino<sup>17</sup> also presented the case of High Damping Rubber (HDR) damper. The HDR damper is characterized by the spring stiffness factor  $K$  and loss factor of rubber material  $\phi$ . Damping force generated by HDR damper  $f(t) = K(1 + \phi i)v(x, t)$ . The damping ratio is formulated in as<sup>17</sup>

$$\frac{\xi_n}{(a/l)} = R_k R_f R_{sn} \frac{\phi \eta_k \bar{K}}{(1 + \eta_k \bar{K})^2 + (\phi \eta_k \bar{K})^2} \quad (1.16)$$

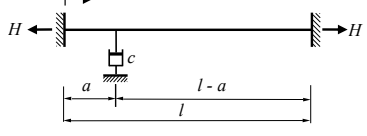
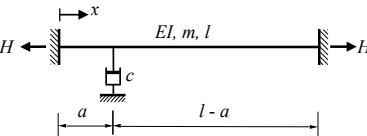
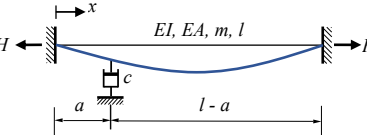
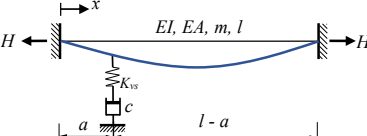
Maximum damping ratio

$$\frac{\xi_n}{(a/l)} = 0.5R_k R_f R_{sn} R_\phi \text{ at } \bar{K}_{opt} = \frac{1}{\eta_k \eta_\phi} \quad (1.17)$$

where  $\bar{K} = Ka/H$  is the dimensionless parameter of spring factor  $K$ ;  $R_\phi = \phi/(1 + \sqrt{1 + \phi^2})$ ; and  $\eta_\phi = \sqrt{1 + \phi^2}$ ; These parameters  $R_\phi$  and  $\eta_\phi$  only depend on loss factor of rubber material  $\phi$ . Other parameters in Eq. (1.16) and Eq. (1.17) are defined the same as viscous damper case. In the design of viscous damper, viscous coefficient

$c$  presented through  $\eta_n$  is a key element; similarly, in the design of HDR damper, spring factor  $K$  is a key parameter.

**TABLE 1.2.** Cable model and optimal damping ratio

No.	Cable model	Maximum damping ratio $\xi_{\max}$ and optimal coefficient $c_{opt}$ .	References
1	<b>Taut-string cable (no sag and no bending stiffness)</b> 	$\xi_{\max} = 0.52 \frac{a}{l}; c_{opt} = \frac{0.1\pi\sqrt{Hm}}{n(a/l)}$ ; $n$ is a targeted mode.	Pacheco et al. <sup>12</sup>
		$\xi_{\max} = 0.5 \frac{a}{l}; c_{opt} = \frac{\sqrt{Hm}}{\pi n(a/l)}$	Krenk <sup>13</sup>
2	<b>Cable with bending stiffness <math>EI</math></b> 	$\xi_{\max} = R_f \times \left(0.5 \frac{a}{l}\right); c_{opt} = \frac{\sqrt{Hm}}{\pi n(a/l)} \left(\frac{1}{\eta_f}\right)$ Where $R_f = \frac{(1-q)^2}{1-q-0.5rq^2}; \eta_f = 1-q-0.5rq^2$ $q = \frac{1-e^{-r}}{r}; r = \frac{a}{l\sqrt{\eta}}; \eta = \frac{EI}{Hl^2}$	Hoang and Fujino <sup>17</sup>
3	<b>Cable with bending stiffness <math>EI</math> and sag effect</b> 	$\xi_{\max} = R_{ns} R_f \times \left(0.5 \frac{a}{l}\right); c_{opt} = \frac{\sqrt{Hm}}{\pi n(a/l)} \left(\frac{1}{\eta_f \eta_{ns}}\right)$ where $R_{ns} = \frac{\left[\tan\left(\frac{1}{2}\beta_n^0 l\right) - \frac{1}{2}\beta_n^0 a\right]^2}{\tan^2\left(\frac{1}{2}\beta_n^0 l\right) + (12/\lambda^2)\left(\frac{1}{2}\beta_n^0 l\right)^2}; \eta_{ns} = \frac{\beta_n^0 l}{n\pi}$ $\lambda^2 = \left(\frac{mgl \cos \varphi}{H}\right)^2 \frac{l}{HL_e / EA}$ $L_e \approx l \left[1 + \frac{1}{8}\left(\frac{mgl \cos \varphi}{H}\right)^2\right]$ $\tan\left(\frac{1}{2}\beta_n^0 l\right) = \frac{\beta_n^0 l}{2} - \frac{4}{\lambda^2} \left(\frac{\beta_n^0 l}{2}\right)^3$ $\varphi =$ inclination angle of cable.	Fujino and Hoang <sup>18</sup>
4	<b>Cable with bending stiffness and sag effect, and support stiffness <math>K_{vs}</math></b> 	$\xi_{\max} = R_k R_{ns} R_f \times \left(0.5 \frac{a}{l}\right); c_{opt} = \frac{\sqrt{Hm}}{\pi n(a/l)} \frac{1}{\eta_k \eta_{ns}}$ where $R_k = \frac{\bar{K}_{vs} \eta_f}{1 + \bar{K}_{vs} \eta_f}; \eta_k = \eta_f + \frac{1}{\bar{K}_{vs}}; \bar{K}_{vs} = \frac{K_{vs} a}{H}$	Fujino and Hoang <sup>18</sup>

### Negative stiffness damper

As mentioned in the previous part that the actual effectiveness of damper is affected by cable sag, bending stiffness and damper support stiffness. More



specifically, these factors trigger the reduction of added damping in cable. It raises a question on how to improve performance of damper by adding enough amount of required damping to cables. One of the solutions is to use negative stiffness dampers. Recently, studies into negative stiffness damper (NSD) have been of interest as a means of improving the damper performance. A common type of the NSD for cable vibration control is the combination of a conventional damper with negative stiffness devices such as pre-compressed springs. In the presence of negative stiffness, the vibration amplitudes of cable at the damper location are amplified because negative stiffness produces forces in the direction of cable motion, resulting in larger attainable damping. Chen et al.<sup>19</sup> was among the first to introduce a NSD applied to cable vibration control, in which the NSD was assembled from a pre-compress spring and a viscous damper; an analytical damping formulation was introduced for a taut cable. Zhou and Li<sup>20</sup> introduced a NSD which was composed of two compressed springs and an oil damper mounted to a taut cable; the control performance of the NSD-cable system was investigated by numerical simulation and experiment. Both studies have come out that the NSD could provide a superior added damping to cable than conventional dampers. Other works related to the vibration control and dynamic behaviors of stay cables with a NSD have been implemented, such as Shi et al.<sup>21</sup>, Shi et al.<sup>22</sup>, Javanbakht et al.<sup>23</sup>, and Dong and Cheng<sup>24</sup>. So far, only negative stiffness viscous dampers were introduced.

### **1.1.2. Vibration-based tension estimation of stay cables**

Cables play an important role in cable-stayed bridges, and cable tension must be measured or estimated accurately during construction and maintenance stages. Currently, tension in cables can be measured directly or estimated indirectly by a vibration method. The direct measurement such as lift-off test could result in accurate tension, but costly and require massive devices, skillful labor<sup>8</sup>. The indirect estimation of cable tension by vibration method has been widely used because of its simplicity, non-destructive implementations, and relatively low cost.

For the estimation of cable tension by vibration method, the natural frequencies of a cable are measured first. Tension is deduced through analytical relationship between measured frequencies, tension, and other cable parameters.

#### **Cable model without sag effect and bending stiffness (taut-string cable)**

The simplest formulation of cable tension is derived based on taut-string theory, where tension in cable  $H$  is a function of cable length, mass per unit length and measured frequencies as

$$H = \frac{4ml^2 f_n^2}{n^2} \quad (1.18)$$

where  $H$  = cable tension;  $m$  = mass per unit length;  $l$  = length of cable; and  $f_n$  = natural frequencies measured at  $n^{\text{th}}$  mode. Eq. (1.18), however, does not include the effect of cable bending stiffness and cable sag.

#### Cable model with sag effect but ignore cable bending stiffness

By considering sag effect, tension can be calculated using a solution of Irvine & Caughey<sup>15</sup>

$$\tan\left(\frac{1}{2}\beta l\right) = \left(\frac{\beta l}{2}\right) - \left(\frac{4}{\lambda^2}\right)\left(\frac{\beta l}{2}\right)^3 \quad (1.19)$$

here  $\beta = 2\pi f_k \sqrt{m/H}$ ;  $\lambda^2 = \left(\frac{mgl}{H}\right)^2 \frac{l}{HL_e/EA}$ ;  $L_e \approx l\left[1 + \frac{1}{8}\left(\frac{mgl}{H}\right)^2\right]$ ;  $EA$  = axial stiffness of cable. Eq. (1.19), however, is transcendental and might cause difficulty. To alleviate that, Ren et al.<sup>25</sup> introduced empirical expression based on range of sag parameter  $\lambda^2$

$$H = 4ml^2 f^2 \quad (\lambda^2 \leq 0.17) \quad (1.20)$$

$$H = \sqrt[3]{ml^2(4f^2 H^2 - 7.569mEA)} \quad (0.17 \leq \lambda^2 \leq 4\pi^2) \quad (1.21)$$

$$H = ml^2 f^2 \quad (4\pi^2 \leq \lambda^2) \quad (1.22)$$

#### Cable model with bending stiffness and sag effect

Zui et al.<sup>5</sup> introduced practical formulas for estimating cable force which account for cable bending stiffness and cable sag.

- 1) Use the measured frequency  $f_1$  of mode 1 (cable with sufficiently small sag  $3 \leq \Gamma$ )

$$H = 4m(f_1 l)^2 \left[ 1 - 2.20 \frac{C}{f_1} - 0.55 \left( \frac{C}{f_1} \right)^2 \right]; \quad (17 \leq \zeta) \quad (1.23)$$

$$H = 4m(f_1 l)^2 \left[ 0.865 - 11.6 \left( \frac{C}{f_1} \right)^2 \right]; \quad (6 \leq \zeta \leq 17) \quad (1.24)$$

$$H = 4m(f_1 l)^2 \left[ 0.828 - 10.5 \left( \frac{C}{f_1} \right)^2 \right]; \quad (0 \leq \zeta \leq 6) \quad (1.25)$$

2) Use measured frequency of mode 2 (cable with relatively large sag  $\Gamma \leq 3$ )

$$H = m(f_2 l)^2 \left[ 1 - 4.40 \frac{C}{f_2} - 1.10 \left( \frac{C}{f_2} \right)^2 \right]; \quad (60 \leq \zeta) \quad (1.26)$$

$$H = m(f_2 l)^2 \left[ 1.03 - 6.33 \frac{C}{f_2} - 1.58 \left( \frac{C}{f_2} \right)^2 \right]; \quad (17 \leq \zeta \leq 60) \quad (1.27)$$

$$H = m(f_2 l)^2 \left[ 0.882 - 85.0 \left( \frac{C}{f_2} \right)^2 \right]; \quad (0 \leq \zeta \leq 17) \quad (1.28)$$

3) Use measured frequency of high-order modes (very long cable  $2 < k$ )

$$H = \frac{4m}{n^2} (f_n l)^2 \left( 1 - 2.20 \frac{nC}{f_2} \right); \quad (200 \leq \zeta) \quad (1.29)$$

here  $C = \sqrt{(EI)/(ml^4)}$ ;  $\Gamma = \sqrt{(mgl)/(128EA\delta^3 \cos^5 \varphi)}[(0.31\zeta + 0.5)]/[(0.31\zeta - 0.5)]$ ;  $\zeta = l\sqrt{H/EI}$ ;  $\delta$  = sag-to-span ratio;  $\varphi$  = inclination angle; and  $EI$  = bending stiffness.

In fact, these formulations of cable tension are only valid for a cable without lateral attachments. As mentioned, stay cables have shown very low inherent damping<sup>26</sup>, thus cross ties<sup>2,27,28</sup> or dampers<sup>18,23,29-31</sup> are often mounted to cables to suppress wind-induced vibration. The presence of the lateral components has made the estimation of cable force even more challenging. Recently, some of emerging optimization algorithms have been adopted to identify not only cable tension but also other parameters like cable bending stiffness, restraint stiffness at cable ends as well as the lateral components (e.g., damper characteristics). The main purpose of the optimization is to minimize the errors between measured and analytical cable frequencies. Kim and Park<sup>32</sup> used the frequency-based sensitivity-updating algorithm (FBSU) to determine tension, bending stiffness and axial stiffness. Ma<sup>33</sup> extended the FBSU for a cable with rotational restraint ends. Zarbaf et al.<sup>34</sup> used Genetic Algorithm (GA) and Particle Swarm Optimization (PSO). Dan et al.<sup>35</sup> also used PSO for the identification of tension and lateral force components (e.g., additional mass, dampers); however, only tension and damping coefficient were successfully identified with acceptable accuracy. Apart from the above optimization solutions,

ZarbaF et al.<sup>36</sup> was among the first to introduce an application of Artificial Neural Networks (ANNs) in estimating tension. In this work, however, cable inclination, restraints at cable ends and lateral components like dampers and cross ties were not incorporated into the cable model.

## 1.2. Problem statement

In this research, the target structure is stay cables with dampers. For this cable-damper structure, damping and tension are obviously two main engineering values. The following points outline the problems addressed in this study.

- 1) **Problem 1**: Actual damping contributed by dampers is usually lower than theoretical values. The performance of dampers could vary from 50% to 70% of theoretical design (Caetano<sup>1</sup>). Cable bending stiffness, cable sag and damper support stiffness have been pointed out by Fujino and Hoang<sup>18</sup> as the reasons for the damper ineffectiveness. Practically, dampers are often installed to cables that also contain attachments between cable and damper like a ring-shaped rubber bushing. These attachments trigger vibration restraints at the damper location and lead to the reduction of damper performance as a result. This problem has not been solved in the past.
- 2) **Problem 2**: Conventional model of cable with damper assumed the perfect boundary conditions at cable ends, usually fixed-fixed end. In fact, restraints at cable ends are complex and rely heavily, for example, on anchorage types, anchoring techniques, and configurations of the supports. Therefore, the determination of damping in cables which accounts for the uncertain boundaries at cable ends like hinged-hinged, fixed-fixed, and rotational restraint ends should be taken into account. This issue is important because dampers are installed near a cable end (at 1%-5% of cable length), and damper performance are greatly affected by shape of cable near cable ends.
- 3) **Problem 3**: In the design of damping in a stay cable with damper, the damping ratio is a function of many parameters like damper location, cable properties, damper characteristics, damper support stiffness, damper stiffness, negative stiffness, etc. Therefore, damping curve varies under influencing parameters. To facilitate the design process, especially for multi-mode vibration control, it is necessary to propose a universal damping curve which is independent of any parameters. As a result, the design process using a single curve will be easier than involving multiple damping curve.

- 4) **Problem 4:** The above points of the problem statement deal with the theoretical development of damping in stay cables with dampers. The verification should be conducted. With that, damping analysis from full-scale measurement data of existing cables of a cable-stayed bridge will be presented in this study. This helps to compare theoretical damping and actual damping. The effectiveness and performance of actual damper can be evaluated. Other issues such as amplitude dependency of damping and amplitude dependency of measured frequencies can also be observed from measurement data.
- 5) **Problem 5:** The estimation of tension of cables without lateral attachment (e.g., dampers and crossties) was fully developed. In the presence of dampers, it becomes challenging. In addition, cable length, mass per unit length and the first few natural frequencies are most likely available to be used for estimating tension. But the other parameters such as bending stiffness, axial stiffness, cable inclination, rotational restraint stiffness at the cable ends, and lateral components are often unknown or uncertain. Under limited information of cable parameters, the formulations of cable tension developed in the past seem to fail to estimate tension. Hence, it raises a question of how to identify tension utilizing just some available parameters but still accounting for unavailable information.

### 1.3. Aims and methodology

This study aims at addressing the 5 problems mentioned in the problem statement (Section 1.2) above. These 5 problems were solved and presented through Chapter 2 to Chapter 5. In details, Chapter 2 solves the Problem 1; Chapter 3 deals with the Problems 2 and 3; Chapter 3 addresses the Problem 4; and Chapter 5 proposes a solution for the Problem 5. The results and conclusions are made in Chapter 6, where all concerning points in the problem statement section are addressed.

The methodology used in this study is analytical model analysis and full-scale experimental validation. For the development of theoretical damping, cable mode is introduced followed by eigen analysis of cable vibration with damper. The formulation of damping is derived based on an asymptotic solution. About field measurement of cable damping, data processing is conducted to extract measured damping and measured frequency. Regarding the estimation of cable tension, the Finite Difference Method is employed in conjunction with the application of Artificial Neural Networks (ANNs).

## 1.4. Structure of the dissertation

This dissertation includes 6 chapters:

**Chapter 1:** Introduction.

**Chapter 2:** Reduction of damping in stay cable with damper under rotational restraint between damper and cable.

**Chapter 3.** Development of universal damping curve for design of cable damping with damper.

**Chapter 4:** Damping analysis of full-scale cables from field measurement data.

**Chapter 5:** Framework for estimation of cable tension under limited information of cable properties by application of artificial neural networks (ANNs)

**Chapter 6:** Conclusions and future study.

## 1.5. Publications

The contents of this research cover 03 published journal papers, 02 published conference papers.

Title	Journal/ Conference	Status	Year
<b>Luu Xuan Le</b> , Hiroshi Katsuchi, and Hitoshi Yamada. 2020. “Effect of Rotational Restraint at Damper Location on Damping of a Taut Cable with a Viscous Damper.” <i>J. Bridge Eng.</i> 25(2): 04019139. <a href="https://doi.org/10.1061/(ASCE)BE.1943-5592.0001520">https://doi.org/10.1061/(ASCE)BE.1943-5592.0001520</a>	Journal of Bridge Engineering (ASCE)	Published	2020
<b>Luu Xuan Le</b> , Hiroshi Katsuchi, and Hitoshi Yamada.2020. “Damping of Cable with HDR Damper Accounting for Restraint Boundary Conditions.” <i>J. Bridge Eng.</i> 25(12): 04020105. <a href="https://doi.org/10.1061/(ASCE)BE.1943-5592.0001641">https://doi.org/10.1061/(ASCE)BE.1943-5592.0001641</a>	Journal of Bridge Engineering (ASCE)	Published	2020
<b>Luu Xuan Le</b> , Hiroshi Katsuchi, Hitoshi Yamada, and BX Luong.2021. “Reduction of Damping in Stay Cable with a Viscous Damper Due to Rotational Restraint between Damper and Cable.” 2nd International Symposium on Dynamics and Aerodynamics of Cables - ISDAC 2021. p49-56.	Conference Proceeding	Published	2021
<b>Luu Xuan Le</b> , Hiroshi Katsuchi, and Hitoshi Yamada. 2021. “Asymptotic Formulas for Vibration-Based Cable Tension Identification Accounting for Uncertain Boundary Conditions.” In book: Bridge Maintenance, Safety, Management, Life-Cycle	Book chapter	Published	2021

Sustainability, and Innovations; DOI: 10.1201/9780429279119-409.			
<b>Luu Xuan Le</b> , Dionysius M. Siringoringo, Hiroshi Katsuchi, and Yozo Fujino. 2022. “ <i>Stay cable tension estimation of cable-stayed bridge under limited information on cable properties using artificial neural networks.</i> ” Struct Control Health Monit.;e3015-1-29. doi:10.1002/stc.3015	Journal of Structural Control and Health Monitoring (SCHM)	Published	2022

## CHAPTER 2. REDUCTION OF DAMPING IN STAY CABLE WITH DAMPER UNDER ROTATIONAL RESTRAINT BETWEEN DAMPER AND CABLE

The actual damping in cable with damper is often lower than designed value. Some factors like cable bending stiffness or cable sag have pointed out as the reasons for this reduction of added damping. This chapter presents another cause of damping reduction which is due to rotational restraint between damper and cable. Additionally, the effects of damper support stiffness and damper stiffness on damper effectiveness are also investigated. The results indicated that by taking the rotational restraint between the damper and cable into account, the achievable damping in the cable is always lower than its value in a non-rotationally restraint case. Cable with viscous damper is studied first, then extending results to cable with High Damping Rubber damper (HDR damper).

### 2.1. Introduction

In cable-stayed bridges, the cable is an undoubtedly important component, due to its loading capacity, economic advantages, and aesthetics. Stay cables, however, are prone to vibration under wind or traffic loads because they have very low intrinsic damping. Gimsing and Georgakis<sup>2</sup> pointed out that the inherent damping ratio of cables is in the order of 0.01% – 0.2%, whereas PTI Guide Specification<sup>11</sup> suggests that a cable damping ratio of  $\zeta$  equal to 0.5 % to 1.0 % would be needed to suppress rain-wind induced vibrations. For that reason, dampers are often externally mounted to a cable to satisfy the required damping. In fact, the measured damping in installed cables is lower than the expected value. For instance, an efficiency ratio of 0.6 for viscous dampers has been reported in an experimental study by Zhou et al.<sup>37</sup> For many years, the problem of damping reduction in a stay cable with an external damper has received the attention of researchers. For instance, a study of Tabatabai and Mehrabi<sup>38</sup>, by numerical method, showed that the cable bending stiffness and sag effect, caused by cable self-weight, result in a lower added damping than the corresponding value of a taut string counterpart. In another study on damping reduction due to the sag extensibility and flexural stiffness of cables, Fujino and Hoang<sup>18</sup> derived reduction factors due to bending and sag by applying an asymptotic solution.



Dampers, practically, are often installed to a cable with attached devices on mechanical and aesthetic grounds, such as cable protective tubes, rubbers at damper location, damper supports, and damper protective tubes. As a matter of fact, these attachments, so-called restraints, have finite stiffness, and as a result, will pose adverse impacts on the damper efficiency. To deal with this issue, some studies<sup>30,39-43</sup> on the effect of these restraints on the attainable damping of a cable have been implemented. These works addressed the problem regarding damper restraints by setting two typical models of the damper system: a damper connected to an elastic spring in series or in parallel. However, rotational restraint at the damper location might also exist because of the presence of cable protective tubes or damper supports. Such influences of the rotational restraint should be considered for calculating achievable cable damping.

For that reason, this chapter aims at investigating the effect of the rotational restraint at the damper location on added damping of a cable with an externally installed damper, in which cable bending stiffness and vertical restraints (damper stiffness and support stiffness) are also included. It is noted that although a traditional single damper does not include the rotational restraints, the cable-damper system might include rotational and vertical restraints when it is installed with attached devices depending on kinds of attached devices.

The remaining of this chapter are as follows: Firstly, a cable model with a viscous damper is introduced accounting for rotational restraint between cable and damper at damper location. Next, the formulation of added damping is accordingly proposed using asymptotic solution which is based on the proposed cable-damper model; the reduction factor of added damping due to the rotational stiffness at damper location is also proposed. Afterwards, the effect of damper stiffness and damper support stiffness on the damper effectiveness are investigated. Finally, the results are extended to cable with High Damping Rubber damper (HDR damper).

## **2.2. Schematic diagram, equation of motion and eigenvalue analysis**

Transverse vibration scheme of a cable with an external viscous damper is shown in Figure 2.1, in which the coordinate  $x$  starts from the left end of the given cable. The cable has length  $l$ , mass per unit length  $m$ , bending stiffness  $EI$ , and tension of cable  $H$ . A viscous damper with damping coefficient  $c$  is attached to the cable at the location  $a$  from the cable's left end. Rotational restraint stiffness at the damper location is denoted as  $K_r$ .

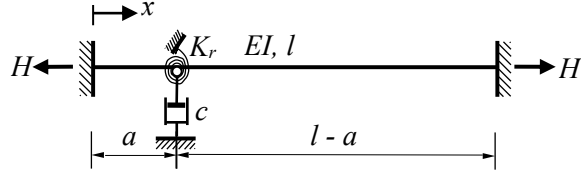


**FIGURE 2. 1.** Cable with a viscous damper.

Equation of motion of each segment,  $0 \leq x \leq a^-$  and  $a^+ \leq x \leq l$  is derived as

$$H \frac{\partial^2 v(x,t)}{\partial x^2} - EI \frac{\partial^4 v(x,t)}{\partial x^4} - m \frac{\partial^2 v(x,t)}{\partial t^2} = 0 \quad (2.1)$$

Displacement of the cable  $v(x,t)$  can be described in terms of the harmonic form as

$$v(x,t) = \tilde{v}(x)e^{\omega it} \quad (2.2)$$

where  $i^2 = -1$ ;  $\omega$  = complex natural frequency of the cable;  $\tilde{v}(x)$  = cable mode shape. Substitution of  $v(x,t)$  from Eq. (2.2) into Eq. (2.1) yields

$$\eta l^2 \frac{d^4 \tilde{v}(x)}{dx^4} - \frac{d^2 \tilde{v}(x)}{dx^2} - \beta^2 \tilde{v}(x) = 0 \quad (2.3)$$

where  $\eta = EI/Hl^2$  is a nondimensional parameter of cable bending stiffness, while  $\beta = \omega \sqrt{m/H}$  is the wave number.

Solving the characteristic equation of the fourth-order ordinary differential equation, Eq. (2.3) yields two real roots and another two complex roots. Hence, the homogeneous solutions of Eq. (2.3) which represents the complex mode shape of the cable in the left segment and the right segment of the damper are determined correspondingly as

$$\tilde{v}_1(x) = C_1 \sinh(\delta_1 x) + C_2 \cosh(\delta_1 x) + C_3 \sin(\delta_2 x) + C_4 \cos(\delta_2 x) \quad (2.4)$$

and

$$\tilde{v}_2(x) = C_5 \sinh \delta_1(x-a) + C_6 \cosh \delta_1(x-a) + C_7 \sin \delta_2(x-a) + C_8 \cos \delta_2(x-a) \quad (2.5)$$

where

$$\delta_{1,2} = \sqrt{\frac{\sqrt{1+4\eta l^2 \beta^2} \pm 1}{2\eta l^2}} \quad (2.6)$$

The constants from  $C_1$  to  $C_8$  are ascertained by satisfying boundary conditions at cable ends and continuity conditions at the damper location. For these conditions, the slope and displacement at both ends of the cable are set to be zero, and the slope and transverse displacements of the cross section in the left span are equal to those in the right span at the damper location. Difference of bending moments on a cross section between two segments as well as its shear forces at the damper are equal to the external moment  $M_r$  contributed from the rotational restraint and the damper force  $F_a$ , correspondingly.

$$\tilde{v}_1(0) = 0; \quad \left. \frac{d\tilde{v}_1}{dx} \right|_{x=0} = 0; \quad \tilde{v}_2(l) = 0; \quad \left. \frac{d\tilde{v}_2}{dx} \right|_{x=l} = 0; \quad (2.7a-d)$$

$$\tilde{v}_1(a) = \tilde{v}_a; \quad \tilde{v}_2(a) = \tilde{v}_a; \quad \left. \frac{d\tilde{v}_1(x)}{dx} \right|_{x=a^-} = \left. \frac{d\tilde{v}_2(x)}{dx} \right|_{x=a^+}; \quad (2.8a-d)$$

$$EI \left. \frac{d^2\tilde{v}_2(x)}{dx^2} \right|_{x=a^+} - EI \left. \frac{d^2\tilde{v}_1(x)}{dx^2} \right|_{x=a^-} = M_r; \quad (2.9)$$

$$EI \left. \frac{d^3\tilde{v}_1(x)}{dx^3} \right|_{x=a^-} - EI \left. \frac{d^3\tilde{v}_2(x)}{dx^3} \right|_{x=a^+} = F_a; \quad (2.10)$$

By solving and simplifying Eqs. from (2.7a) to (2.9) with respect to  $\tilde{v}_a$ , constants in Eq. (2.4) and Eq. (2.5) are obtained as follows:

$$C_1 = \frac{\tilde{v}_a(K_r f_1 + f_2)}{K_r f_3 + f_4}; \quad C_2 = \frac{\tilde{v}_a(K_r f_5 + f_6)}{K_r f_3 + f_4}; \quad C_3 = \left( \frac{-\delta_1}{\delta_2} \right) C_1; \quad C_4 = -C_2 \quad (2.11a-d)$$

$$C_5 = \frac{\tilde{v}_a(K_r f_7 + f_8)}{K_r f_3 + f_4}; \quad C_6 = \frac{\tilde{v}_a(K_r f_9 + f_{10})}{K_r f_3 + f_4}; \quad C_7 = \frac{\tilde{v}_a(K_r f_{11} + f_{12})}{K_r f_3 + f_4} \quad (2.12a-d)$$

where  $f_1$  to  $f_{12}$  are expressed in terms of sine, cosine, hyperbolic sine, and hyperbolic cosine as shown in the Appendix from Eq. (2.48) to Eq. (2.59). Substituting the determined complex mode shape of each segment into Eq. (2.10), and simplifying them, the equation for complex eigenfrequencies of the cable  $\omega$  is derived in the subsequent form

$$\frac{K_r f_{13} + EI(\delta_1^2 + \delta_2^2)^2 \{2\delta_1 \delta_2 [\cos(\delta_2 l) \cosh(\delta_1 l) - 1] - (\delta_1^2 - \delta_2^2) \sin(\delta_2 l) \sinh(\delta_1 l)\}}{K_r f_3 + f_4} = \frac{F_a}{\tilde{v}_a EI \delta_1 \delta_2} \quad (2.13)$$

The formula  $f_{13}$  is shown in Eq. (2.60) in the Appendix. Obviously, Eq. (2.13) is transcendental and quite mathematical cumbersome, in which the first term of the numerator and denominator of the left-hand-side part reflects the influence of the

rotational restraint on the dynamic characteristics of the cable. The numerator of the right-hand-side part is the damper force  $F_a$  applying to the cable at the damper location. To verify the reliability of the proposed solution herein, if the effect of the rotational restraint is neglected,  $K_r = 0$ , Eq. (2.13) results naturally in the same expression derived by Hoang and Fujino<sup>17</sup>. In addition, without having a damper ( $c = 0$ ) and rotational restraint ( $K_r = 0$ ), the numerator of the left-hand-side part is equal to zero, and as a result, Eq. (2.13) leads fairly to the exact form of the characteristic equation of a vibrating cable introduced by Zui et al.<sup>5</sup> This transcendental equation, Eq. (2.13), contains imaginary number  $i$  in the term of  $F_a$  in the right-hand side while the opposite side consists of sine, cosine and hyperbolic functions. So that, it is not easy to achieve explicit solution of the Eq. (2.13). To alleviate that, the next section will present an asymptotic solution applied to obtain an explicit formulation of damping ratio.

### 2.3. Attainable cable damping

The asymptotic solution is employed in this section to derive damping formulation from Eq. (2.13). The asymptotic solution is under the assumption that the perturbation in terms of a wave number between the cable with a damper and a taut string without a damper ( $\beta_m = n\pi/l$ ) is small (Hoang and Fujino<sup>17</sup>). Based on that, the following approximation is made using the Taylor expansion

$$\tan(\beta_n l) \cong \beta_n l - n\pi \quad (2.14)$$

Practically, the damper is often installed close to one end of the cable,  $a/l \ll 1$ . Therefore,

$$\cos(\beta_n a) \cong 1; \quad \sin(\beta_n a) \cong \beta_n a \quad (2.15)$$

In addition, the non-dimensional parameter of the cable bending stiffness  $\eta$ , which was introduced in the preceding section, is also small for cables of cable-stayed bridges,  $\eta \ll 1$ . The practical range is around  $2.8 \times 10^{-6} - 1 \times 10^{-2}$  (Hoang and Fujino<sup>17</sup>). By referencing the work of (Hoang and Fujino<sup>17</sup>), the subsequent approximations are rationally introduced.

$$\delta_1 \cong \frac{1}{\sqrt{\eta l}}; \quad \delta_2 \cong \beta_m; \quad \delta_1^2 + \delta_2^2 \cong \delta_1^2 - \delta_2^2 = \frac{1}{\eta l^2}; \quad \sinh \delta_1 l \gg 1 \quad (2.16a-d)$$

$$\sinh \delta_1 (a-l) = -\cosh \delta_1 (a-l) \cong -e^{-r} \sinh \delta_1 l; \quad (2.17)$$

$$\sinh \delta_1 (2a-l) = -\cosh \delta_1 (2a-l) \cong -e^{-2r} \sinh \delta_1 l. \quad (2.18)$$

Substitution of these approximations from Eqs. (2.15) to (2.18) into Eq. (2.13) leads to the asymptotic form of eigenfrequencies. Hence,

$$\tan(\beta_n l) = \beta_n l \left( \frac{a}{l} \right) \frac{\frac{2}{r} + \frac{F_a a}{H \tilde{v}_a} \left( 1 - \frac{2}{r^2} + \frac{2+2r}{r^2 e^r} \right) + A}{1 + \frac{F_a a}{H \tilde{v}_a} \left( 1 - \frac{3}{2r} - \frac{1-4e^r}{2re^{2r}} \right) + B} \quad (2.19)$$

where

$$A = \frac{K_r}{H a e^r} (3e^r - 2) + \frac{2F_a K_r}{H^2 \tilde{v}_a} \left( \frac{2+r}{re^r} - \frac{1}{r} - \frac{1+r}{re^{2r}} \right) \quad (2.20)$$

$$B = \frac{K_r}{H} \left[ \frac{(\beta_m)^2 a (2-e^r)}{e^r} + \frac{r(e^{2r}-1)}{2ae^{2r}} \right] - \frac{F_a K_r}{H^2 \tilde{v}_a} \left( 1 - \frac{re^r+4}{2e^r} + \frac{2+r}{2e^{2r}} \right) \quad (2.21)$$

and  $r = \frac{a}{l\sqrt{\eta}}$ , a nondimensional parameter of the damper location.

Components  $A$  and  $B$  which contain the rotational stiffness  $K_r$  represent the effect of the rotational restraint on the eigenfrequencies. It is straightforward to verify that if the rotational restraint is not considered in the cable model ( $A = B = 0$ ), then Eq. (2.19) shifts to the same form as proposed by Hoang and Fujino<sup>17</sup>.

Since the natural frequencies of the cable are complex, its form can be illustrated through cable damping ratio  $\xi_n$  and its frequency magnitude  $|\omega_n|$  (Krenk<sup>13</sup>).

$$\omega_n = |\omega_n| (\sqrt{1 - \xi_n^2} + \xi_n i) \quad (2.22)$$

From which, the damping ratio can be deduced as the imaginary part of Eq. (2.22)

$$\xi_n = \frac{\text{Im}[\omega_n]}{|\omega_n|} \quad (2.23)$$

Rewriting Eq. (2.23) in the form of the wave number  $\beta_n$ , then combining it with Eqs. (2.14) and (2.19) yields the explicit form of the damping ratio as

$$\xi_n = \text{Im} \left[ \left( \frac{a}{l} \right) \frac{\frac{2}{r} + \frac{F_a a}{H \tilde{v}_a} \left( 1 - \frac{2}{r^2} + \frac{2+2r}{r^2 e^r} \right) + A}{1 + \frac{F_a a}{H \tilde{v}_a} \left( 1 - \frac{3}{2r} - \frac{1-4e^r}{2re^{2r}} \right) + B} \right] \quad (2.24)$$

It can confirm that when the rotational restraint is not included ( $A = B = 0$ ), then Eq. (2.24) becomes the same expression proposed by Hoang and Fujino<sup>17</sup> for a

flexural cable with a conventional viscous damper. Substitution of the damper force  $F_a = ci\omega\tilde{v}_a$  (Hoang and Fujino<sup>17</sup>) into Eq. (2.24) yields

$$\frac{\xi_n}{(a/l)} = R_r R_f \frac{\eta_r \eta_f \eta_n}{(1 + \eta_{r1} \bar{k}_r)^2 + [\eta_f + \eta_{r2} \bar{k}_r]^2 \eta_n^2} \quad (2.25)$$

where  $\bar{k}_r = K_r/(Ha)$  is the nondimensional rotational restraint stiffness at damper location;  $q = (1 - e^{-r})/r$  is the intermediate parameter of cable bending stiffness;  $R_f = (1 - q)^2/\eta_f$  characterizes a reduction factor of the maximum cable damping caused by the cable bending stiffness;  $\eta_f = (1 - q - 0.5rq^2)$  denotes a modification factor of the damper characteristic due to the cable bending stiffness;  $\eta_n = n\pi ca/(l\sqrt{Hm})$  is the dimensionless damper coefficient corresponding to the  $n^{\text{th}}$  vibration mode;  $R_r$  is the damping reduction factor due to rotational restraint between damper and cable;  $\eta_r$ ,  $\eta_{r1}$  and  $\eta_{r2}$  are the modification factors of the damping characteristic.

$$R_r = \left( \frac{\eta_{r3} \bar{k}_r^2 + \eta_{r4} \bar{k}_r}{(1 - q)^2} + 1 \right) \frac{\eta_f}{(1 + \eta_{r1} \bar{k}_r)(\eta_f + \eta_{r2} \bar{k}_r)} \quad (2.26)$$

$$\eta_r = \frac{(1 + \eta_{r1} \bar{k}_r)(\eta_f + \eta_{r2} \bar{k}_r)}{\eta_f}; \quad \eta_{r1} = n^2 \pi^2 (1 - 2qr) \left( \frac{a}{l} \right)^2 - \frac{(qr - 2)qr^2}{2} \quad (2.27a,b)$$

$$\eta_{r2} = (1 - q - 0.5qr)qr^2; \quad \eta_{r3} = -2qr(qr + q - 1)\eta_{r1} - (1 + 2qr)\eta_{r2} \quad (2.28a,b)$$

$$\eta_{r4} = \frac{-2\eta_{r2}}{r} - (1 + 2qr)\eta_f + \left( 1 - 2q - \frac{2q}{r} + \frac{2}{r} \right) \eta_{r1} - 2qr(qr + q - 1) \quad (2.29)$$

The maximum added damping and its optimal damper coefficient are

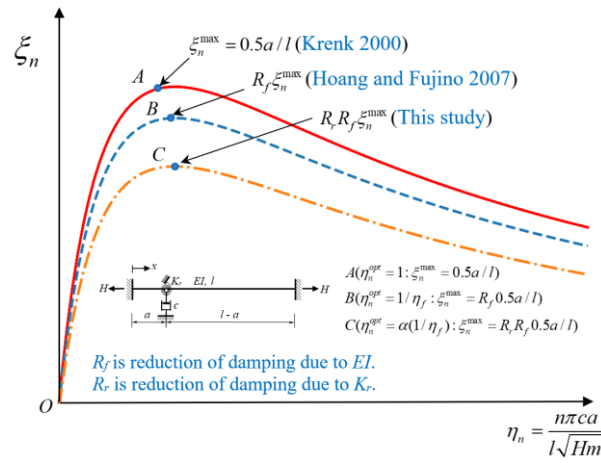
$$\frac{\xi_{\max}}{(a/l)} = 0.5R_r R_f \quad \text{when} \quad \eta_n^{\text{opt}} = \alpha \left( \frac{1}{\eta_f} \right) \quad (2.30a,b)$$

here,  $\alpha$  is a modification factor of the optimal damper coefficient due to the rotational restraint at the damper location.

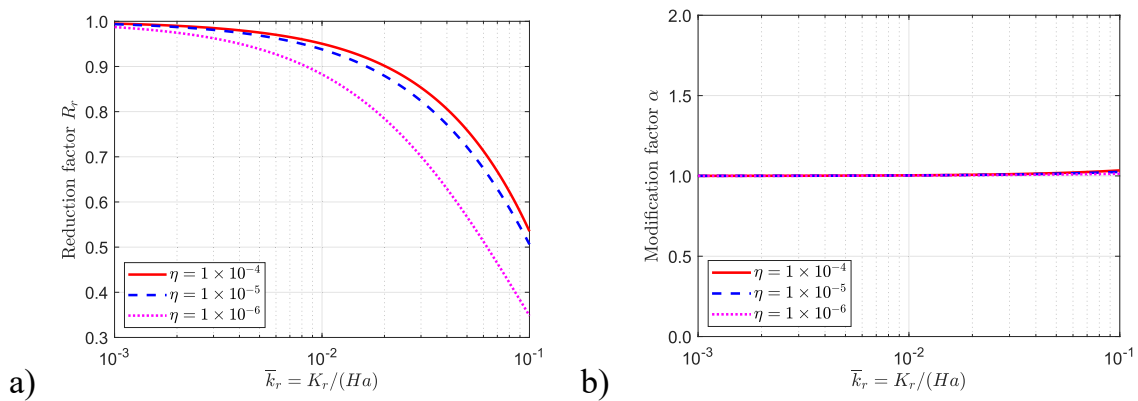
$$\alpha = \frac{\eta_{r1} \bar{k}_r + 1}{(\eta_{r2} \bar{k}_r / \eta_f + 1)} \quad (2.31)$$

Figure 2.2 shows the damping curve of stay cable with viscous damper. For a taut-string cable (without cable sag and bending stiffness), Krenk (2000)<sup>13</sup> proposed the

damping curve and pointed out that the maximum damping ratio is  $\xi_{\max} = 0.5(a/l)$ . In a study of Hoang and Fujino<sup>17</sup>, they indicated that the maximum damping ratio is reduced by the factor  $R_f$  due to cable bending stiffness, making  $\xi_{\max} = 0.5R_f(a/l)$ . In this study, we propose a damping curve which accounts for the impact of rotational restraint at damper location; damping ratio is further reduced by a reduction factor  $R_r$  in comparison with damping value from study of Hoang and Fujino<sup>17</sup>. Also, the optimal coefficient of a viscous damper is modified by the factor  $\alpha$ . Physically, the factors  $R_r$  and  $\alpha$  mean that the peak of the cable damping curve proposed by Hoang and Fujino<sup>17</sup>, will be vertically and horizontally shifted from an original value to a new location. Figure 2.3 shows the reduction factor  $R_r$  and modification factor  $\alpha$  due to the rotational restraint between a damper and cable.



**FIGURE 2. 2.** Damping curve of cable with viscous damper under rotational restraint.



**FIGURE 2. 3.** a) Reduction factor  $R_r$  of the maximum modal damping; and b) modification factor  $\alpha$  of the optimal damper coefficient with different cable bending stiffness ( $a/l = 0.02$ ).

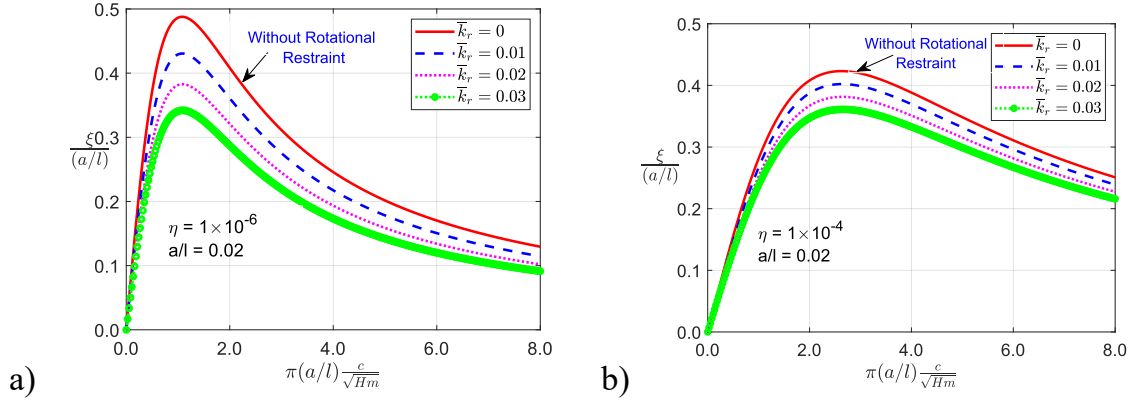


**FIGURE 2. 4.** Modal damping in a cable with a viscous damper accounting for the rotational restraint between the damper and cable: a) small bending stiffness; and b) large bending stiffness.

As can be seen from Figure 2.3a, the increase in rotational restraint between damper and cable results in a decrease in attainable damping, which is much larger for cables with small bending stiffness. For the installation of stay cables to a bridge, ring-shaped rubber bushings are sometimes attached to cables inside the steel guide tubes to reduce the bending stress, especially at anchorages. In a scenario where the rubber bushing is mounted at the damper location, the installation might trigger rotational restraint between damper and cable leading to the ineffectiveness of an installed damper. Another point, based on the view of the beam-cable theory, is that the rotational angle of a cable cross section is inversely proportional to the cable bending stiffness  $EI$ . Therefore, an increase in  $EI$  (increase  $\eta$ ) causes a decrease in rotational angle at the damper location, which reduces the impact of the rotational restraint on the damper performance. Figure 2.3b indicates that the rotational restraint at the damper location does not significantly modify much the optimal damper coefficient. This modification factor  $\alpha$  of the optimal damper coefficient is nearly unity. It means that the peak of the damping curve is not horizontally shifted. It almost vertically drops as clearly shown in Figure 2.4. This interesting observation hints at the design of the cable damping with a viscous damper under the rotational restraint consideration that the achievable cable damping ratio can be re-identified by multiplying the designed damping of a conventional case by the reduction factor  $R_r$ . The numerical investigations on the influence of the rotational restraint at the damper location on the added damping is shown in Figure 2.4 while Figure 2.5 displays



damping of different modes. Figure 2.5 indicates that damping drops remarkably from Mode 1 to Mode 3, and the reduction percentage from the Mode 1 to Mode 3 between two schemes (with and without having restraints) is nearly the equal, around 40%. Cable with  $l = 100$  m,  $m = 78.3$  kg/m,  $H = 3 \times 10^6$  N, and  $a/l = 0.02$  was used.

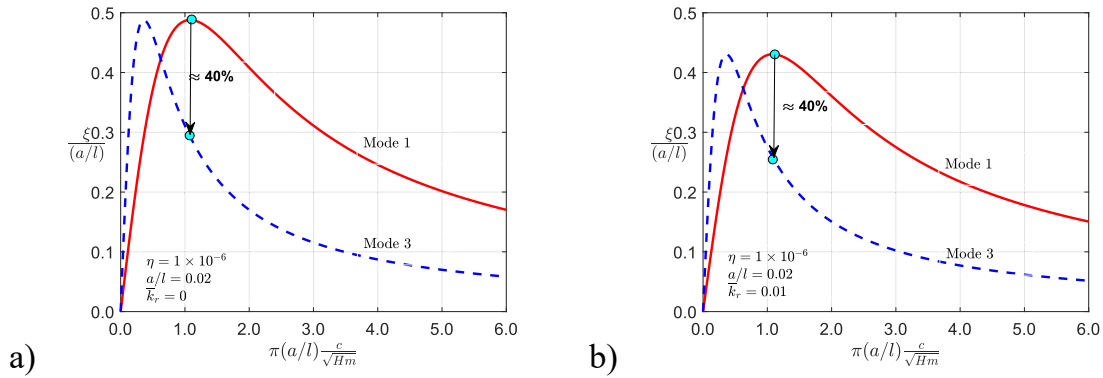


**FIGURE 2. 5.** Modal damping Mode 1 and Mode 3: a) without rotational restraint ( $\bar{k}_r = 0$ ); and, b) with rotational restraint ( $\bar{k}_r = 0.01$ ).

#### 2.4. Effect of damper support stiffness and damper stiffness on damping

Translational restraint stiffness connected to the viscous damper in series or in parallel is modelled with linear elastic springs  $K_{vs}$  and  $K_{vp}$ , representing the damper support stiffness and damper stiffness, respectively. The schematic diagrams are shown in Figure 2.6.

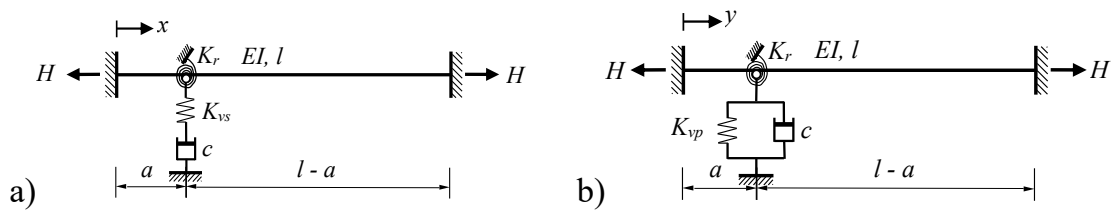


**FIGURE 2. 6.** Cable with a viscous damper accounting for: a) Damper support stiffness; and b) damper stiffness.

In the presence of damper support stiffness or damper stiffness, the damper force expression is calculated using Eq. (2.32a) or Eq. (2.32b), respectively (Le et al.<sup>29</sup>).

$$F_a = \frac{\tilde{v}_a i \omega}{\left( \frac{i \omega}{K_{vs}} + \frac{1}{c} \right)}; \quad (2.32a)$$

$$F_a = \tilde{v}_a (K_{vp} + ci \omega) \quad (2.32b)$$

**Effect of Damper Support Stiffness:** By substituting damper force  $F_a$  from Eq. (2.32a) into Eq. (2.24), the modal damping ratio of a cable is obtained as

$$\frac{\xi}{(a/l)} = R_{vs} R_r R_f \frac{\eta_{vs} \eta_r \eta_f \eta_n}{\left[ (1 + \eta_{r1} \bar{k}_r) + (\eta_f + \eta_{r2} \bar{k}_r) \left( \frac{\eta_n^2}{\eta_n^2 + \bar{k}_{vs}^2} \right) \bar{k}_{vs} \right]^2 + \left( \frac{\bar{k}_{vs}^2}{\eta_n^2 + \bar{k}_{vs}^2} \right)^2 (\eta_f + \eta_{r2} \bar{k}_r)^2 \eta_n^2} \left( \frac{\bar{k}_{vs}^2}{\eta_n^2 + \bar{k}_{vs}^2} \right) \quad (2.33)$$

where  $\bar{k}_{vs} = K_{vs} a/H$  characterizes the nondimensional damper support stiffness;  $R_{vs}$  and  $\eta_{vs}$  are the reduction factors for cable damping and its modification factor for the damper characteristic due to damper support stiffness, respectively.

$$R_{vs} = \frac{1}{\eta_{vs}}; \quad \eta_{vs} = 1 + \frac{(1 + \eta_{r1} \bar{k}_r)}{(\eta_f + \eta_{r2} \bar{k}_r)} \left( \frac{1}{\bar{k}_{vs}} \right) \quad (2.34a,b)$$

The maximum modal damping ratio and its optimal damper coefficient are

$$\frac{\xi}{(a/l)} = 0.5 R_{vs} R_r R_f \quad \text{when} \quad \eta_n^{opt} = \left( \frac{\alpha \beta}{\alpha + \beta} \right) \left( \frac{1}{\eta_f} \right) \quad (2.35a,b)$$

where  $\alpha$  is defined as Eq. (2.31) related to rotational restraint at damper location; and  $\beta = \bar{k}_{vs} \eta_f$ . When the effect of damper support stiffness is neglected ( $\bar{k}_{vs} = \infty$ ), the factors  $\eta_{vs} = 1$  and  $R_{vs} = 1$ , making Eq. (2.33) to become Eq. (2.25) and Eq. (2.35a,b) to become Eq. (2.30a,b).

**Effect of Damper Stiffness:** By substitution of damper force  $F_a$  from Eq. (2.32b) into Eq. (2.24), the modal damping ratio of a cable is obtained as

$$\frac{\xi}{(a/l)} = R_{vp} R_r R_f \frac{\eta_{vp} \eta_r \eta_f \eta_n}{\left[ (1 + \eta_{r1} \bar{k}_r) + (\eta_f + \eta_{r2} \bar{k}_r) \bar{k}_{vp} \right]^2 + (\eta_f + \eta_{r2} \bar{k}_r)^2 \eta_n^2} \quad (2.36)$$

where  $\bar{k}_{vp} = K_{vp} a/H$  characterizes the nondimensional damper stiffness;  $R_{vp}$  and  $\eta_{vp}$  are the reduction factor for cable damping and its modification factor for the damper characteristic due to damper stiffness, respectively.

$$R_{vp} = \frac{1}{\eta_{vp}} ; \text{ and } \eta_{vp} = 1 + \left( \frac{\eta_f + \eta_{r2} \bar{k}_r}{1 + \eta_{r1} \bar{k}_r} \right) \bar{k}_{vp} \quad (2.37a,b)$$

The maximum modal damping ratio and its optimal damper coefficient are

$$\frac{\xi_n}{(a/l)} = 0.5 R_{vp} R_r R_f \text{ when } \eta_n^{opt} = (\kappa + \alpha) \left( \frac{1}{\eta_f} \right) \quad (2.38a,b)$$

in which  $\kappa = \bar{k}_{vp} \eta_f$  represents the modification factor for the optimal damper coefficient due to damper stiffness. It can be confirmed that by neglecting damper stiffness ( $\bar{k}_{vp} = 0$ ), the factors  $\eta_{vp}$  and  $R_{vs}$  are unity, thus Eq. (2.36) results in Eq. (2.25) and Eq. (2.38a,b) become Eq. (2.30a,b).

The graphic of damping in cable which considers the effect of damper support stiffness or damper stiffness is shown in Figure 2.7a and Figure 2.7b, respectively. In the presence of these constraints, attainable damping is always lower than cases without constraints. The reductions of added damping due to the constraints are presented through the proposed reduction factor  $R_{vs}$  due to damper support stiffness and  $R_{vp}$  due to damper stiffness. Figures 2.8 plots the reduction factors  $R_{vs}$  and  $R_{vp}$ . Figure 2.9 illustrates the damping curve with different values of damper support stiffness  $K_{vs}$  and damper stiffness  $K_{vp}$ . Cable with  $l = 100$  m,  $m = 78.3$  kg/m,  $H = 3 \times 10^6$  N, and  $a/l = 0.02$  was used.

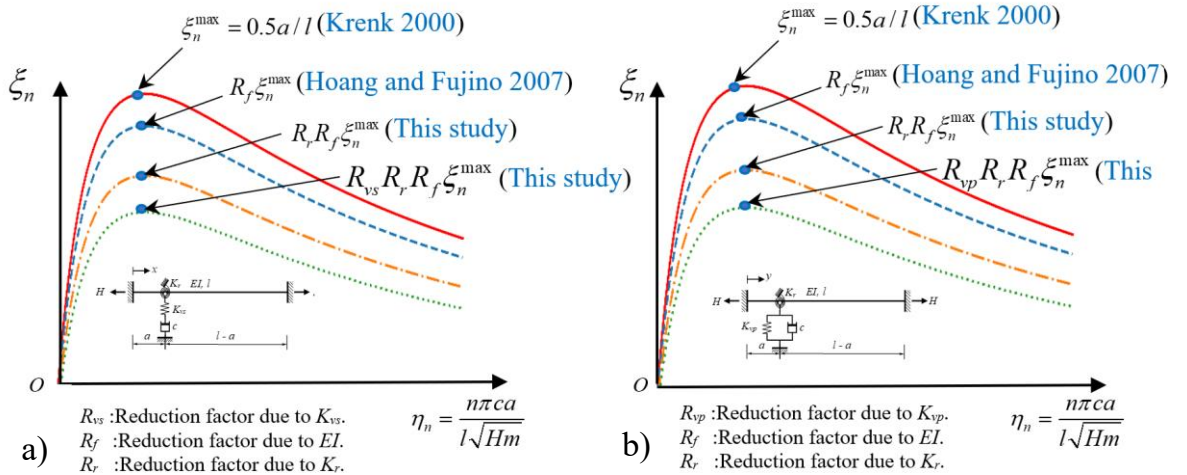


**FIGURE 2. 7.** Demonstration of damping curve of cable with viscous damper considering for: a) damper support stiffness; and b) damper stiffness.

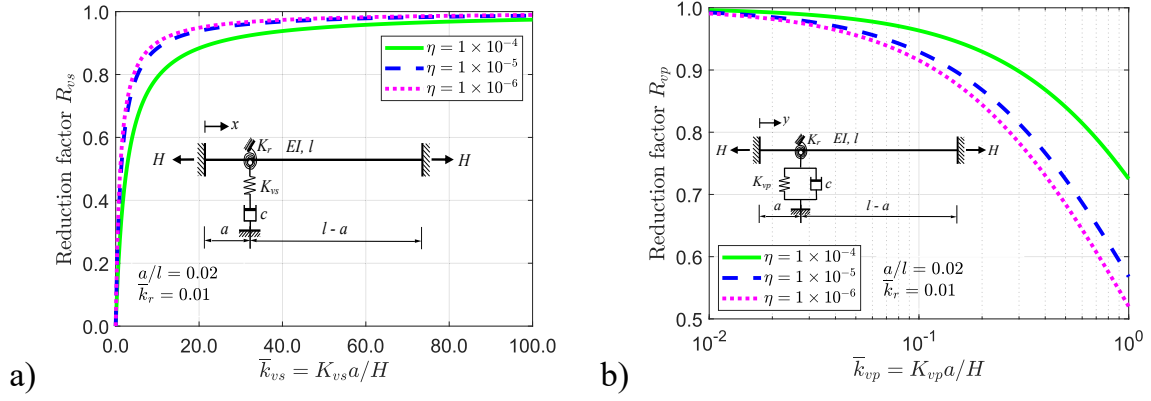


FIGURE 2. 8. Reduction factors of damping: a)  $R_{vs}$ ; and b)  $R_{vp}$ .

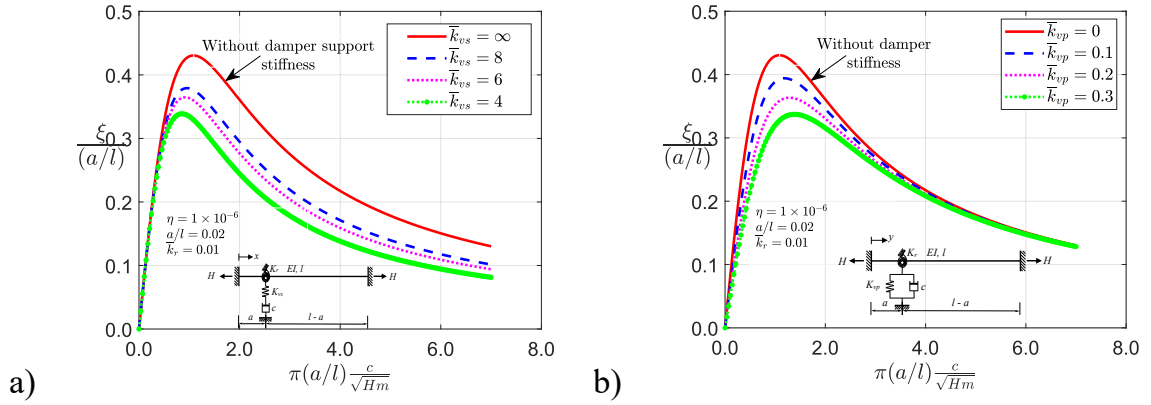


FIGURE 2. 9. Damping curve: a) different values of damper support stiffness  $K_{vs}$ ; and b) different values of damper stiffness  $K_{vp}$ .

Overall, a damper with flexible support stiffness  $K_{vs}$  produces less added damping ( $R_{vs} < 1$ ) compared to rigid damper support. A damper with damper stiffness  $K_{vp}$  also triggers less added damping than damper without having damper stiffness. Since the damper support stiffness and damper stiffness are the culprits of the damping reduction in a cable, the design of a cable-damper system should consider these factors to avoid overestimation of the achievable damping.

## 2.5. Extend results to cable with High Damping Rubber Damper (HDR damper)

Expanding the results of damping in cable with viscous damper in the preceding sections, the reduction of damping in the HDR damper-cable system due to the rotational restraint between at damper location is proposed in this section. For a ring-

shaped HDR damper with a finite length of rubber along the cable, the interval displacement ( $\Delta$ ) between both ends of rubber would trigger the rotational restraint. Figure 2.10 shows a model of cable with an HDR damper.

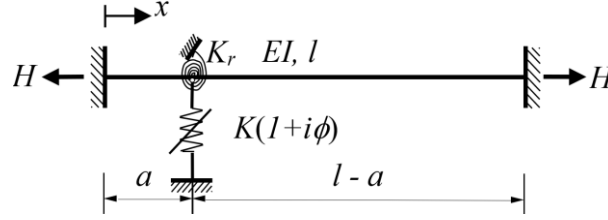


FIGURE 2. 10. Model of cable with HDR damper.

The characteristics of the HDR damper are illustrated as complex-valued impedance with the damper force is given as the independent form of frequency (Fujino and Hoang<sup>18</sup>).

$$F_a = K(1+i\phi)\tilde{v}_a \quad (2.39)$$

where  $i^2 = -1$ ;  $K$  = spring factor of the HDR damper;  $\phi$  = loss factor of rubber material; and  $\tilde{v}_a$  = amplitudes of the cable mode shape at  $x = a$ .

By inserting the HDR damper force from Eq. (2.39) into Eq. (2.24), the damping ratio can be found as

$$\frac{\xi_n}{(a/l)} = R_{rd}R_f \frac{\eta_{rd}\eta_f\phi\bar{K}}{(1+\eta_{rd1}\eta_f\bar{K})^2 + (\phi\eta_{rd2}\eta_f\bar{K})^2} \quad (2.40)$$

The maximum added damping ratio and the optimal damper spring factor are

$$\frac{\xi_n^{max}}{(a/l)} = 0.5R_{rd}R_fR_\phi \quad \text{when} \quad \bar{K}_{rd}^{opt} = \frac{1}{(\eta_{rd2}^2/\eta_{rd})} \left( \frac{1}{\eta_f\sqrt{1+\phi^2}} \right) \quad (2.41a,b)$$

in which the definitions of  $\eta_f$  and  $R_f$  are the same as in the section of viscous damper;  $\bar{K} = Ka/H$ ;  $R_\phi = \phi/(1 + \sqrt{1 + \phi^2})$ ; and  $R_{rd}$  is the reduction factor of the maximum cable damping due to the rotational restraint at the damper location

$$R_{rd} = \frac{1}{\eta_{rd}} \left[ \frac{(f_1f_2 + 2f_3f_4)}{(1-q)^2} \bar{k}_r^2 + \frac{(f_5f_4r - f_1f_6r + 2f_3r + 2f_2)}{r(1-q)^2} \bar{k}_r + 1 \right] \quad (2.42)$$

$$\eta_{rd} = 1 + \left( f_4 - \frac{f_2}{f_6} \right) \bar{k}_r - \frac{f_2 f_4}{f_6} \bar{k}_r^2 \quad \eta_{rd1} = \left[ 1 + \left( \frac{f_4}{f_6 \bar{K}} - \frac{f_2}{f_6} \right) \bar{k}_r \right]; \quad (2.43a,b)$$

$$\eta_{rd2} = \left( 1 - \frac{f_2}{f_6} \bar{k}_r \right) \quad f_1 = 1 + 2rq; \quad (2.44a,b)$$

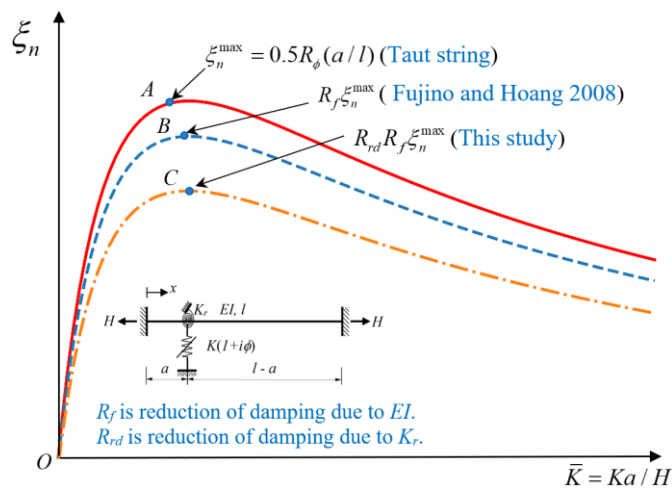
$$f_2 = 0.5qr^2(rq + 2q - 2); \quad f_3 = rq(1 - q - rq) \quad (2.45a,b)$$

$$f_4 = \left( \frac{a}{l} \right)^2 n^2 \pi^2 (1 - 2rq) - 0.5qr^2(rq - 2); \quad f_5 = 1 - 2q + \frac{2}{r}(1 - q) \quad (2.46a,b)$$

$$f_6 = 1 - q - 0.5rq^2 \quad (2.47)$$

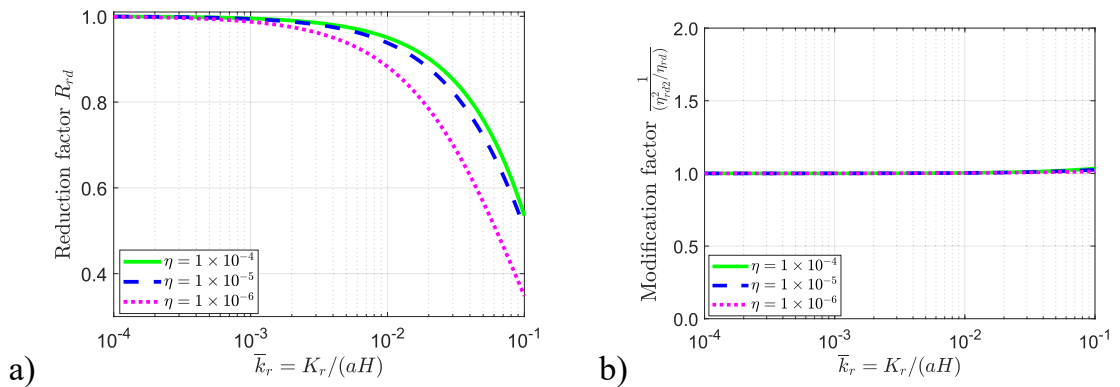
It is noted that without the rotational restraint ( $\bar{k}_r = 0$ ), such components  $R_{rd} = 1$ ,  $\eta_{rd} = \eta_{rd1} = \eta_{rd2} = 1$ , Eq. (2.40) is the same as damping proposed by Fujino and Hoang<sup>18</sup>.

Figure 2.11 displays the damping curve of HDR damper under the consideration of rotational restraint in comparison with previous works. It can be explained as the following: Taut-string cable with HDR damper can have maximum added damping is  $\xi_n^{max} = 0.5R_\phi(a/l)$ . Fujino and Hoang<sup>18</sup> pointed out that this value of optimal damping  $\xi_n^{max}$  is reduced by factor  $R_f$  due to the effect of cable bending stiffness. If rotational restraint between cable and damper is considered, the optimal damping  $\xi_n^{max}$  is further reduced by factor  $R_{rd}$  proposed in this study.



**FIGURE 2. 11.** Damping curve of cable with HDR damper under rotational restraint.

Figure 2.12a depicts the reduction factor  $R_{rd}$  of the modal damping ratio against the rotational restraint stiffness. Its corresponding modification factor of the optimal damper coefficient  $1/(\eta_{rd2}^2/\eta_{rd})$  is presented in Figure 2.12b. In fact, the added damping decreases ( $R_{rd} < 1$ ) in the presence of the rotational restraint between the cable and damper. This reduction, also shown in Figure 2.13, depends on the smooth transition between the damper and cable at the attached point. The higher rotational stiffness is, the lower additional cable damping gains. Another point is that the increase in the bending stiffness  $\eta$  leads to less effect of restraint on the added damping as represented in Figure 2.12a. For example, with  $\bar{k}_r = 0.01$ ,  $R_{rd} = 0.88$  for  $\eta = 1 \times 10^{-6}$  and  $R_{rd} = 0.95$  for  $\eta = 1 \times 10^{-4}$ . It is understandable from the view of the beam-cable theory that the rotational angle of a cable cross section is inversely proportional to the cable bending stiffness  $EI$ . Therefore, the increase in  $EI$  (increase  $\eta$ ) causes the decrease in the rotational angle at the damper location, which leads to the small impact of the rotational restraint on the damper performance. About optimal damper coefficient, Figure 2.12b indicates that the rotational restraint at the damper location does not modify the optimal damper coefficient much; this modification factor of the optimal damper coefficient is nearly 1. It means that the peak of the damping curve is not horizontally shifted. It almost vertically drops as clearly shown in Figure 2.13. This interesting observation releases a hint in the design of the cable damping with a HDR damper under the rotational restraint consideration such that the achievable cable damping ratio can be re-identified by multiplying the designed damping of a conventional case by the reduction factor  $R_{rd}$ .



**FIGURE 2. 12.** (a) Reduction factor  $R_{rd}$  of damping ratio; and b) Modification factor damper coefficient.

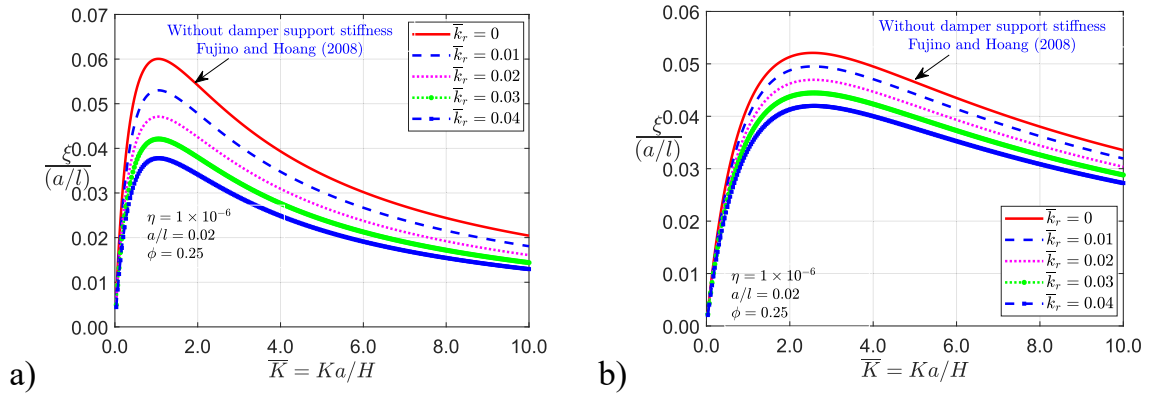


**FIGURE 2. 13.** Damping ratio in a cable with an HDR damper accounting for the rotational restraint between the damper and cable: a) small bending stiffness; and b) large bending stiffness.

For a HDR damper without the rotational restraint at the attached location, the modal damping ratio is independent of the vibration modes (Fujino and Hoang<sup>18</sup>). In the existence of the rotational restraint, the achievable damping, on the other hand, is dependent on the vibration modes, but Figure 2.14 shows that this dependency can be neglected. This characteristic is unique for the HDR damper because the cable with a viscous damper has reduction in the damping by around 40 % from the peak of Mode 1 to the corresponding point of Mode 3.

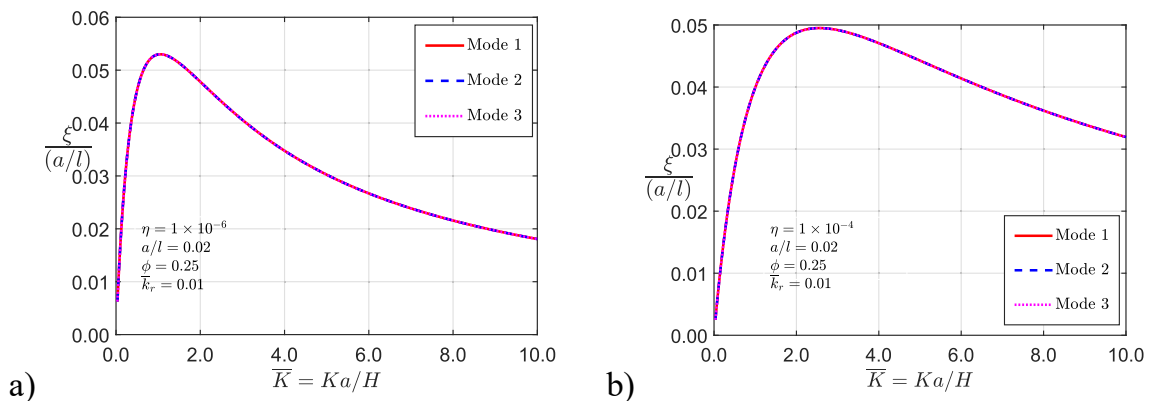


**FIGURE 2. 14.** Damping ratio with different vibration modes: a) small bending stiffness; and b) large bending stiffness.



## 2.6. Full-scale experimental validation

Several reduction factors of damping have been proposed in this chapter. The improvement of damping estimation will be examined using full-scale experimental data in the literature. An experiment conducted by Yoneda et al.<sup>44</sup> in the literature will be used for the validation. Table 2.1 shows the cable properties used in the experiments. A viscous-shear damper was installed to the cable at a damper location  $a = 0.72$  m. Table 2.2 summarizes measured damping, damper characteristics, estimated damping, and estimation accuracy. The damping ratio is estimated using formulations by Krenk<sup>13</sup>, Hoang and Fujino<sup>17</sup>, and the proposed damping formular in this study. It is worth mentioning again that Krenk<sup>13</sup> did not consider the effect of cable bending stiffness; Hoang and Fujino<sup>17</sup> considered the reduction of damping due to cable bending stiffness; the proposed solution in this study simultaneously considers the reduction of damping due to cable bending stiffness and damper stiffness. The results illustrated in the Table 2.2 clearly indicate that by taking reduction of damping owing to cable bending stiffness and damper stiffness, the estimation accuracy is significantly improved. The estimated damping ratio by our proposed formulation is closer to measured damping in comparison to others.

**TABLE 2. 1.** Cable properties in the experimental validation

Cable length $l$ (m)	Mass per unit length $m$ (kg/m)	Bending stiffness $EI$ (N.m <sup>2</sup> )	Cable tension $H$ (N)	Cable diameter $D$ (m)	Damper location $a$ (m)
100.23	100.7	5.52E+06	4.20E+06	0.155	4.72

**TABLE 2. 2.** Improvement of damping estimation

Mode	Measured damping ratio $\xi$ (%)	Viscous coefficient $c$ (N.s/m)	Damper stiffness $K_{vp}$ (N/m)	Estimated damping ratio (%)			Estimation accuracy		
				By Krenk <sup>13</sup>	by Hoang and Fujino <sup>17</sup>	This study	By Krenk <sup>13</sup>	by Hoang and Fujino <sup>17</sup>	This study
1	1.27	1.56E+05	8.09E+05	2.34	2.01	1.01	0.54	0.63	1.26
2	0.97	1.10E+05	1.11E+06	2.13	2.12	1.01	0.46	0.46	0.96

## 2.7. Summary

In this chapter, the reduction of damping ratio due to rotational restraint at damper location, damper support stiffness and damper stiffness was studied. The formulation of damping ratio was proposed accordingly using asymptotic solution,

and the reduction of the added damping were presented through reduction factors. Viscous damper and High Damping Rubber damper (HDR damper) were used as targeted dampers in this study. The conclusions are as follows:

 **Effect of rotational restraint at damper location on cable damping**

- 1) In the presence of rotational restraint, the added damping is always lower than its value in a non-rotational restraint. This reduction of damping is presented through the proposed reduction factor.
- 2) When rotational restraint stiffness between cable and damper is large, the damper works ineffectively.
- 3) Although the value of damping ratio decreases due to the restraint, this restraint does not modify much the optimal damper coefficient compared to a conventional case (without the rotational restraint).
- 4) In the design cable-damper structure which accounts for the rotational restraint, damping is re-identified by multiplying the designed damping of a conventional case by the reduction factor proposed in this study.
- 5) For viscous damper, the damping ratio decreases remarkably from the first mode to the higher modes, but the difference in terms of the reduction percentage between with and without rotational restraints is not significant.
- 6) For HDR damper, the damping is almost equal for all vibration modes regardless of rotational restraint effect.

 **Effect of damper stiffness and damper support stiffness on cable damping**

- 1) Damper stiffness and damper support stiffness caused low damper performance. The reduction of damping is presented through the proposed reduction factor.
- 2) Dampers with small support stiffness generate small amount of damping and vice versa. Similarly, dampers with large damper stiffness result in small amount of damping and vice versa.

## Appendix: Formulas in from Eq. (2.11) to (2.13)

The following formulas partly appear in Eq. (2.11) to Eq. (2.13)

$$f_1 = -\delta_2(\delta_1 \sinh \delta_1 a + \delta_2 \sin \delta_2 a) \{(\delta_1^2 - \delta_2^2) \sinh \delta_1(a-l) \sin \delta_2(a-l) - 2\delta_1 \delta_2 [\cosh \delta_1(a-l) \cos \delta_2(a-l) - 1]\} \quad (2.48)$$

$$f_2 = EI \delta_2 (\delta_1^2 + \delta_2^2) \{ \delta_1 \delta_2 (\cos \delta_2 a + \cosh \delta_1 a) [(\cosh \delta_1(a-l) \cos \delta_2(a-l) - 1) + \sinh \delta_1(a-l) \sin \delta_2(a-l)] \\ \times (\delta_2^2 \cos \delta_2 a - \delta_1^2 \cosh \delta_1 a) + (\delta_1 \sinh \delta_1 a + \delta_2 \sin \delta_2 a) [\delta_1 \sin \delta_2(a-l) \cosh \delta_1(a-l) - \delta_2 \sinh \delta_1(a-l)] \\ \times \cos \delta_2(a-l) \} \} \quad (2.49)$$

$$f_3 = \frac{1}{2} \delta_1^2 \delta_2^2 \{ \cos \delta_2 l [\cosh \delta_1(2a-l) + 3 \cosh \delta_1 l] + \cos \delta_2(2a-l) [3 \cosh \delta_1(2a-l) + \cosh \delta_1 l] - 8 [\cosh \delta_1(a-l) \\ \times \cos \delta_2(a-l) + \cosh(\delta_1 a) \cos(\delta_2 a) - 1] \} - \delta_1 \delta_2 (\delta_1^2 - \delta_2^2) [\sinh \delta_1(2a-l) \times \sin \delta_2(2a-l) + \sin(\delta_2 l) \sinh(\delta_1 l) \\ - 2 \sinh(\delta_1 a) \sin(\delta_2 a) - 2 \sinh \delta_1(a-l) \sin \delta_2(a-l)] - \frac{1}{4} (\delta_1^4 + \delta_2^4) [\cos \delta_2(2a-l) - \cos \delta_2 l] \times [\cosh \delta_1(2a-l) \\ - \cosh \delta_1 l] \quad (2.50)$$

$$f_4 = -\frac{1}{2} EI (\delta_1^2 + \delta_2^2) \{ \delta_1^3 \sinh \delta_1 l [\cos \delta_2 l - \cos \delta_2(2a-l)] + \delta_2^2 \delta_2 \sin \delta_2 l [3 \cosh \delta_1 l + \cosh \delta_1(2a-l)] - 4 \delta_1^2 \delta_2 \\ \times [\sin(\delta_2 a) \cosh(\delta_1 a) - \sin \delta_2(a-l) \cosh \delta_1(a-l)] - \delta_1 \delta_2^2 \sinh \delta_1 l [3 \cos \delta_2 l + \cos \delta_2(2a-l)] + [\cos(\delta_2 a) \\ \times \sinh(\delta_1 a) - \sinh \delta_1(a-l) \cos \delta_2(a-l)] 4 \delta_1 \delta_2^2 - \delta_2^3 \sin \delta_2 l [\cosh \delta_1 l - \cosh \delta_1(2a-l)] \} \quad (2.51)$$

$$f_5 = -\delta_1 \delta_2 (\cosh \delta_1 a - \cos \delta_2 a) \{ 2 \delta_1 \delta_2 [\cosh \delta_1(a-l) \cos \delta_2(a-l) - 1] - (\delta_1^2 + \delta_2^2) \sinh \delta_1(a-l) \sin \delta_2(a-l) \} \quad (2.52)$$

$$f_6 = -EI \delta_1 \delta_2 (\delta_1^2 + \delta_2^2) [\cosh \delta_1(a-l) \cos \delta_2(a-l) (\delta_2 \sinh \delta_1 a + \delta_1 \sin \delta_2 a) + \delta_1 \cosh \delta_1(a-l) (\cosh \delta_1 a - \cos \delta_2 a) \\ \times \sin \delta_2(a-l) - \delta_2 \sinh \delta_1 a - \delta_1 \sin \delta_2 a - \delta_2 \cos \delta_2(a-l) \sinh \delta_1(a-l) (\cosh \delta_1 a - \delta_2 \cos \delta_2 a) - \sinh \delta_1(a-l) \\ \times \sin \delta_2(a-l) (\delta_1 \sinh \delta_1 a - \delta_2 \sin \delta_2 a)] \quad (2.53)$$

$$f_7 = -\delta_2 \{ 2 \delta_1 \delta_2 [\cosh(\delta_1 a) \cos(\delta_2 a) - 1] - (\delta_1^2 - \delta_2^2) \sinh(\delta_1 a) \sin(\delta_2 a) \} \times [\delta_2 \cosh \delta_1(a-l) \sin \delta_2(a-l) + \delta_1 \\ \times \cos \delta_2(a-l) \sinh \delta_1(a-l)] \quad (2.54)$$

$$f_8 = -\delta_2 EI (\delta_1^2 + \delta_2^2) \{ \delta_1 \delta_2 \cosh \delta_1(a-l) \cosh \delta_1 a [\cos \delta_2(a-l) \cos \delta_2 a + \sin \delta_2(a-l) \sin \delta_2 a] + \delta_2^2 \cosh \delta_1(a-l) \\ \times \sinh \delta_1 a [\cos \delta_2(a-l) \sin \delta_2 a - \sin \delta_2(a-l) \cos \delta_2 a] + \delta_1^2 \sinh \delta_1(a-l) \cosh \delta_1 a [\cos \delta_2(a-l) \sin \delta_2 a - \cos \delta_2 a \\ \times \sin \delta_2(a-l)] + \delta_1^2 [\sinh \delta_1(a-l) \sin \delta_2(a-l) - \sinh \delta_1 a \sin \delta_2 a] - \delta_1 \delta_2 \sinh \delta_1(a-l) \sinh \delta_1 a [\cos \delta_2(a-l) \\ \times \cos \delta_2 a + \sin \delta_2(a-l) \sin \delta_2 a] - \delta_1 \delta_2 [\cosh \delta_1(a-l) \cos \delta_2(a-l) - \cosh \delta_1 a \cos \delta_2 a + 1] \} \quad (2.55)$$

$$f_9 = \delta_2 \{ (\delta_1^2 - \delta_2^2) \sinh(\delta_1 a) \sin(\delta_2 a) - 2 \delta_1 \delta_2 [\cosh(\delta_1 a) \cos(\delta_2 a) - 1] \} \times [\delta_1 \cosh \delta_1(a-l) \cos \delta_2(a-l) - \delta_1 \\ + \delta_2 \sin \delta_2(a-l) \sinh \delta_1(a-l)] \quad (2.56)$$

$$f_{10} = -(\delta_1^2 + \delta_2^2) \{ \delta_1 \delta_2 \cosh \delta_1(a-l) \sinh(\delta_1 a) [\cos \delta_2(a-l) \cos(\delta_2 a) + \sin \delta_2 a \sin \delta_2(a-l)] - \delta_1^2 \cosh \delta_1(a-l) \\ \times \cosh \delta_1 a [\cos \delta_2(a-l) \sin \delta_2 a - \sin \delta_2(a-l) \cos \delta_2 a] - \delta_1^2 [\cosh \delta_1(a-l) \sin \delta_2(a-l) + \sin \delta_2 a \cosh \delta_1 a] \\ - \delta_2^2 \sinh \delta_1(a-l) \sinh \delta_1 a [\cos \delta_2(a-l) \sin \delta_2 a - \sin \delta_2(a-l) \cos \delta_2 a] - \delta_1 \delta_2 \sinh \delta_1(a-l) \cosh \delta_1 a \\ \times [\cos \delta_2(a-l) \cos \delta_2 a - \sin \delta_2 a \sin \delta_2(a-l)] + \delta_1 \delta_2 [\cos \delta_2(a-l) \sinh \delta_1(a-l) - \sinh \delta_1 a \cos \delta_2 a] \} EI \delta_2 \quad (2.57)$$

$$f_{11} = -\delta_1 \{ 2 \delta_1 \delta_2 [\cosh(\delta_1 a) \cos(\delta_2 a) - 1] - (\delta_1^2 - \delta_2^2) \sinh(\delta_1 a) \sin(\delta_2 a) \} [\delta_2 \cosh \delta_1(a-l) \sin \delta_2(a-l) \\ + \delta_1 \cos \delta_2(a-l) \sinh \delta_1(a-l)] \quad (2.58)$$

$$f_{12} = EI \delta_1 (\delta_1^2 + \delta_2^2) \{ \delta_1 \delta_2 \cosh \delta_1(a-l) \cosh \delta_1 a [\cos \delta_2(a-l) + \sin \delta_2(a-l) \sin \delta_2 a] - \delta_2^2 \cos \delta_2(a-l) \sin \delta_2 a \\ \times [\cosh \delta_1(a-l) \sinh \delta_1 a - \cosh \delta_1 a \sinh \delta_1(a-l)] - \delta_2^2 \sin \delta_2(a-l) \cos \delta_2 a [\cosh \delta_1(a-l) \sinh \delta_1 a + \cosh \delta_1 a \\ \times \sinh \delta_1(a-l)] - \delta_1 \delta_2 \sinh \delta_1(a-l) \sinh \delta_1 a [\cos \delta_2(a-l) \cos \delta_2 a + \sin \delta_2(a-l) \sin \delta_2 a] - \delta_1 \delta_2 [-\delta_1 \delta_2 \\ \times \cosh \delta_1 a \cos \delta_2 a + \cosh \delta_1(a-l) \cos \delta_2(a-l) + 1] - \delta_2^2 [\sinh \delta_1(a-l) \sin \delta_2(a-l) - \sinh \delta_1 a \sin \delta_2 a] \} \quad (2.59)$$

$$f_{13} = \frac{1}{2} (\delta_1^2 + \delta_2^2) \{ \delta_1^2 \delta_2 [4 \sinh \delta_1(a-l) \cos \delta_2(a-l) - 4 \cos(\delta_2 a) \sinh(\delta_1 a) + 3 \cos(\delta_2 l) \sinh(\delta_1 l) + \cos \delta_2(2a-l) \\ \times \sinh \delta_1 l] - \delta_1 \delta_2^2 [4 \sin(\delta_2 a) \cosh(\delta_1 a) - 3 \sin(\delta_2 l) \cosh(\delta_1 l) - 4 \cosh \delta_1(a-l) \sin \delta_2(a-l) - \cosh \delta_1(2a-l) \\ \times \sin \delta_2 l] + \delta_1^2 \sin \delta_2 l [\cosh \delta_1(2a-l) - \cosh \delta_1 l] - \delta_2^3 \sinh \delta_1 l [\cos \delta_2 l - \cos \delta_2(2a-l)] \} \quad (2.60)$$

## CHAPTER 3. DEVELOPMENT OF UNIVERSAL DAMPING CURVE FOR DESIGN OF CABLE DAMPING WITH DAMPER

This chapter proposes a universal damping curve for the design of cable damping with dampers. A cable model is proposed which accounts for uncertain boundary conditions at cable ends. The formulation of damping is then derived using asymptotic solution. By grouping cable-damper parameters, the universal damping curve is rationally established in which the cable-damper parameters like cable bending stiffness, boundary conditions at cable ends (hinged, fixed or restraint ends), damper stiffness, damper support stiffness and added negative stiffness are incorporated into a single curve. The unique proposed curve is independent of any influencing parameter. Additionally, the design examples are illustrated, and the results indicated that the proposed universal damping curve is useful in the design of a cable damping, especially targeting multi-mode vibration.

### 3.1. Introduction

Cables in cable-stayed bridges have very low intrinsic damping.<sup>9,12,26</sup> The amount of this inherent damping ratio<sup>1,2,9,45</sup> is typically in the order of 0.01% – 0.20% that triggers the susceptibility of cables to unwanted vibrations, such as rain-wind induced vibration, vortex excitation and dry inclined cable galloping. Among the above vibration types, rain-wind induced vibration, which is caused by the simultaneous combination between wind and rain, is the most documented in field observations (95% of the reported cases)<sup>9,45</sup>.

In the design of a stay cable under wind excitation, a modal damping ratio of around 0.5 % to 1.0 %, which is equivalent to a Scruton number of at least 10, is often required to suppress or mitigate extreme vibrations.<sup>11,46</sup> Since the intrinsic damping of cables is far lower than the required damping, dampers are often mounted to cables to generate the added damping. Although several dampers have been introduced, viscous damper (VD) and High Damping Rubber (HDR) damper types are commonly adopted in many cable-stayed bridges, especially in Japan. For instance, when Fujino et al.<sup>9</sup> summarized Japanese experiences on the countermeasures of cable vibrations (e.g., dampers, cross ties, spacer, and aerodynamic treatments) in 47 cable-stayed bridges, there were around 20/47 and 13/47 of bridges adopting HDR dampers and viscous dampers, respectively.

For cables with viscous damper, the universal damping curve was introduced by Pacheco et al.<sup>12</sup> for the first time by the numerical complex eigenvalue analysis. This universal curve of damping has been proving the effectiveness and capability in: (1) the design of a damper (damping coefficient, damper location) under a required amount of added damping ratio; (2) the estimation of the added damping in an actual cable with an existing damper. In addition to the numerical analysis, Krenk<sup>13</sup> proposed a universal damping curve by an asymptotic solution, which was similar in the shape and mathematical format to the curve presented by Pacheco et al.<sup>12</sup> These curves of damping, however, were originally developed for an ideal nonflexural cable (taut-string cable) with a traditional viscous damper and ignored several influencing factors such as cable bending stiffness, restraints at cable ends, damper stiffness, damper support stiffness and added negative stiffness. Some researchers have turned their attention to more realistic cable-damper models that took some of these factors into account. Fujino and Hoang<sup>18</sup> proposed a formulation of the modal damping ratio for a fixed-fixed end cable, in which cable sag, cable bending stiffness and damper support stiffness were considered. Le et al.<sup>29</sup> investigated the impact of rotational restraint at a damper location on the reduction of the added damping. Also, the adverse effects of damper support stiffness and/or damper stiffness on damper performance have been pointed out in several published works.<sup>39,41-43</sup> To sum up, although some damping formulations have been proposed to improve one derived from taut-string cable, the universal damping curve which accounts for these influencing factors has not been previously discussed, to the best of our knowledge.

For cables with HDR dampers, several advantages over viscous dampers have been mentioned in the past,<sup>47,48</sup> e.g., it raises nearly equal damping in all directions, reducing additional stress sparked by live load, the independence of vibration modes, temperature stability, aesthetics, and easy maintenance. Cu and Han<sup>49</sup> derived an asymptotic form of the attainable damping contributed by an HDR damper to a taut-string cable while Fujino and Hoang<sup>18</sup> accounted for the effects of cable bending stiffness, cable sag and support stiffness on the added damping. The combined benefits of a viscous damper and an HDR damper was also investigated.<sup>47,50</sup> recently. In the design of a cable with an HDR damper, a universal damping curve is still a question mark.

In this chapter, the universal damping curve for a stay cable with an HDR damper or a viscous damper is proposed. The proposed damping curve is unique and independent of any influencing factors such as cable properties, damper

characteristics, restraints at cable ends, damper stiffness, damper support stiffness and added negative stiffness.

### 3.2. Cable model

A schematic diagram of a cable with damper is depicted in Figure 3.1, which considers rotational restraint at cable ends. Assuming that the cable tension is much larger than its self-weight, cable sag is neglected in this analysis. The cable has a length  $l$ , tension  $H$ , mass per unit length  $m$ , and bending stiffness  $EI$ . The coordinate with  $x$  starts from the left end of the cable. Restraints at cable ends were assumed to be treated as the linear rotational springs with stiffness  $K_r$ .

In this present study, several types of HDR dampers and viscous dampers are considered as depicted in Figures 3.2 and 3.3, respectively. For a conventional HDR damper (Figure 3.2a), two intrinsic damper characteristics are the damper spring factor  $K$  and material loss factor  $\phi$ . When damper supports are not perfectly rigid, its support stiffness  $K_{vs}$  is added to the damper (Figures 3.2b and 3.2d). The negative stiffness HDR dampers (Figures 3.2c and 3.2d) are the equivalent models of the combination between a conventional HDR damper and negative stiffness devices such as pre-compressed springs; the equivalent negative stiffness is  $K_{NS}$ .

Figure 3.3 shows four viscous damper types which are a conventional viscous damper with damping coefficient  $c$ , viscous damper with damper support stiffness  $K_{vs}$ , viscous damper with damper stiffness  $K_{vp}$ , and viscous damper with both damper stiffness  $K_{vs}$  and damper support stiffness  $K_{vp}$ . Mathematically, a negative stiffness viscous damper is the case when  $K_{vp}$  takes negative values.<sup>19,23,43</sup>

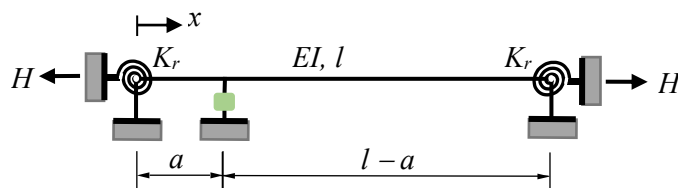


**FIGURE 3. 1.** Schematic diagram of a stay cable with a damper.

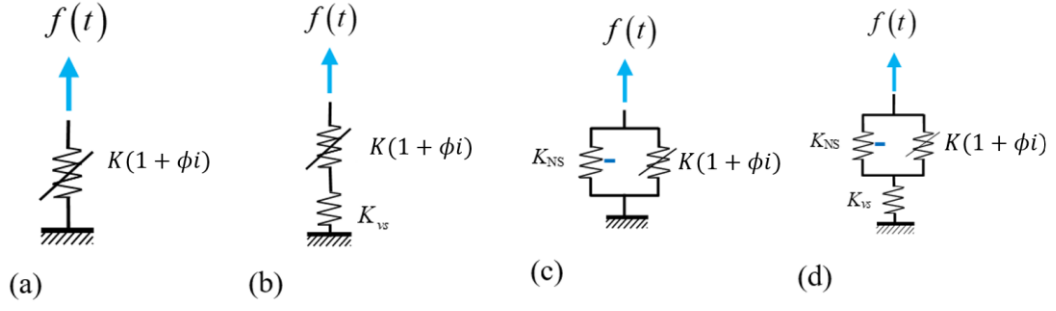


**FIGURE 3. 2.** HDR damper types: a) conventional HDR damper; b) HDR damper with damper support stiffness; c) negative stiffness HDR damper; and d) negative stiffness HDR damper with damper support stiffness.

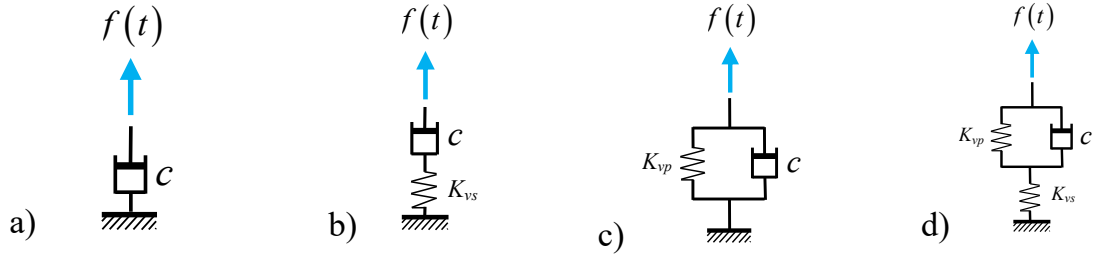


**FIGURE 3. 3.** Viscous damper types: a) conventional viscous damper; b) viscous damper with damper support stiffness; c) viscous damper with damper stiffness; and d) viscous damper with both damper stiffness and damper support stiffness.

### 3.3. Governing equation and eigenfrequency analysis

The governing equation of the in-plane motion in each cable segment,  $0 \leq x \leq a^-$  and  $a^+ \leq x \leq l$ , can be presented as

$$H \frac{\partial^2 v(x,t)}{\partial x^2} - EI \frac{\partial^4 v(x,t)}{\partial x^4} - m \frac{\partial^2 v(x,t)}{\partial t^2} = 0 \quad (3.1)$$

Since Eq. (3.1) describes the undamped free vibration of the cable, transverse displacement of the cable can be taken as a harmonic form with

$$v(x,t) = \tilde{v}(x)e^{oit} \quad (3.2)$$

where  $i^2 = -1$ ;  $\omega$  = complex natural frequency of the cable; and  $\tilde{v}(x)$  = cable mode shape.

The mode shape of each cable segment  $\tilde{v}_1(x)$  and  $\tilde{v}_2(x)$  can be obtained by solving the characteristic formulation of Eq. (3.1) which should be addressed after the substitution of the cable displacement from Eq. (3.2) into Eq. (3.1).

The first segment,  $0 \leq x \leq a$ :

$$\tilde{v}_1(x) = C_1 \sinh(\delta_1 x) + C_2 \cosh(\delta_1 x) + C_3 \sin(\delta_2 x) + C_4 \cos(\delta_2 x) \quad (3.3)$$

The second segment,  $a+ \leq x \leq l$ :

$$\tilde{v}_2(x) = C_5 \sinh \delta_1(x-a) + C_6 \cosh \delta_1(x-a) + C_7 \sin \delta_2(x-a) + C_8 \cos \delta_2(x-a) \quad (3.4)$$

where

$$\delta_{1,2} = \sqrt{\frac{\sqrt{1+4\eta l^2 \beta^2} \pm 1}{2\eta l^2}} \quad (3.5)$$

where  $\eta = EI/Hl^2$  characterizes the nondimensional parameter of cable bending stiffness; and  $\beta = \omega\sqrt{m/H}$  is the wave number.

The constants from  $C_1$  to  $C_8$  are obtained by inserting the cable mode shapes from Eq. (3.3) and Eq. (3.4) into the boundary conditions at cable ends ( $x = 0$  and  $x = l$ ), and into the continuity conditions at the damper location  $x = a$  as the following expressions:

At  $x = 0$ :

$$\tilde{v}_1(0) = 0; \quad (3.6)$$

$$K_r \tilde{v}'_1(0) = EI \tilde{v}''_1(0) \quad (3.7)$$

At  $x = a$ :

$$\tilde{v}_1(a^-) = \tilde{v}_2(a^+) = \tilde{v}_a; \quad \tilde{v}'_1(a^-) = \tilde{v}'_2(a^+); \quad EI \tilde{v}''_1(a^-) = EI \tilde{v}''_2(a^+); \quad EI \tilde{v}''_1(a^-) - EI \tilde{v}''_2(a^+) = F_a \quad (3.8a-d)$$

At  $x = l$ :

$$\tilde{v}_2(l) = 0; \quad K_r \tilde{v}'_2(l) = -EI \tilde{v}''_2(l) \quad (3.9a,b)$$

Solving Eqs. From (3.6) to (3.9) except for Eq. (3.8d), yields the constants (from  $C_1$  to  $C_8$ ) of the cable mode shapes with respect to  $\tilde{v}_a$  (value of cable mode shape at damper location  $y = a$ ) as

$$C_1 = \frac{\tilde{v}_a(\Psi_1 K_r^2 + \Psi_2 K_r + \Psi_3)}{\Psi_4 K_r^2 + \Psi_5 K_r + \Psi_6}; \quad C_2 = \frac{\tilde{v}_a(\Psi_7 K_r^2 + \Psi_8 K_r)}{\Psi_4 K_r^2 + \Psi_5 K_r + \Psi_6} \quad (3.10a,b)$$

$$C_3 = \frac{\tilde{v}_a(\Psi_9 K_r^2 + \Psi_{10} K_r + \Psi_{11})}{\Psi_4 K_r^2 + \Psi_5 K_r + \Psi_6}; \quad C_4 = -\frac{\tilde{v}_a(\Psi_7 K_r^2 + \Psi_8 K_r)}{\Psi_4 K_r^2 + \Psi_5 K_r + \Psi_6} \quad (3.10c,d)$$



$$C_5 = \frac{\tilde{v}_a(\Psi_{12}K_r^2 + \Psi_{13}K_r + \Psi_{14})}{\Psi_4K_r^2 + \Psi_5K_r + \Psi_6}; \quad C_6 = \frac{\tilde{v}_a(\Psi_{15}K_r^2 + \Psi_{16}K_r + \Psi_{17})}{\Psi_4K_r^2 + \Psi_5K_r + \Psi_6} \quad (3.10e,f)$$

$$C_7 = \frac{\tilde{v}_a(\Psi_{18}K_r^2 + \Psi_{19}K_r + \Psi_{20})}{\Psi_4K_r^2 + \Psi_5K_r + \Psi_6}; \quad C_8 = \tilde{v}_a - \frac{\tilde{v}_a(\Psi_{15}K_r^2 + \Psi_{16}K_r + \Psi_{17})}{\Psi_4K_r^2 + \Psi_5K_r + \Psi_6} \quad (3.10g,h)$$

Details of the functions from  $\Psi_1$  to  $\Psi_{20}$  are referred to the Appendix; and  $F_a =$  damper force. After having the above constants, the substitution of the determined mode shapes  $\tilde{v}_1(x)$  and  $\tilde{v}_2(x)$  into Eq. (3.8d) results in the eigenfrequency formulation as

$$\frac{\Psi_{21}K_r^2 + \Psi_{22}K_r + \Psi_{23}}{2(\Psi_4K_r^2 + \Psi_5K_r + \Psi_6)} = \frac{F_a}{\tilde{v}_a EI} \quad (3.11)$$

where

$$\Psi_{21} = 2\delta_1\delta_2(\delta_1^2 + \delta_2^2)\{2\delta_1\delta_2[1 - \cos(\delta_2l)\cosh(\delta_1l)] + (\delta_1^2 - \delta_2^2)\sin(\delta_2l)\sinh(\delta_1l)\} \quad (3.12)$$

$$\Psi_{22} = 4EI\delta_1\delta_2(\delta_1^2 + \delta_2^2)[\delta_1\sin(\delta_2l)\cosh(\delta_1l) - \delta_2\cos(\delta_2l)\sinh(\delta_1l)] \quad (3.13)$$

$$\Psi_{23} = 2EI^2\delta_1\delta_2(\delta_1^2 + \delta_2^2)^3\sin(\delta_2l)\sinh(\delta_1l) \quad (3.14)$$

For a cable with a fixed boundaries at cable ends,  $K_r \rightarrow \infty$ , the left-hand side of Eq. (3.11) becomes  $\Psi_{21}/(2\Psi_4)$ , and this fraction is exactly the same as the formula of the eigenfrequency proposed by Hoang and Fujino<sup>17</sup>. This form of the eigenfrequencies is implicit, transcendental and quite cumbersome. This study, on the other hand, focuses on an explicit form of the cable damping, hence an asymptotic solution will be applied to approximate such transcendental terms of Eq. (3.11), and to derive the formulation of the attainable damping ratio.

### 3.4. Attainable cable damping

In the presence of the damper, the natural frequencies of the cable become complex numbers. The complex natural frequencies  $\omega_n$  can be presented through the cable damping ratio  $\xi_n$  and its frequency magnitude  $|\omega_n|$  (Krenk<sup>13</sup>). The damping ratio, then, can be deduced from the imaginary part of the complex frequencies as

$$\xi_n = \frac{\text{Im}[\omega_n]}{|\omega_n|} \quad (3.15)$$

In principle,  $\omega_n$  is directly derived from Eq. (3.11). However, Eq. (3.11) is transcendental as mentioned, the direct establishment of the attainable cable damping

from Eq. (3.11) is challenging. To alleviate this, an asymptotic solution is properly applied to simplify Eq. (3.11) and derive the complex circular frequencies  $\omega_n$ . The asymptotic solution employed herein assumes that the perturbation of the wave number  $\Delta\beta_n$  between a bending-stiff cable with a damper ( $\beta_n = \omega_n\sqrt{m/H}$ ) and a taut string without a damper ( $\beta_m = n\pi/l$ ) is small (Hoang and Fujino<sup>17</sup>). Practically, a damper is commonly installed near the cable end; therefore,  $a/l \ll 1$ . Regarding cable bending stiffness, 95 % of stay cables have  $\eta < 1 \times 10^{-4}$  as reported by Mehrabi and Tabatabai<sup>16</sup>. Based on the previous features, the following approximations have been made (Hoang and Fujino<sup>17</sup>).

$$\tan(\beta_n l) \cong \beta_n l - n\pi; \quad (3.16)$$

$$\cos(\beta_n a) \cong 1; \quad (3.17)$$

$$\sin(\beta_n a) \cong \beta_n a \quad (3.18)$$

$$\delta_1 \cong \frac{1}{\sqrt{\eta l}}; \quad (3.19)$$

$$\delta_2 \cong \beta_n; \quad (3.20)$$

$$\sinh \delta_1 l \gg 1 \quad (3.21)$$

$$\delta_1^2 + \delta_2^2 \cong \delta_1^2 - \delta_2^2 = \frac{1}{\eta l^2} \quad (3.22)$$

$$\sinh \delta_1(a-l) = -\cosh \delta_1(a-l) \cong -e^{-r} \sinh \delta_1 l \quad (3.23)$$

$$\sinh \delta_1(2a-l) = -\cosh \delta_1(2a-l) \cong -e^{-2r} \sinh \delta_1 l \quad (3.24)$$

Substitution of the above approximations into Eq. (3.11), then combining this with Eq. (3.15) results in the formulation of the modal damping ratio as

$$\frac{\xi_n}{(a/l)} = \text{Im} \left\{ \frac{\left[ \frac{2}{r} + \frac{F_a a}{H\tilde{V}_a} \left( 1 - \frac{2}{r^2} + \frac{2+2r}{r^2 e^r} \right) \right] K_r^2 + \Psi_{24} K_r + \Psi_{25}}{\left[ 1 + \frac{F_a a}{H\tilde{V}_a} \left( 1 - \frac{3}{2r} - \frac{1-4e^r}{2re^{2r}} \right) \right] K_r^2 + \Psi_{26} K_r + \Psi_{27}} \right\} \quad (3.25)$$

where

$$\Psi_{24} = \left[ \frac{2Ha}{r^2} + \left( \frac{F_a a^2}{\tilde{V}_a r^3} \right) \left( \frac{1+2re^r}{e^{2r}} + 2r^2 - 1 \right) \right]; \quad (3.26)$$

$$\Psi_{25} = \left( \frac{2rF_a}{\tilde{v}_a} \right) \left( \frac{Ha^3}{2r^3} \right) \quad (3.27)$$

$$\Psi_{26} = \left[ \frac{2aH}{r} - \frac{2a^2F_a}{\tilde{v}_ar^2} \left( 1 - \frac{re^r + 1}{e^r} \right) \right]; \quad (3.28)$$

$$\Psi_{27} = \left( \frac{Ha^3}{2r^3} \right) \left[ \frac{2rH}{a} + \frac{F_a}{\tilde{v}_a} \left( \frac{1 - e^{2r}}{e^{2r}} + 2r \right) \right] \quad (3.29)$$

and  $r = a / (l\sqrt{\eta})$ , a nondimensional parameter of the damper location.

**TABLE 3. 1.** Damper force component  $F_a$  of the dampers

No.	Damper types	Damper force component $F_a$	References
1	Conventional HDR damper	$F_a = K(1 + \phi i)\tilde{v}_a$	Figure 3.2a
2	HDR damper with damper support stiffness	$F_a = \frac{K_{vs}K(1 + \phi i)}{K_{vs} + K(1 + \phi i)}\tilde{v}_a$	Figure 3.2b
3	Negative stiffness HDR damper	$F_a = K(1 + K_{NS}/K)(1 + \frac{\phi}{1 + K_{NS}/K}i)\tilde{v}_a$	Figure 3.2c
4	Negative stiffness HDR damper with damper support stiffness	$F_a = \frac{K_{vs}K(1 + K_{NS}/K)(1 + \frac{\phi}{1 + K_{NS}/K}i)}{K_{vs} + K(1 + K_{NS}/K)(1 + \frac{\phi}{1 + K_{NS}/K}i)}\tilde{v}_a$	Figure 3.2d
5	Conventional viscous damper	$F_a = ci\omega\tilde{v}_a$	Figure 3.3a
6	Viscous damper with damper support stiffness	$F_a = \frac{i\omega}{(i\omega/K_{vs} + 1/c)}\tilde{v}_a$	Figure 3.3b
7	Viscous damper with damper stiffness	$F_a = (K_{vp} + ci\omega)\tilde{v}_a$	Figure 3.3c
8	Viscous damper with both damper stiffness and damper support stiffness	$F_a = \frac{(K_{vp} + ci\omega)K_{vs}}{(K_{vp} + ci\omega) + K_{vs}}\tilde{v}_a$	Figure 3.3d

Note:  $i^2 = -1$ ; and  $\omega$  is the natural circular frequency.

Since Eq. (3.25) presents the added damping of a cable model with the rotational restraint ends, it covers the cases of hinged-hinged or fixed-fixed ends by approaching  $K_r$  to 0 or  $\infty$ , respectively. Therefore, it is easy to verify that when  $K_r \rightarrow \infty$  (fixed ends), taking the limitation of the right-hand side section of Eq. (3.25) results in the eliminations of the last two terms in both the numerator and denominator. Therefore,

the remaining parts inside the square brackets are the same as the formulation of the modal damping ratio derived by Hoang and Fujino<sup>17</sup> for a fixed-fixed cable.

Based on Eq. (3.25), the universal damping curve will be developed. It is noted that different types of dampers in Figures 3.2 and 3.3 leads to different damper force  $F_a$ . The force component  $F_a$  of the dampers is derived through the force equilibrium equations, displacement compatibility, and force-displacement relationships between cable and damper. Table 3.1 summarizes the damper force component  $F_a$  with respect to each given damper.

### 3.5. Propose universal damping curve for design of cable damping

#### 3.5.1. Universal damping curve for cable with HDR damper

The case of the negative stiffness HDR damper with damper support stiffness as in Figure 3.2d mathematically covers the three remaining cases. Hence, the universal damping curve for this damper will be proposed, so the remaining ones (Figures 3.2a-3.2c) can be easily deduced. The force component  $F_a$  of this damper is taken from Table 3.1 as

$$F_a = \frac{K_{vs}K(1+K_{NS}/K)(1+\frac{\phi}{1+K_{NS}/K}i)}{K_{vs}+K(1+K_{NS}/K)(1+\frac{\phi}{1+K_{NS}/K}i)}\tilde{v}_a \quad (3.30)$$

Inserting damper force  $F_a$  from Eq. (3.30) into Eq. (3.25), the modal damping ratio can be obtained as

$$\frac{\xi_n}{(a/l)} = R_1R_2R_3\frac{\eta_1\eta_2\eta_3\phi\bar{K}}{(1+\eta_1\eta_2\eta_3\bar{K})^2+(\eta_1\eta_2\eta_3\phi\bar{K})^2} \quad (3.31)$$

Maximum modal damping ratio and its optimal damper coefficient

$$\frac{\xi_n}{(a/l)} = 0.5R_1R_2R_3R_\phi \text{ at } \bar{K}_{opt} = \frac{1}{\eta_1\eta_2\eta_3\eta_\phi} \quad (3.32)$$

where  $R_\phi = \phi/(1+\sqrt{1+\phi^2})$ ;  $\eta_\phi = \sqrt{1+\phi^2}$ ;  $\bar{K} = Ka/H$  is the dimensionless parameter of  $K$ ; and  $(R_1, \eta_1)$ ,  $(R_2, \eta_2)$  and  $(R_3, \eta_3)$  are modification factors of the damping ratio due to rotational restraints at cable ends, damper support stiffness and negative stiffness, respectively.

Modification factors  $(R_1, \eta_1)$  due to rotational restraints  $K_r$  at the cable ends

$$R_1 = \frac{(1-q)^2 \bar{K}_r^2 + \frac{2(1-q)}{r} \bar{K}_r + \frac{1}{r^2}}{\left(1-q - \frac{1}{2}rq^2\right) \bar{K}_r^2 + \frac{2(1-q)}{r} \bar{K}_r + \left(1-q + \frac{1}{2}rq^2\right) \frac{1}{r^2}} \quad (3.33)$$

and

$$\eta_1 = \frac{\left(1-q - \frac{1}{2}rq^2\right) \bar{K}_r + \left(1-q + \frac{1}{2}rq^2\right) \frac{1}{r}}{\bar{K}_r + \frac{1}{r}} \quad (3.34)$$

where  $q = (1 - e^{-r})/r$  is intermediate parameter of  $\eta$ ; and  $\bar{K}_r = K_r/(Ha)$  is the dimensionless stiffness of  $K_r$ .

Modification factors ( $R_2$ ,  $\eta_2$ ) due to damper support stiffness  $K_{vs}$

$$R_2 = \frac{\bar{K}_{vs} \eta_1}{1 + \bar{K}_{vs} \eta_1} \quad \text{and} \quad \eta_2 = 1 + \frac{1}{\bar{K}_{vs} \eta_1} \quad (3.35a,b)$$

where  $\bar{K}_{vs} = (K_{vs} \times a)/H$  is the dimensionless stiffness of  $K_{vs}$ .

Modification factors ( $R_3$ ,  $\eta_3$ ) due to negative stiffness  $K_{NS}$

$$R_3 = \frac{1}{1 + \eta_1 \eta_2 \bar{K}_{NS}} \quad \text{and} \quad \eta_3 = \frac{1}{1 + \eta_1 \eta_2 \bar{K}_{NS}} \quad (3.36a,b)$$

where  $\bar{K}_{NS} = (K_{NS} \times a)/H$  is the dimensionless stiffness of  $K_{NS}$ . Although  $R_3$  and  $\eta_3$  mathematically takes the same form, we set two different symbols because  $R_3$  is the modification factor of optimal damping whereas  $\eta_3$  is the modification factor of damper coefficient.

The modification factors ( $R_1$ ,  $\eta_1$ ), ( $R_2$ ,  $\eta_2$ ) and ( $R_3$ ,  $\eta_3$ ) in Eq. (3.32) can be explained as: the damping ratio  $\xi$  and the optimal damper coefficient  $\bar{K}_{opt}$  will be modified in comparison with a conventional case. The conventional case is the case of a nonflexural cable ( $\eta = 0$  and  $K_r = 0$ ) with a conventional HDR damper ( $K_{NS} = 0$ ) and rigid damper support ( $K_{vs} \rightarrow \infty$ ); it makes  $R_1 = \eta_1 = R_2 = \eta_2 = R_3 = \eta_3 = 1$  according to Eq. (3.33), Eq. (3.34), Eq. (3.35) and Eq. (3.36). In the conventional case, Eq. (3.31) is the same the damping ratio formulation introduced by Cu and Han<sup>49</sup>. When cable includes bending stiffness ( $\eta \neq 0$ ) together with rotational restraints at cable ends ( $K_r \neq 0$ ), the damping ratio  $\xi$  and the optimal damper coefficient  $\bar{K}_{opt}$  are modified by the factors  $R_1$  and  $\eta_1$ , respectively. Similarly, if damper consists of damper support stiffness ( $K_{vs} > 0$ ),  $\xi$  and  $\bar{K}_{opt}$  are then modified by the factors  $R_2$  and  $\eta_2$ , correspondingly. Also, if damper includes negative stiffness

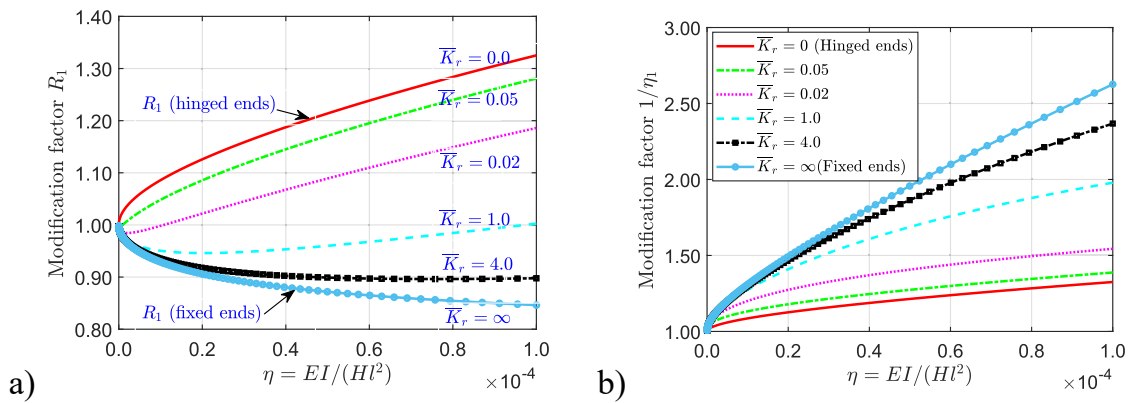
( $K_{NS} < 0$ ),  $\xi$  and  $\bar{K}_{opt}$  are further modified by the factors  $R_3$  and  $\eta_3$ , respectively. Table 3.2 summarizes factors of Eq. (3.32)

**TABLE 3. 2.** Factors of the modal damping ratio and optimal damper coefficient for HDR damper

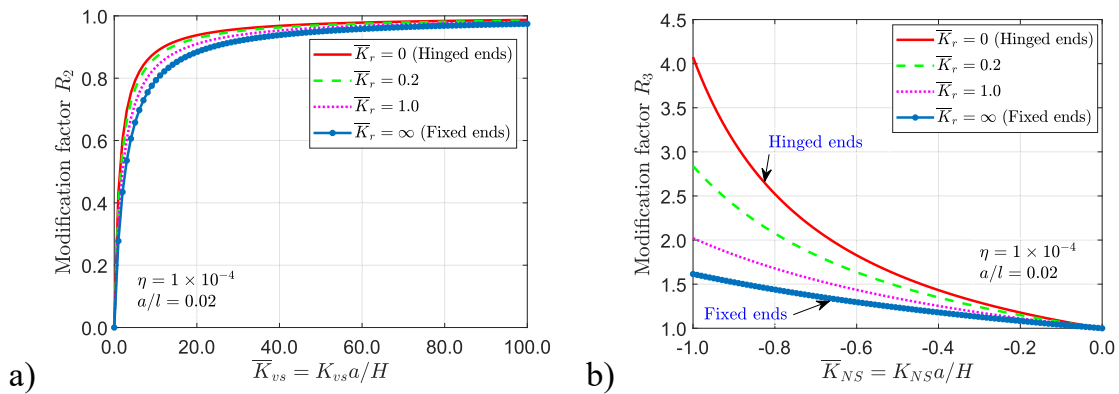
No.	HDR damper types	Factors in Eq. (3.32)	References
1	Conventional HDR damper ( $K_{vs} \rightarrow \infty, K_{NS} = 0$ )	$R_1$ (Eq. 3.33); $\eta_1$ (Eq. 3.34); $R_2 = \eta_2 = 1$ ; $R_3 = \eta_3 = 1$ .	Figure 3.2a
2	HDR damper with damper support stiffness ( $K_{vs} > 0, K_{NS} = 0$ )	$R_1$ (Eq. 3.33); $\eta_1$ (Eq. 3.34); $R_2$ and $\eta_2$ (Eq. 3.35a,b); $R_3 = \eta_3 = 1$ .	Figure 3.2b
3	Negative stiffness HDR damper ( $K_{NS} < 0, K_{vs} \rightarrow \infty$ )	$R_1$ (Eq. 3.33); $\eta_1$ (Eq. 3.34); $R_2 = \eta_2 = 1$ ; $R_3$ and $\eta_3$ (Eq. 3.36a,b).	Figure 3.2c
4	Negative stiffness HDR damper with damper support stiffness ( $K_{NS} < 0, K_{vs} > 0$ )	$R_1$ (Eq. 3.33); $\eta_1$ (Eq. 3.34); $R_2$ and $\eta_2$ (Eq. 3.35a,b); $R_3$ and $\eta_3$ (Eq. 3.36a,b).	Figure 3.2d

Figure 3.4a shows the modification factor of damping  $R_1$  due to rotational restraint at cable ends. For the fixed-fixed end,  $R_1$  is always  $< 1$  regardless of small or large cable bending stiffness, hence bending stiffness triggers reduction of damping which was noted by Fujino and Hoang<sup>18</sup>. In contrast, for the hinged-hinged cable,  $R_1$  is always  $> 1$  such that cable gains more added damping from a damper. For a cable with the rotational restraint ends,  $R_1$  varies between fixed-fixed end cable and hinged-hinged end cable. Consequently, a damper will work more effectively or less effectively relying on the fixity degree of the supports and cable bending stiffness values. More importantly, the difference in term of the maximum modal damping between hinged end and fixed end is also significant, especially cable with large bending stiffness. For instance,  $\frac{R_1(hinged) - R_1(fixed)}{R_1(hinged)} \times 100 \approx 37\%$  when  $\eta = 1 \times 10^{-4}$ . It is noted that the cable bending stiffness  $\eta < 1 \times 10^{-4}$  covers 95 % of stay cables (Mehrabi and Tabatabai<sup>16</sup>). In addition, short cables often have large bending stiffness parameter; therefore, design of the damper system for short cables, if required, should seriously consider the boundary conditions at cable ends.

Figure 3.4b demonstrates the modification factors of the optimal damper coefficient  $1/\eta_l$ . The modification here means that adjustment of the optimal damping coefficient was made against that value of the taut-string cable. Since these factors are always greater than 1, the peak of the modal damping curve will always be shifted to the right-hand side of the corresponding peak of a taut string. It is pointed out that the increase in cable bending stiffness (increase  $\eta$ ) leads to an increase of the optimal damper coefficient, and this increase is much larger for the fixed ends case.



**FIGURE 3. 4.** Modification factor of damping due to restraint at cable ends ( $a/l = 0.02$ ).



**FIGURE 3. 5.** Modification factor of damping due to damper support stiffness  $R_2$ , and due to negative stiffness damper  $R_3$ .

Figure 3.5 illustrates the modification of damping due to damper support stiffness as well as negative stiffness. Overall, damper support stiffness poses the reduction of

damping since the factor  $R_2$  is always  $< 1$  (in Figure 3.5 a); this remark was already mentioned in Chapter 2. In contrast, Figure 3.5b indicates that  $R_3$  is always  $> 1$ , and it means that negative stiffness could provide higher damping to cable compared to conventional damper (without negative stiffness  $K_{NS} = 0$ ).

Eq. (3.31) shows that the damping ratio depends heavily on several influencing factors such as cable properties, damper location  $a$ , boundary conditions at cable ends (fixed, hinged, or restraint ends), damper support stiffness  $K_{vs}$ , negative stiffness  $K_{NS}$  (if included) and loss factor of rubber material  $\phi$ . Figure 3.6 investigates the variations in the modal damping ratio versus influencing factors. As it appeared, higher material loss factor  $\phi$  results in higher added damping (Figure 3.6a); bending stiffness and damper support stiffness causes the reduction of added damping (Figures 3.6b and 3.6e, respectively); the damper location installed far from a cable end leads to higher optimal provided damping (Figures 3.6c); a cable with hinged ends gained more damping than fixed end counterparts (Figure 3.6d); and a negative stiffness damper ( $K_{NS} < 0$ ) generated superior damping to a cable than the conventional damper without negative stiffness (Figure 3.6f).

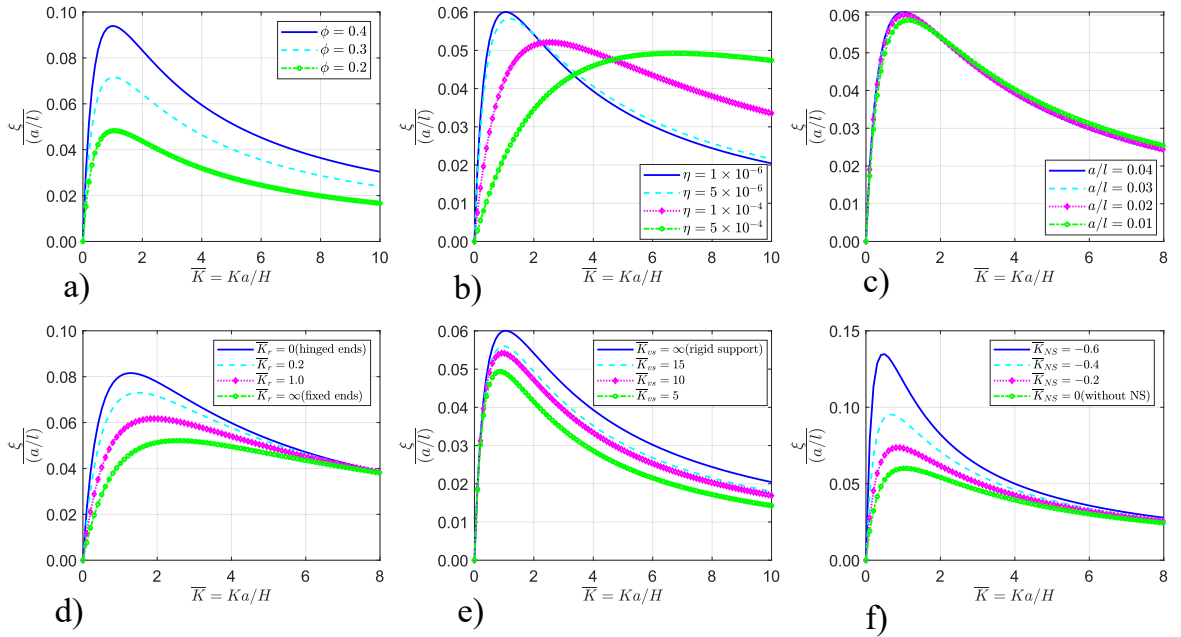


**FIGURE 3. 6.** Variations in modal damping ratio of HDR damper versus different factors: a) material loss factor  $\phi$  ( $\bar{K}_r = \infty$ ;  $\bar{K}_{vs} = \infty$ ;  $\bar{K}_{NS} = 0$ ;  $\eta = 1 \times 10^{-6}$ ;  $a/l = 0.02$ ) ; b) cable bending stiffness parameter  $\eta$  ( $\bar{K}_r = \infty$ ;  $\bar{K}_{vs} = \infty$ ;  $\bar{K}_{NS} = 0$ ;  $\phi = 0.25$ ;  $a/l = 0.02$ ) ; c) damper location  $a/l$  ( $\bar{K}_r = \infty$ ;  $\bar{K}_{vs} = \infty$ ;  $\bar{K}_{NS} = 0$ ;  $\phi = 0.25$ ;  $\eta = 1 \times 10^{-6}$ ) ; d) restraints at cable ends  $\bar{K}_r$  ( $\bar{K}_{vs} = \infty$ ;  $\bar{K}_{NS} = 0$ ;  $\eta = 1 \times$



$10^{-4}$ ;  $\phi = 0.25$ ;  $a/l = 0.02$ ); e) damper support stiffness  $\bar{K}_{vs}$  ( $\bar{K}_r = \infty$ ;  $\bar{K}_{NS} = 0$ ;  $\eta = 1 \times 10^{-6}$ ;  $\phi = 0.25$ ;  $a/l = 0.02$ ); and, f) negative stiffness  $\bar{K}_{NS}$  ( $\bar{K}_r = \infty$ ;  $\bar{K}_{vs} = \infty$ ;  $\eta = 1 \times 10^{-6}$ ;  $\phi = 0.25$ ;  $a/l = 0.02$ ).

Since the damping curve involves in various factors as illustrated in Figure 3.6, it might spark some difficulties in the design of cable-damper system. Therefore, it is useful to propose a single damping curve that is independent of those influencing factors. In this regard, Eq. (3.31) is reformed as

$$Y = \frac{(1 + \sqrt{1 + \phi^2})\sqrt{1 + \phi^2} X}{(\sqrt{1 + \phi^2} + X)^2 + (\phi X)^2} \quad (3.37)$$

in which  $X = K\left(\frac{a}{H}\right)\sqrt{1 + \phi^2}(\eta_1 \eta_2 \eta_3)$  and  $Y = \frac{\xi_n}{(a/l)R_1 R_2 R_3 R_\phi}$  are the horizontal and vertical axes of the damping curve, respectively.

Eq. (3.37) is derived by observing that the modal damping ratio in Eq. (3.31) and its optimal value in Eq. (3.32), then grouping Eq. (3.31) into a new version as Eq. (3.37). An interesting feature of Eq. (3.37) is that it always yields the maximum  $Y = 0.5$  at  $X = 1$  regardless of  $\phi$ ; therefore, Eq. (3.37) is simpler. However, it still includes the loss factor  $\phi$ . In fact, the High Damping Rubber (HDR) damper is commonly considered as an equivalent complex-stiffness model<sup>18,49</sup>, in which the complex modulus  $E$  is featured by the real component  $E^R$  (storage modulus) and the imaginary modulus  $E^I$  (loss modulus).<sup>49,51</sup> The loss factor  $\phi = E^I / E^R$ . According to some test results,  $\phi$  ranged from 0.12 to 0.18 for the natural rubber (NR60)<sup>52</sup>, from 0.30 to 0.41 for the butyl rubber (BR60)<sup>52</sup>, and around 0.67 for the neoprene rubber<sup>53</sup>. The loss factor  $\phi$  of HDR dampers used for the vibration control of cables of Shinminato Bridge in Japan was 0.62. To the best of our knowledge, commercial rubbers with the loss factor  $\phi < 1$  are widely manufactured and used.

Figure 3.7a plots damping curves by Eq. (3.37) with  $\phi$  varying from 0.1 to 0.9. These curves are then normalized into one practical universal damping curve in Figure 3.7b with a correlation of 99.99% on average.

The practical universal damping curve which is normalized from Eq. (3.37) with an average correlation of 99.99% is proposed as below

$$Y = \frac{2.299X}{(1.097 + X)^2 + 0.203X^2} \quad (3.38)$$

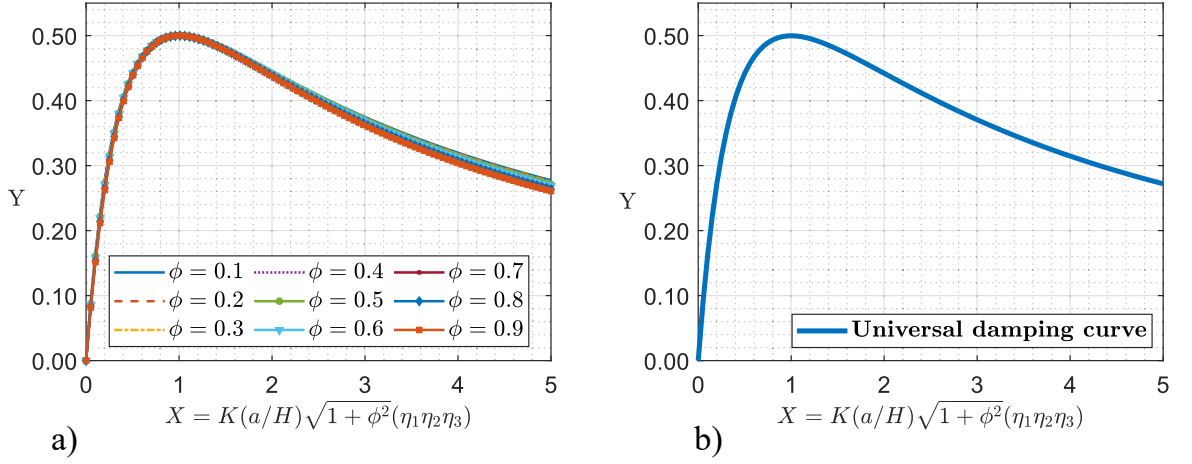


**FIGURE 3. 7.** Damping curve: a) by Eq. (3.37); and b) by the proposed universal curve.

This proposed universal damping curve for an HDR damper is unique and independent of any factors. The factors like cable properties, damper characteristics, damper location, restraints at cable ends, damper support stiffness and negative stiffness are incorporated into  $X$  and  $Y$  axes.

### 3.5.2. Universal damping curve for cable with viscous damper

There are four types of viscous dampers are considered as shown in Figure 3.3. The damper forces are given in Table 3.1. Since the case of a viscous damper with damper stiffness and damper support stiffness (Figure 3.3d) also covers the remaining cases, this type of damper will be used to derive the universal damping curve. The damper force is taken from Table 3.1 as

$$F_a = \frac{(K_{vp} + ci\omega)K_{vs}}{(K_{vp} + ci\omega) + K_{vs}} \tilde{v}_a \quad (3.39)$$

On making use of Eq. (3.39), the modal damping ratio  $\xi_n$  from Eq. (3.25) becomes

$$\frac{\xi_n}{(a/l)} = R_1 R_2 R_3 \frac{\eta_1 \eta_2 \eta_3 \bar{c}_n}{1 + (\eta_1 \eta_2 \eta_3 \bar{c}_n)^2} \quad (3.40)$$

where  $\bar{c}_n = \left(\frac{a}{l}\right) \frac{n\pi c}{\sqrt{Hm}}$ ; and  $n$  is the  $n^{th}$  vibration mode.

Maximum modal damping ratio and optimal damper coefficient

$$\frac{\xi_n}{(a/l)} = 0.5R_1R_2R_{3'}, \text{ at } \bar{c}_n^{opt} = \frac{1}{\eta_1\eta_2\eta_{3'}} \quad (3.41)$$

in which  $(R_1, \eta_1)$  and  $(R_2, \eta_2)$  are the modification factors of damping due to restraints at cable ends and damper support stiffness, respectively. These factors are defined in a previous section; and  $(R_{3'}, \eta_{3'})$  are the modification factors due to damper stiffness  $K_{vp}$ .

$$R_{3'} = \frac{1}{1 + \eta_1\eta_2\bar{K}_{vp}} \text{ and } \eta_{3'} = \frac{1}{1 + \eta_1\eta_2\bar{K}_{vp}} \quad (3.42a,b)$$

in which  $\bar{K}_{vp} = (K_{vp} \times a)/H$  is the dimensionless stiffness of  $K_{vp}$ . It is noted that  $R_{3'}$  and  $\eta_{3'}$  take the same formula, we use two different symbols because  $R_{3'}$  reflects the modification of the optimal damping ratio while  $\eta_{3'}$  presents the modification of the optimal damping coefficient.

Eq. (3.40) can be verified with previous publications. Case 1 is a nonflexural cable (taut-string cable) with a conventional viscous damper ( $\eta = 0, K_{vs} \rightarrow \infty, K_{vp} = 0$ ). They lead to  $R_1 = \eta_1 = 1, R_2 = \eta_2 = 1$ , and  $R_{3'} = \eta_{3'} = 1$ , respectively. In this case, Eq. (3.40) is the same as one proposed by Krenk<sup>13</sup>. Case 2 is a flexural cable with fixed ends and a viscous damper without damper stiffness ( $\eta \neq 0, K_r \rightarrow \infty, K_{vp} = 0$ ). These conditions result in the factors  $R_1 = (1 - q)^2/(1 - q - 0.5rq^2)$ ,  $\eta_1 = (1 - q - 0.5rq^2)$ , and  $R_{3'} = \eta_{3'} = 1$ . In this case, Eq. (3.40) becomes one introduced by Fujino and Hoang<sup>18</sup>. The factors  $(R_1; \eta_1; R_2; \eta_2; R_{3'}; \eta_{3'})$  in Eq. (3.40) and Eq. (3.41) mean the modification of the damping compared to the case 1. Table 3.4 summarizes the factors in Eq. (3.40).

By grouping components in Eq. (3.40), the universal damping curve for the viscous damper types is proposed in a simplest form as

$$Y = \frac{X}{1 + X^2} \quad (3.43)$$

where  $X = (\eta_1\eta_2\eta_{3'}) \left(\frac{a}{l}\right) \frac{n\pi c}{\sqrt{Hm}}$  and  $Y = \frac{\xi_n}{(a/l)R_1R_2R_{3'}}$  are the horizontal and vertical axes of the proposed universal damping curve, respectively.

Figure 3.8 shows the proposed universal curve. This universal damping curve is unique and independent of any influencing factors. The factors of damping such as damper location, cable properties, damping coefficient  $c$ , effects of damper support stiffness, damper support stiffness as well as boundary conditions at cable ends (hinged, fixed or restraint ends) only appear in  $X$  and  $Y$  axes.

**TABLE 3. 3.** Factors of the modal damping ratio and optimal damper coefficient for viscous damper types

No.	HDR damper types	Factors in Eq. (3.40)	References
1	Conventional viscous damper ( $K_{vs} \rightarrow \infty, K_{vp} = 0$ )	$R_1$ (Eq. 3.33); $\eta_1$ (Eq. 3.34); $R_2 = \eta_2 = 1$ ; $R_3 = \eta_3 = 1$ .	Figure 3.3a
2	Viscous damper with damper support stiffness ( $K_{vs} > 0, K_{vp} = 0$ )	$R_1$ (Eq. 3.33); $\eta_1$ (Eq. 3.34); $R_2$ and $\eta_2$ (Eq. 3.35a,b); $R_3 = \eta_3 = 1$ .	Figure 3.3b
3	Viscous damper with damper stiffness ( $K_{vs} \rightarrow \infty, K_{vp} > 0$ )	$R_1$ (Eq. 3.33); $\eta_1$ (Eq. 3.34); $R_2 = \eta_2 = 1$ ; $R_3$ and $\eta_3$ (Eq. 3.42a,b).	Figure 3.3c
4	Viscous damper with both damper support stiffness and damper stiffness ( $K_{vs} > 0, K_{vp} > 0$ )	$R_1$ (Eq. 3.33); $\eta_1$ (Eq. 3.34); $R_2$ and $\eta_2$ (Eq. 3.35a,b); $R_3$ and $\eta_3$ (Eq. 3.42a,b).	Figure 3.3d

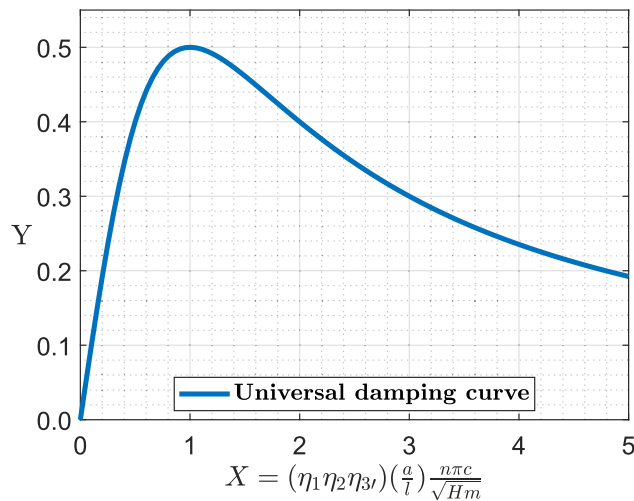


**FIGURE 3. 8.** Universal damping curve for viscous damper types.

### 3.6. Design example

#### 3.6.1. Single-mode vibration control

**Example 1:** This example illustrates the design of a HDR damper ( $K$  and  $\phi$ ) to suppress rain-wind induced vibration of a stay cable. The cable with  $l = 184.72$  m,  $H$

$= 3.55 \times 10^6 \text{ N}$ ,  $m = 60.2 \text{ kg/m}$ ,  $D = 0.12 \text{ m}$  (cable diameter),  $EI = 1.98 \times 10^6 \text{ N.m}^2$  is used. The air density  $\rho$  is set to be  $1.23 \text{ kg/m}^3$ .

According to the Post-Tensioning Institute Cable-Stayed Bridge Committee (PTI)<sup>11</sup>, the amount of an added damping ratio required to avoid rain-wind induced vibration is as

$$\frac{m\xi}{\rho D^2} \geq 10 \quad (3.44)$$

Inserting the cable properties into Eq. (3.44) results in  $\xi \geq 0.295 \%$ .

An HDR damper is supposed to attach to the cable at the location  $a = 5.85 \text{ m}$  from the cable end due to installation conditions. A couple of design conditions are as follows: the loss factor of rubbers  $\phi = 0.62$ ; the damper support is rigid ( $K_{vs} \rightarrow \infty$ ); negative stiffness is not added to the damper ( $K_{NS} = 0$ ); and cable ends are fixed ( $K_r \rightarrow \infty$ ). Based on these conditions,  $R_1 = 0.941$  from Eq. (3.33),  $\eta_1 = 0.809$  from Eq. (3.34),  $R_2 = \eta_2 = 1$  from Eq. (3.35), and  $R_3 = \eta_3 = 1$  from Eq. (3.36).

The ordinate on the  $Y$  axis of the universal damping curve as

$$Y = \frac{\xi}{(a/l)R_1R_2R_3R_\phi} = \frac{0.00295}{(5.85/184.72) \times 0.941 \times 1 \times 1 \times 0.285} = 0.347 \quad (3.45)$$

where  $R_\phi = \phi / (1 + \sqrt{1 + \phi^2}) = 0.285$ .

The line  $Y = 0.347$  crosses the universal curve of damping at two points  $A$  and  $B$  as can be seen in Figure 3.9. As a result, any point lying along the curve from  $A$  to  $B$  will yields damping higher than the required value.

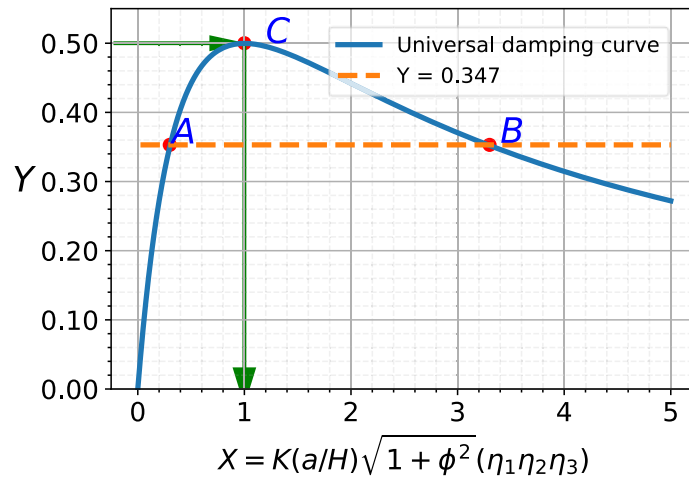


**FIGURE 3. 9.** Design HDR damper using the proposed universal damping curve.

In this scenario, the peak at point  $C(1.00; 0.50)$  is chosen for the design in this example because it poses the highest added damping ratio. From that, the spring factor  $K$  of the HDR damper is calculated as

$$K = \frac{X_c}{(a/H)\sqrt{1+\phi^2}(\eta_1\eta_2\eta_3)} = \frac{1}{(5.85/3.55 \times 10^6)\sqrt{1+0.62^2}(0.809 \times 1 \times 1)} = 637.52 \times 10^3 \text{ N/m} \quad (3.46)$$

In conclusions, an HDR damper is designed with  $\phi = 0.62$  and  $K = 637.52 \times 10^3$  N/m, and it can produce an added damping ratio  $\xi = Y_C \times (a/l) \times R_1 R_2 R_3 R_\phi \times 100 = 0.5 \times (5.85/184.72) \times 0.941 \times 1 \times 1 \times 0.285 \times 100 = 0.425 \%$ .

**Example 2:** This example presents the design of a viscous damper for a single-mode vibration control. Cable properties and the required added damping ratio ( $\xi > 0.295 \%$ ) presented in the Example 1 are used in this example. This example aims at designing a viscous damper (damping coefficient  $c$ ), which can generate the added damping to a cable larger than the required damping, and targeting a single vibration mode (e.g., mode 1).

The set of design conditions are as follows: cable ends are fixed ( $K_r \rightarrow \infty$ ); damper support is rigid ( $K_{vs} \rightarrow \infty$ ); damper stiffness  $K_{vp} = 202.34 \times 10^3$  N/m; and the damper is installed to the cable at damper location  $a = 5.85$  m due to installation restrictions.

In this example, the targeted vibration mode is the mode 1, and a viscous damper is designed to generate the optimal added damping ratio at the mode 1. The optimal point on the universal damping curve (Figure 3.8) is always at the peak, where  $(X_{opt}; Y_{opt}) = (1.0; 0.5)$ . The optimal damping coefficient  $c_{opt}$  as

$$c_{opt} = X_{opt} \frac{\sqrt{Hm}}{n\pi} \left( \frac{l}{a} \right) \left( \frac{1}{\eta_1\eta_2\eta_3} \right) = 1.0 \times \frac{\sqrt{3.55 \times 10^6 \times 60.2}}{1 \times \pi} \left( \frac{184.72}{5.85} \right) \left( \frac{1}{0.809 \times 1 \times 0.788} \right) = 2.306 \times 10^5 \text{ N.s.m}^{-1} \quad (3.47)$$

where  $n = 1$  because the mode 1 is assigned,  $\eta_1 = 0.809$  from Eq. (3.34),  $\eta_2 =$  from Eq. (3.35b), and  $\eta_3 = 0.788$  from Eq. (3.42b).

The optimal added damping ratio as

$$\xi_{opt} = Y_{opt} \left( \frac{a}{l} \right) R_1 R_2 R_3 \times 100 = 0.5 \times \left( \frac{5.85}{184.72} \right) \times 0.941 \times 1 \times 0.788 \times 100 = 1.17 \% \quad (3.48)$$

where  $R_1 = 0.941$  from Eq. (3.33),  $R_2 = 1$  from Eq. (3.35a), and  $R_3 = 0.788$  from Eq. (3.42a).

This amount of added damping is greatly larger than the required damping ratio.

### 3.6.2. Multi-Mode Vibration Control

Multi-mode vibration control for the cable with a viscous damper will be discussed in this example. The set of design conditions are as the same as in Example 2 of Section 3.6.1: damper location  $a = 5.85$  m, cable ends is fixed, damper support is rigid, and damper stiffness  $K_{vp} = 202.34 \times 10^3$  N/m.

The required added damping for suppressing rain-wind induced vibration is  $\xi \geq 0.295\%$ , according to Eq. (3.44).

Based on these conditions, the ordinate on the  $Y$  axis of the universal damping curve as

$$Y = \frac{\xi}{(a/l)R_1R_2R_3} = \frac{0.00295}{(5.85/184.72) \times 0.941 \times 1 \times 0.788} = 0.126 \quad (3.49)$$

The line  $Y = 0.126$  crosses the universal curve at points  $A(0.128; 0.126)$  and  $B(7.830; 0.126)$  as shown in Figure 3.10a. Any point resting on the curve from  $A$  to  $B$  will have the added damping higher than the required damping  $\xi$ . If we start to control mode 1 at point  $A$  ( $n_A = 1$ ), the designed damping coefficient  $c$  is calculated as

$$c = X_A \frac{\sqrt{Hm}}{n_A \pi} \left( \frac{l}{a} \right) \left( \frac{1}{\eta_1 \eta_2 \eta_3} \right) = 0.128 \times \frac{\sqrt{(3.55 \times 10^6) \times 60.2}}{1 \times \pi} \left( \frac{184.72}{5.85} \right) \left( \frac{1}{0.809 \times 1 \times 0.788} \right) = 29.52 \times 10^3 \text{ N.s.m}^{-1} \quad (3.50)$$

The number of controlled modes which have damping ratio higher than required value  $\xi \geq 0.295\%$  will increase from 1 (at point  $A$ ) to  $k$  (at point  $B$ ). The vibration mode at point  $B$  as

$$k = \frac{X_B}{X_A} n_A = \frac{7.830}{0.128} \times 1 = 61 \quad (3.51)$$

It means that a designed viscous damper with  $c = 29.52 \times 10^3$  N.s.m<sup>-1</sup> can control 61 consecutive vibration modes started from the mode 1 to mode 61. Eq. (3.51) also points out that if a starting mode at the point  $A$  is not the mode 1 ( $n_A > 1$ ), the number of controlled modes will be more than 61 modes.

Figure 3.10b shows the added damping ratio of 61 controlled modes. In this scenario, mode 8 gained the maximum added damping ratio ( $\xi = 1.17\%$ ) while the mode 1 and mode 61 possessed the lowest value ( $\xi = 0.295\%$ ).

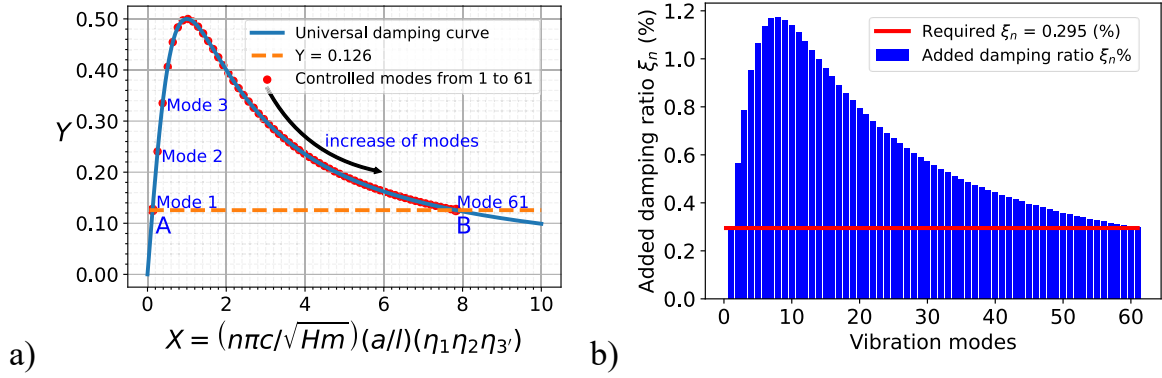


**FIGURE 3. 10.** Damping of multi-mode control: a) locations of modes on the universal damping curve; and b) added damping ratio for each mode.

In practice, the rain-wind induced vibration of a cable often observed at a frequency range from 0 to 3.0 Hz and predominantly at the mode 2, according to U.S. Department of Transportation, Federal Highway Administration<sup>10</sup>. With that concern, the damping coefficient  $c$ , in this example, will be obtained to achieve the maximum damping ratio at the mode 2 ( $n = 2$ ).

$$c = X \frac{\sqrt{Hm}}{n\pi} \left( \frac{l}{a} \right) \left( \frac{1}{\eta_1\eta_2\eta_3} \right) = 1 \times \sqrt{\frac{(3.55 \times 10^6) \times 60.2}{2 \times \pi}} \left( \frac{184.72}{5.85} \right) \left( \frac{1}{0.809 \times 1 \times 0.788} \right) = 115.30 \times 10^3 \text{ N.s.m}^{-1} \quad (3.52)$$

Additionally, for the cable in this example, frequencies of the first five modes (mode 1 to mode 5) will likely fall within 0 to 3.0 Hz. The added damping ratios of the first five modes is plotted in Figure 3.11a, in which the attainable damping ratio of the mode 2 was the highest value with  $\xi = 1.17\%$ .

Some other useful applications of the proposed universal damping curve could be listed as: the identification of the added damping of existing cable-damper system; the design of damper support stiffness or damper stiffness in which the reductions of damping due to these stiffnesses are within an allowable range; the optimization of the multi-mode vibration control of a cable, etc.



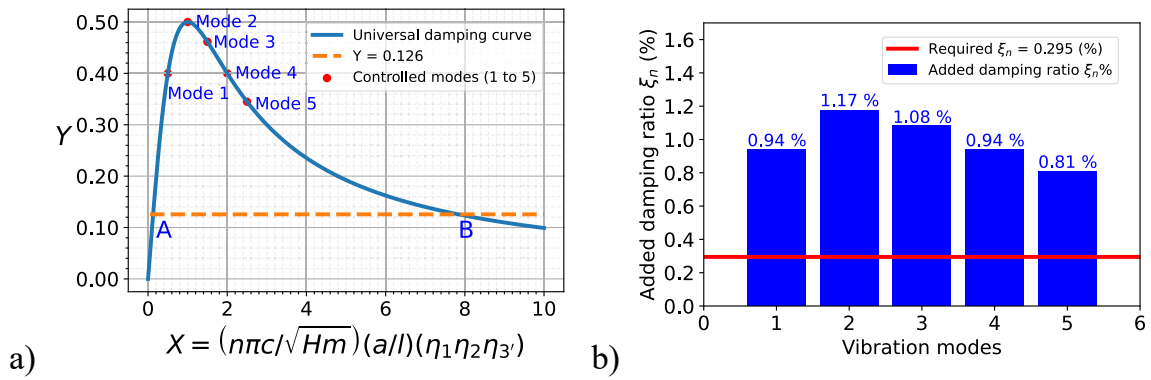


**FIGURE 3. 11.** Damping of the five controlled modes: a) locations of modes on the universal damping curve; and b) added damping ratio for each mode.

It is fair through this section to say that the proposed universal damping curve for an HDR damper and a viscous damper are profoundly convenient in the design of a cable with an attached damper for multi-mode vibration control. The simplicity and practicality can be understood because the proposed curve is a single curve and independent of any factors.

### 3.7. Summary

A model of cable-damper is proposed in this chapter, which accounts for several factors such as cable bending stiffness, restraint at cable ends, damper stiffness, damper support stiffness and negative stiffness damper. The formulation of damping ration is derived, and its universal damping curve is accordingly proposed. The conclusions are as follows

- 1) Cable bending stiffness triggered a reduction of the damping ratio for a fixed-fixed end cable whereas an inverse observation was found for a hinged-hinged end counterpart. By adjusting supports at cable ends with finite rotational restraint stiffness, the damper works more effectively.
- 2) The discrepancy in term of the added damping between a hinged-hinged and fixed-fixed end cable was remarkable when the cable bending stiffness was large.
- 3) In the presence of negative stiffness, the negative stiffness damper generates superior added damping to the cable in comparison to conventional damper.
- 4) The universal damping curve was proposed for a stay cable with an HDR damper or a viscous damper, which has only a single curve. This universal

damping curve is independent of any influencing factors like cable properties, damper characteristics, damper support stiffness, damper stiffness, added negative stiffness and boundary condition at cable ends (hinged, fixed and restraint ends).

- 5) The simplicity and practicality of the proposed universal damping curve in the design of a damper for cable vibration controls were shown through design examples; the design of a damper targeted multiple vibration modes can be easily performed using the proposed universal damping curve.

## Appendix: Formulas in Eqs. (3.10a-h)

The formulas that appear in Eqs. (3.10a-h).

$$\Psi_1 = \delta_1 \delta_2^2 [\cos(\delta_2 a) + \cosh(\delta_1 a) - \cosh \delta_1 (a-l) \cos(\delta_2 l) - \cos \delta_2 (a-l) \cosh(\delta_1 l)] - \delta_2 \delta_1^2 \sin \delta_2 (a-l) \sinh(\delta_1 l) + \delta_2^3 \sinh \delta_1 (a-l) \sin(\delta_2 l) \quad (3.53)$$

$$\Psi_2 = 2EI \delta_2^2 (\delta_1^2 + \delta_2^2) \sinh \delta_1 (a-l) \cos(\delta_2 l) + EI \delta_2 \delta_1^3 [\cosh \delta_1 (a-l) \sin(\delta_2 l) - \sin \delta_2 (a-l) \cosh(\delta_1 l) - \sin(\delta_2 a)] + EI \delta_1 \delta_2^3 [\cosh \delta_1 (a-l) \sin(\delta_2 l) - \sin \delta_2 (a-l) \cosh(\delta_1 l) - \sin(\delta_2 a)] \quad (3.54)$$

$$\Psi_3 = -EI^2 \delta_2 (\delta_1^4 + \delta_2^4) \sinh \delta_1 (a-l) \sin(\delta_2 l) - 2EI^2 \delta_1^2 \delta_2^2 \sinh \delta_1 (a-l) \sin(\delta_2 l) \quad (3.55)$$

$$\Psi_4 = \frac{1}{2} \delta_1^3 \sinh \delta_1 l [\cos \delta_2 l - \cos \delta_2 (2a-l)] + \frac{1}{2} \delta_1^2 \delta_2 \sin \delta_2 l [3 \cosh \delta_1 l + \cosh \delta_1 (2a-l)] + \frac{1}{2} \delta_1^3 \sin \delta_2 l [\cosh \delta_1 (2a-l) - \cosh \delta_1 l] + 2\delta_1^2 \delta_2 [\sin \delta_2 (a-l) \cosh \delta_1 (a-l) - \sin(\delta_2 a) \cosh(\delta_1 a)] - 2\delta_1 \delta_2^2 [\cos \delta_2 (a-l) \sinh \delta_1 (a-l) - \cos \delta_2 a \sinh \delta_1 a] - \frac{1}{2} \delta_1 \delta_2^2 \sinh \delta_1 l [3 \cos \delta_2 l + \cos \delta_2 (2a-l)] \quad (3.56)$$

$$\Psi_5 = 2EI \delta_1 \delta_2 (\delta_1^2 + \delta_2^2) [\sinh(\delta_1 l) \sin(\delta_2 l) - \sinh(\delta_1 a) \sin(\delta_2 a) - \sinh \delta_1 (a-l) \sin \delta_2 (a-l)] + EI (\delta_1^4 - \delta_2^4) \cosh(\delta_1 l) \cos(\delta_2 l) + EI (\delta_1^2 + \delta_2^2) [\delta_2^2 \cosh \delta_1 (2a-l) \cos(\delta_2 l) - \delta_1^2 \cos \delta_2 (2a-l) \cosh(\delta_1 l)] \quad (3.57)$$

$$\Psi_6 = \frac{1}{2} EI^2 (\delta_1^4 + \delta_2^4) [\delta_2 \cosh(\delta_1 l) \sin(\delta_2 l) + \delta_1 \cos(\delta_2 l) \sinh(\delta_1 l) - \delta_2 \sin(\delta_2 l) \cosh \delta_1 (2a-l) - \delta_1 \sinh(\delta_1 l) \cos \delta_2 (2a-l)] - EI^2 \delta_1^2 \delta_2^2 \sin \delta_2 l [\cosh \delta_1 (2a-l) - \cosh(\delta_1 l)] + EI^2 \delta_1^3 \delta_2^2 \sinh(\delta_1 l) [\cos(\delta_2 l) - \cos \delta_2 (2a-l)] \quad (3.58)$$

$$\Psi_7 = \delta_1 \delta_2^2 [\cos(\delta_2 l) \sinh \delta_1 (a-l) + \sinh(\delta_1 l) \cos \delta_2 (a-l) - \sinh(\delta_1 a)] + \delta_2 \delta_1^2 [\cosh(\delta_1 l) \sin \delta_2 (a-l) - \sin(\delta_2 a) + \sin(\delta_2 l) \cosh \delta_1 (a-l)] \quad (3.59)$$

$$\Psi_8 = EI \delta_1 \delta_2 (\delta_1^2 + \delta_2^2) [\sinh(\delta_1 l) \sin \delta_2 (a-l) - \sin(\delta_2 l) \sinh \delta_1 (a-l)] \quad (3.60)$$

$$\Psi_9 = \delta_1^2 \delta_2 [\cos(\delta_2 a) + \cosh(\delta_1 a) - \cos \delta_2 (a-l) \cosh(\delta_1 l) - \cos(\delta_2 l) \cosh \delta_1 (a-l)] + \delta_1 \delta_2^2 \sinh \delta_1 (a-l) \sin(\delta_2 l) - \delta_1^3 \sinh(\delta_1 l) \sin \delta_2 (a-l) \quad (3.61)$$

$$\Psi_{10} = EI \delta_1 (\delta_1^2 + \delta_2^2) [\delta_2 \sinh(\delta_1 a) - 2\delta_1 \sin \delta_2 (a-l) \cosh(\delta_1 l) - \delta_2 \cos \delta_2 (a-l) \sinh(\delta_1 l) + \delta_2 \cos(\delta_2 l) \sinh \delta_1 (a-l)] \quad (3.62)$$

$$\Psi_{11} = -\delta_1 EI^2 [(\delta_1^4 + \delta_2^4) \sin \delta_2 (a-l) \sinh(\delta_1 l) + 2\delta_1^2 \delta_2^2 \sin \delta_2 (a-l) \sinh(\delta_1 l)] \quad (3.63)$$

$$\Psi_{12} = -\frac{1}{2} \delta_2 \delta_1^2 \sin(\delta_2 l) [\sinh(\delta_1 l) - \sinh \delta_1 (2a-l)] + \frac{1}{2} \delta_2^3 \sin(\delta_2 l) [\sinh(\delta_1 l) + \sinh \delta_1 (2a-l)] + \delta_1 \delta_2^2 [\cosh(\delta_1 a) \cos(\delta_2 a) + \cos(\delta_2 l) \cosh(\delta_1 l)] + \delta_2 \delta_1^2 [\sin \delta_2 (a-l) \sinh \delta_1 (a-l) - \sinh(\delta_1 a) \sin(\delta_2 a)] - \delta_1 \delta_2^2 [\cosh \delta_1 (a-l) \cos \delta_2 (a-l) + 1] \quad (3.64)$$

$$\Psi_{13} = EI \delta_2 (\delta_1^2 + \delta_2^2) [\delta_2 \cos(\delta_2 l) \sinh \delta_1 (2a-l) - \delta_1 \cosh(\delta_1 l) \sin(\delta_2 l) + \delta_2 \cos(\delta_2 l) \sinh(\delta_1 l) - \delta_1 \cosh(\delta_1 a) \sin(\delta_2 a) - \delta_1 \sin \delta_2 (a-l) \cosh \delta_1 (a-l)] \quad (3.65)$$

$$\Psi_{14} = -\frac{1}{2} EI^2 \delta_2 (\delta_1^4 + \delta_2^4) [\sin(\delta_2 l) \sinh \delta_1 (2a-l) + \sin(\delta_2 l) \sinh(\delta_1 l)] - EI^2 \delta_1^2 \delta_2^3 \sin(\delta_2 l) [\sinh(\delta_1 l) + \sinh \delta_1 (2a-l)] \quad (3.66)$$

$$\Psi_{15} = -\frac{1}{2} \delta_2 (\delta_1^2 + \delta_2^2) \sin(\delta_2 l) \cosh \delta_1 (2a-l) - \frac{1}{2} \delta_2 (\delta_1^2 - \delta_2^2) \cosh(\delta_1 l) \sin(\delta_2 l) - \delta_1 \delta_2^2 [\sinh(\delta_1 a) \cos(\delta_2 a) - \sinh(\delta_1 l) \cos(\delta_2 l)] - \delta_2 \delta_1^2 [\sin \delta_2 (a-l) \cosh \delta_1 (a-l) - \cosh(\delta_1 a) \sin(\delta_2 a)] + \delta_1 \delta_2^2 \sinh \delta_1 (a-l) \cos \delta_2 (a-l) \quad (3.67)$$

$$\Psi_{16} = EI \delta_2 (\delta_1^2 + \delta_2^2) [\delta_1 \sinh(\delta_1 a) \sin(\delta_2 a) + \delta_2 \cos(\delta_2 l) \cosh(\delta_1 l) - \delta_1 \sinh(\delta_1 l) \sin(\delta_2 l) - \delta_2 \cos(\delta_2 l) \cosh \delta_1 (2a-l) + \delta_1 \sin \delta_2 (a-l) \sinh \delta_1 (a-l)] \quad (3.68)$$

$$\Psi_{17} = \frac{1}{2} EI^2 \delta_2 (\delta_1^4 + \delta_2^4) [\sin(\delta_2 l) \cosh \delta_1 (2a-l) - \cosh(\delta_1 l) \sin(\delta_2 l)] - EI^2 \delta_1^2 \delta_2^3 \sin(\delta_2 l) [\cosh(\delta_1 l) - \cosh \delta_1 (2a-l)] \quad (3.69)$$

$$\Psi_{18} = \frac{1}{2} \delta_1 (\delta_1^2 + \delta_2^2) \sinh(\delta_1 l) \sin \delta_2 (2a-l) + \frac{1}{2} \delta_1 (\delta_1^2 - \delta_2^2) \sinh(\delta_1 l) \sin(\delta_2 l) + \delta_1 \delta_2^2 \sinh \delta_1 (a-l) \sin \delta_2 (a-l) - \delta_1 \delta_2 [\delta_2 \sin(\delta_2 a) \sinh(\delta_1 a) + \delta_1 \cos(\delta_2 a) \cosh(\delta_1 a) + \delta_1 \cos(\delta_2 l) \cosh(\delta_1 l)] + \delta_1^2 \delta_2 [\cos \delta_2 (a-l) \cosh \delta_1 (a-l) + 1] \quad (3.70)$$

$$\Psi_{19} = EI \delta_1 (\delta_1^2 + \delta_2^2) [\delta_1 \cosh(\delta_1 l) \sin \delta_2 (2a-l) - \delta_2 \cos \delta_2 (a-l) \sinh \delta_1 (a-l) - \delta_2 \cos(\delta_2 a) \sinh(\delta_1 a) - \delta_2 \cos(\delta_2 l) \sinh(\delta_1 l) + \delta_1 \sin(\delta_2 l) \cosh(\delta_1 l)] \quad (3.71)$$

$$\Psi_{20} = \frac{1}{2} EI^2 \delta_1 (\delta_1^4 + \delta_2^4) \sinh(\delta_1 l) [\sin \delta_2 (2a-l) + \sin(\delta_2 l)] + EI^2 \sinh(\delta_1 l) \delta_1^3 \delta_2^2 [\sin(\delta_2 l) + \sin \delta_2 (2a-l)] \quad (3.72)$$

## CHAPTER 4. DAMPING ANALYSIS OF FULL-SCALE CABLES FROM FIELD MEASUREMENT DATA

Damping in stay cable contributed by damper was theoretically studied in Chapters 2 and 3. While the previous chapters mainly emphasized on theoretical aspect, this chapter compares measured damping of full-scale cables to theoretical damping for the evaluation of damper performance. The measurement was conducted on stay cables of a cable-stayed bridge in Japan, in which HDR dampers were installed to the cables. Overall, the effectiveness of damper was greater than 0.7 for most of selected cables. Moreover, the analysis on the amplitude dependency of damping ratios and frequencies was presented and the result showed that frequencies were almost stable over amplitudes whereas the variation of damping over amplitudes was significant.

**Keywords:** Full-scale cables; Field measurement; High Damping Rubber (HDR) damper; Damping analysis; Measured damping; Theoretical damping; Amplitude dependency.

### 4.1. Target bridge and measurement

#### 4.1.1. Bridge information

The field measurement of damping in stay cables of Shinminato Bridge in Japan was conducted. The Bridge is in Imizu, Toyama Prefecture, was recently opened in September 2012. It is the largest cable-stayed bridge on the Sea of Japan coast and links the east and west districts around the Toyama Shinminato Harbor entrance. The bridge has a total length of 600 m, in which the main span length is 360 m as shown in Figure 4.1.

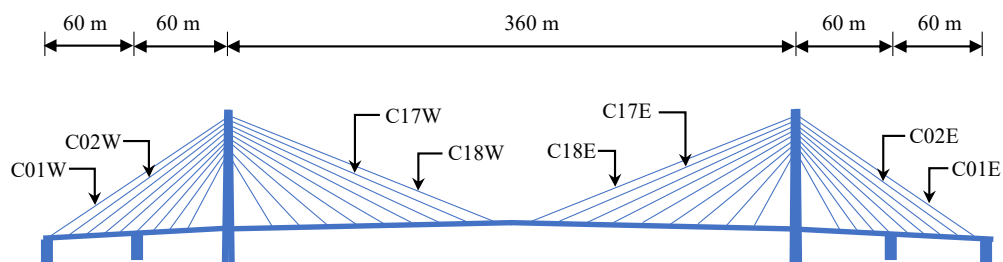
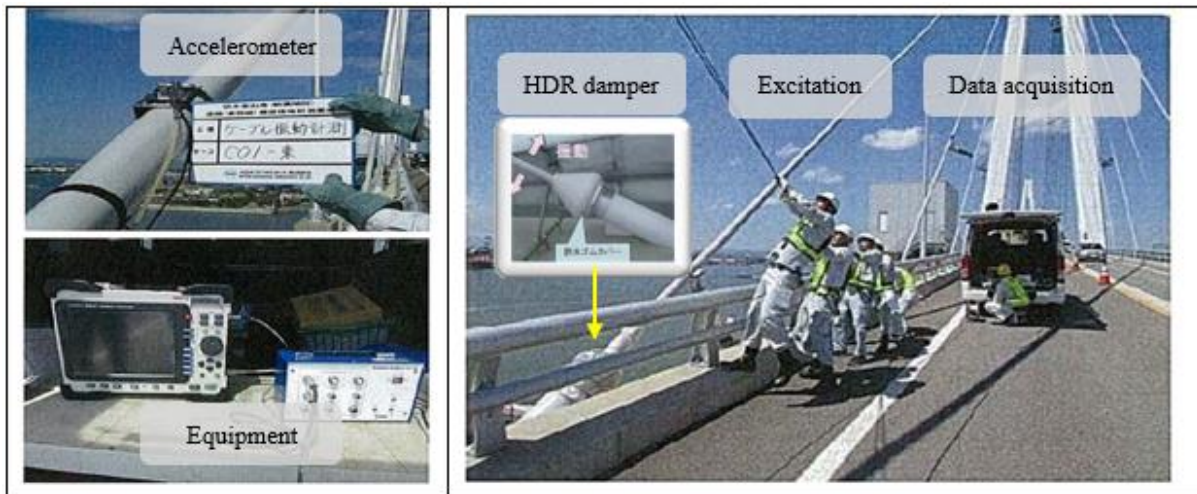


FIGURE 4. 1. Layout of the bridge.

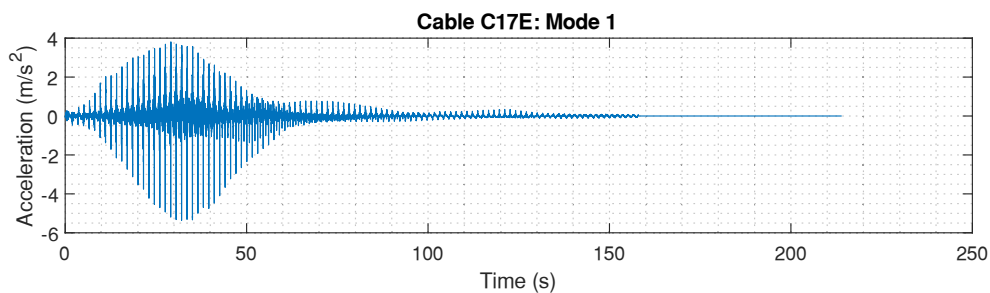
The measurement of the cable vibration in six selected cables with HDR dampers (C01E, C02E, C17E, C18E, C17W and C18W) was implemented to evaluate the cable damping. For each cable, the vibration of the mode 1, mode 2 and mode 3 was individually excited, and the measurement was conducted for each vibration mode. During the measurement, average temperature was recorded at 18.6°C and wind speed averaged 5.3 m/s. Sampling frequency of the accelerometer was 1000 Hz. The measurement setup and excitation are depicted in Figure 4.2.

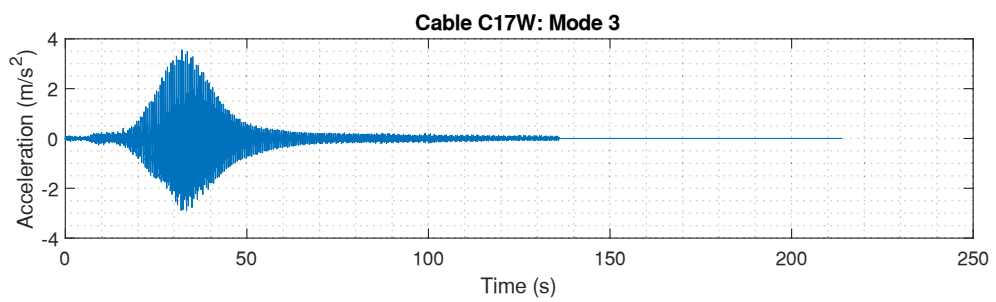
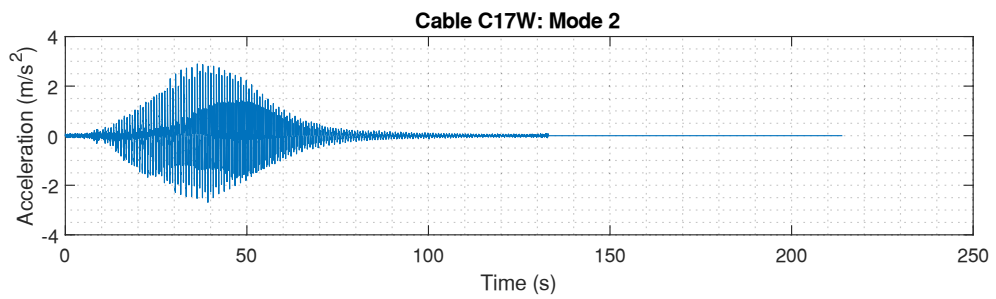
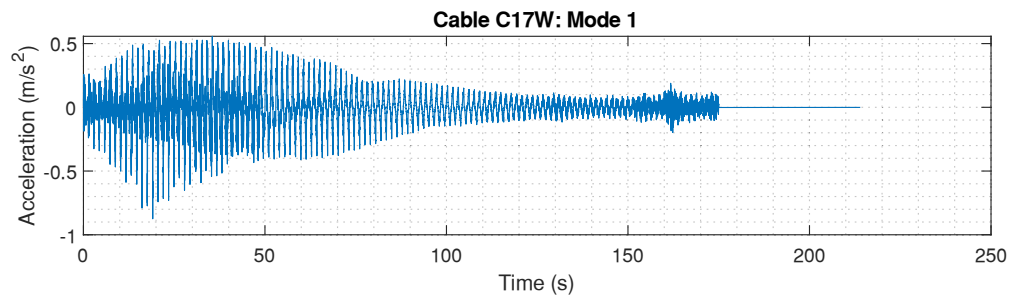
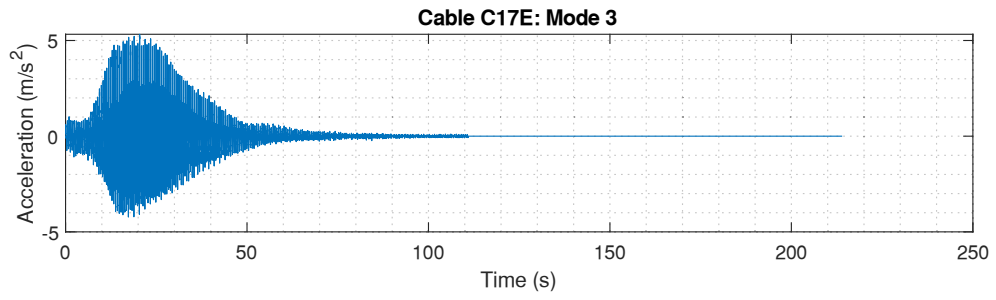
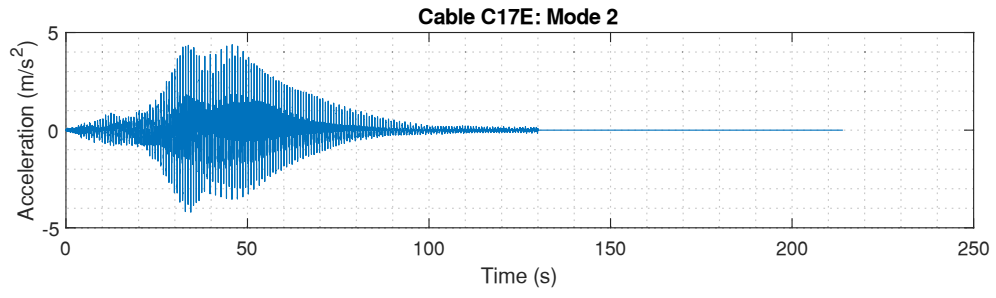


**FIGURE 4. 2.** The measurement setup and data acquisition.

#### 4.1.2. Measurement data

Figure 4.3 displays the raw acceleration data of the vibrations of some cables as examples (C17E, C17W and C18W). The vibration data in Figure 4.3 shows two vibration phases, which are a forced vibration throughout the excitation period and a free-decay vibration phase after releasing the excitation. The identification of the measured natural frequencies and damping ratios will be implemented during the free-decay vibration phase.





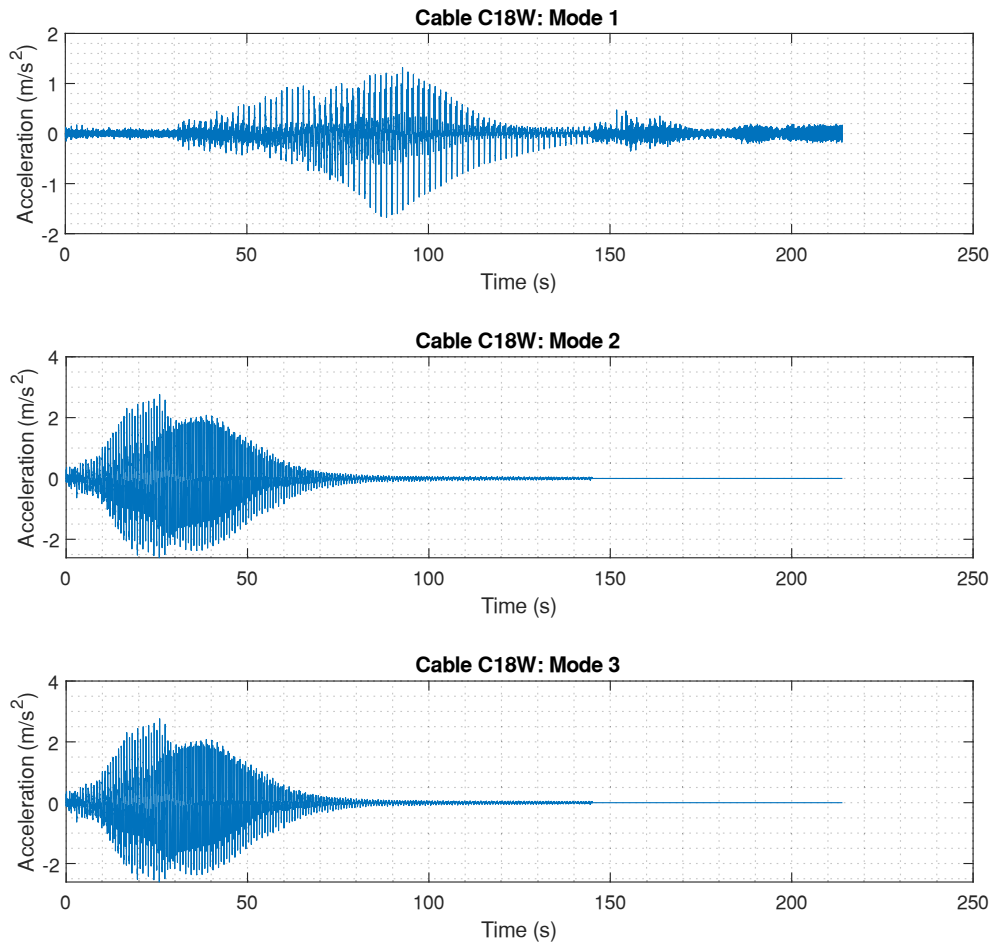


**FIGURE 4. 3.** Raw acceleration data of cables C17E, C17W, 18W.

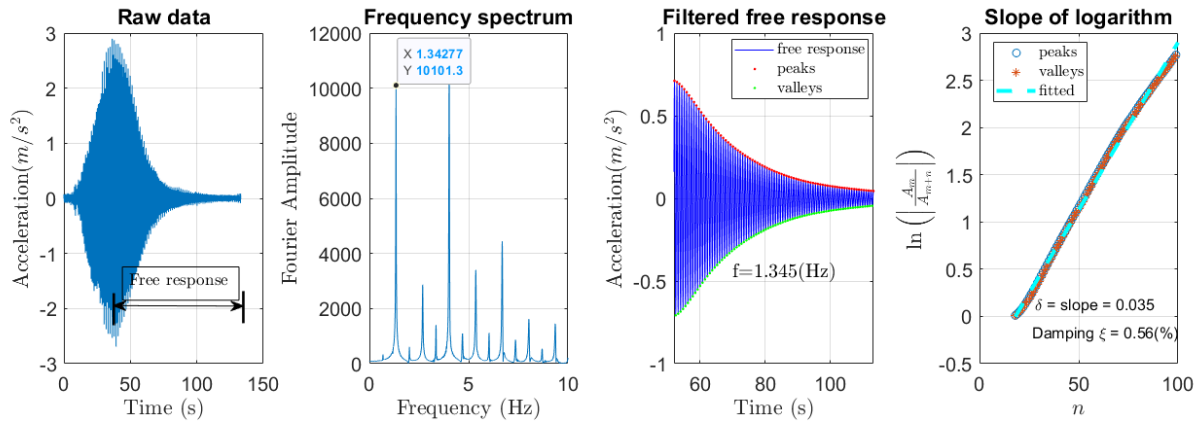
## 4.2. Damping analysis of full-scale stay cables from field measurement

### 4.3.1. Damping analysis procedure

Figure 4.4 shows the 4-step procedures for identifying cable frequencies and damping ratios from the raw acceleration; the measurement data of cable 17W is used to demonstrate the step-by-step implementation. Step 1 is to select a window of free-decay response from the raw signal. Step 2 is to transform the free-decay response from time domain into frequency domain by using Fourier spectrum analysis, in which the frequencies of vibration modes are extracted at the prominent peaks in the spectrum. Step 3 is to pass the free-decay vibration through a Butterworth filter to eliminate ripples and unassigned vibration modes. After being filtered, the filtered accelerations with clear peaks/valleys are displayed. Step 4 is to plot the natural logarithm graph of both peaks' amplitudes and valleys' amplitudes, and the damping ratio  $\xi$  can be deduced from the natural logarithm graph.<sup>54</sup>

$$\xi \approx \frac{\delta}{2\pi} = \frac{1}{2\pi n} \ln \left| \frac{A_m}{A_{m+n}} \right| \quad (4.1)$$

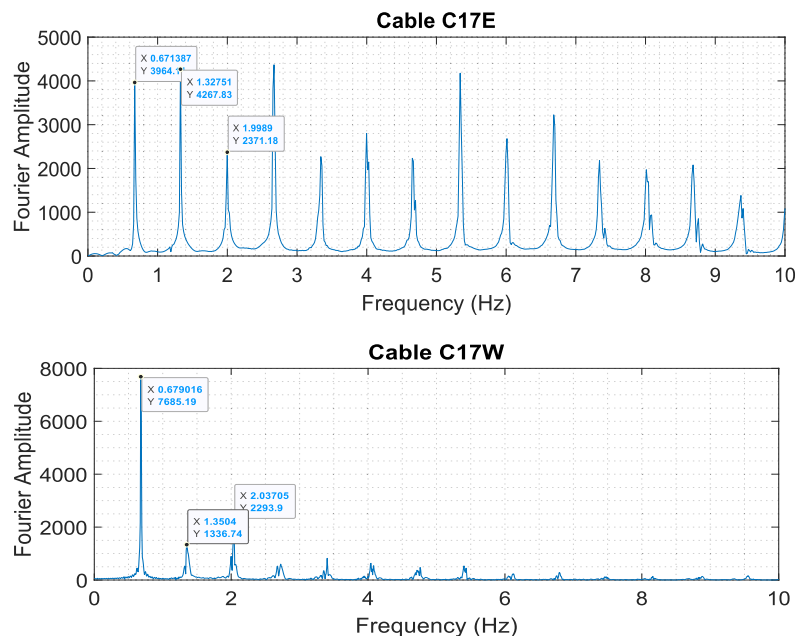
where  $A_m$  and  $A_{m+n}$  are the amplitudes of the filtered free-decay responses at the  $m$  and  $m+n$  peaks (or valleys), respectively; and  $\delta$  is the logarithmic decrement (slope of the natural logarithm line).



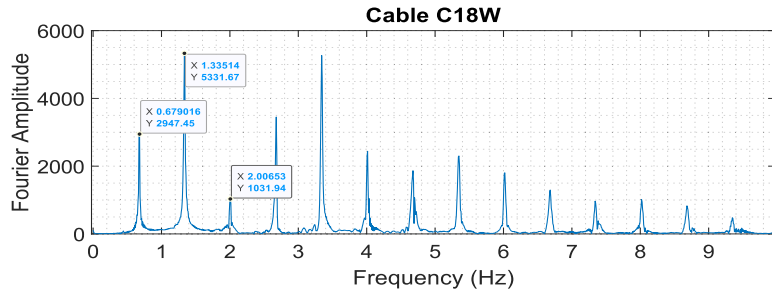
**FIGURE 4. 4.** Four-step procedures for identifying cable damping ratio  $\xi$ .

### 4.3.2. Results of measured damping and measured frequencies

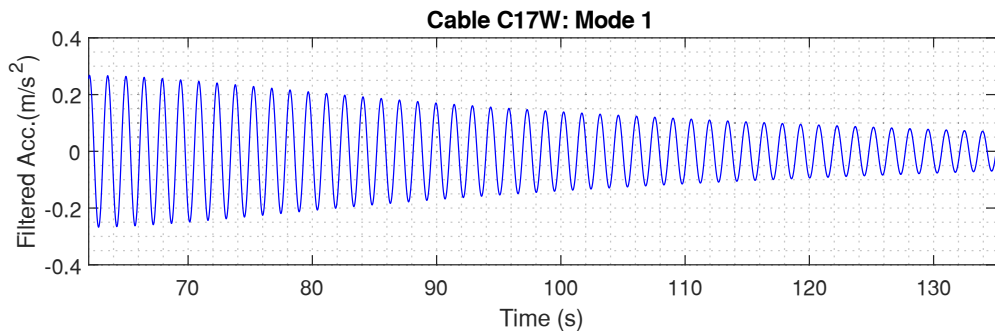
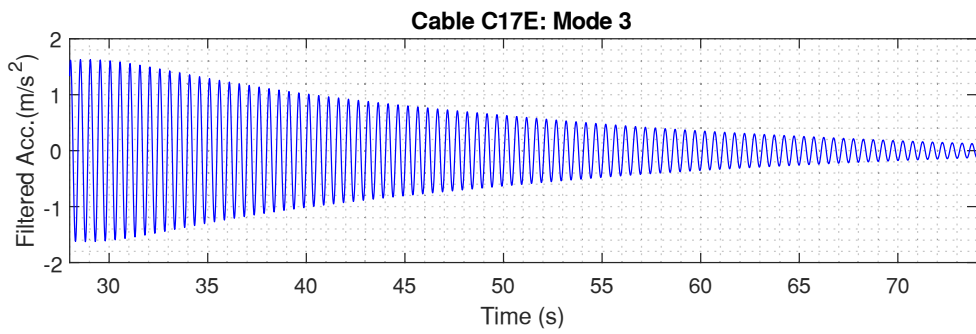
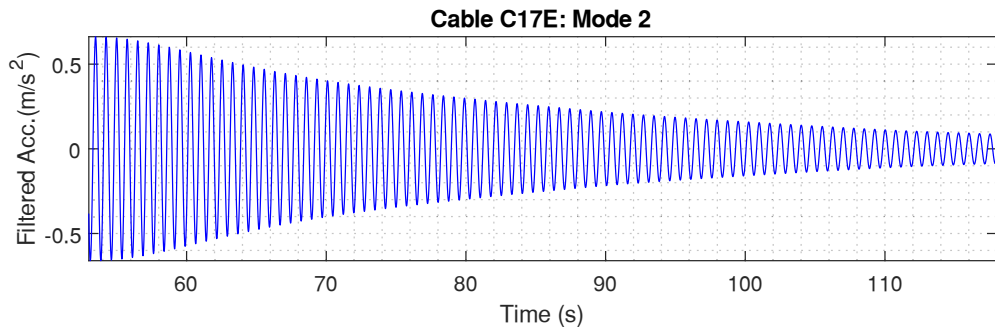
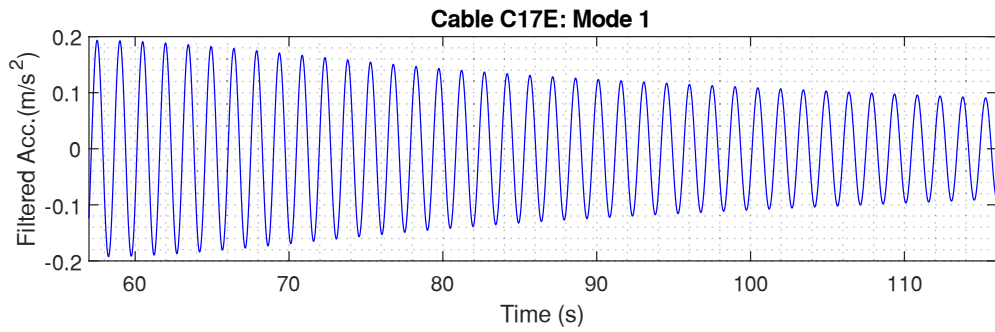
The procedure shown in Figure 4.4 was applied to all selected cables. The frequency spectrum analysis and the filtered free response of raw data (C17E, C17W, 18W in Figure 4.3) are plotted in Figure 4.5 and Figure 4.6 as example, respectively.







**FIGURE 4. 5.** Fourier spectrum analysis.



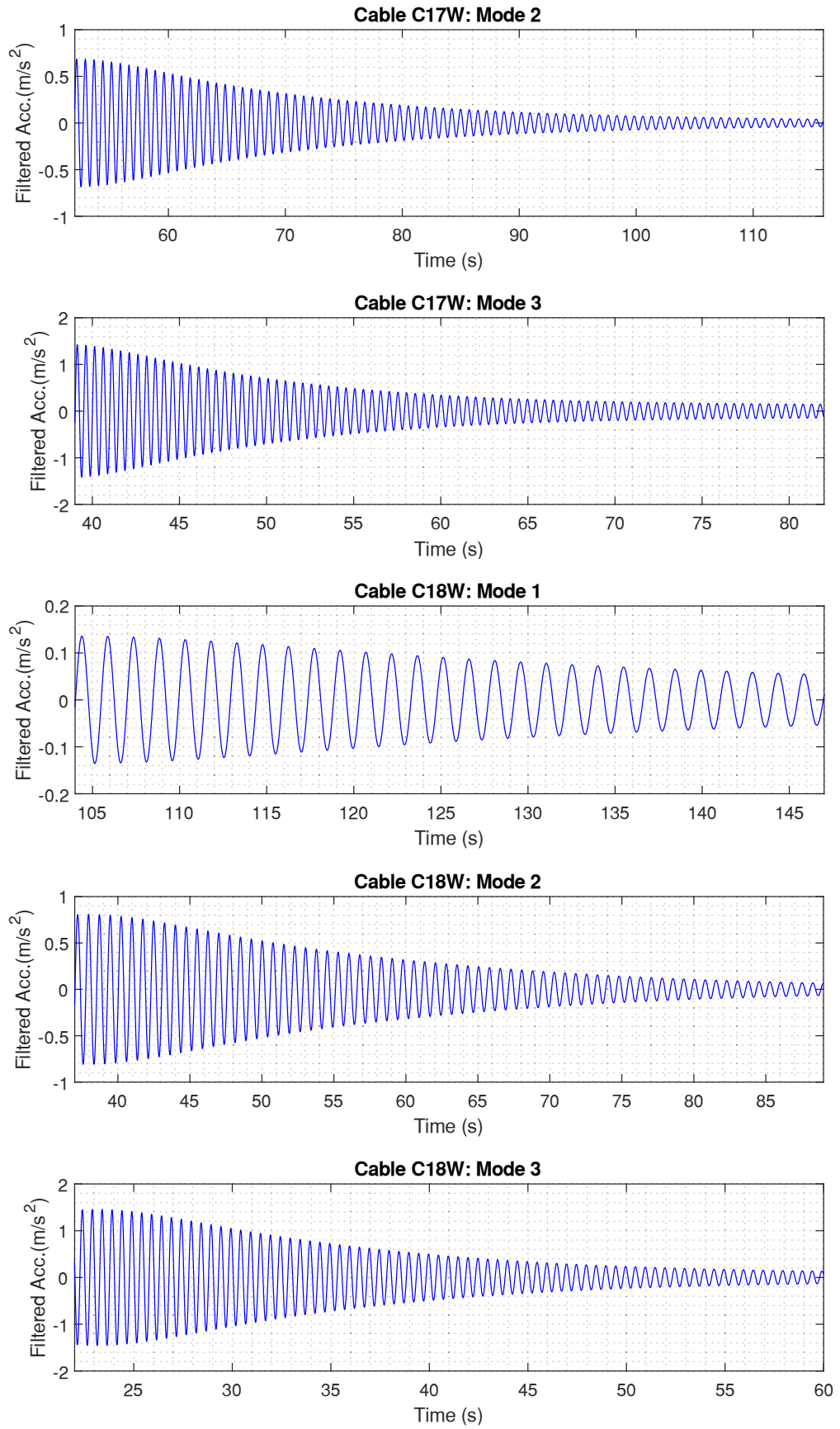


**FIGURE 4. 6.** Filtered acceleration of free-decay responses.

The measured frequencies are extracted from frequency spectrum and damping ratio is computed from Eq. (4.1). The results are listed in Table 4.1. As can be seen in Table 4.1, the measured damping ratios vary around 0.32% - 0.70 % for mode 1, 0.40% - 0.60% for mode 2, and 0.35% - 0.55% for mode 3, respectively. Also, the measured frequencies are less than 1 Hz, 2 Hz, 3Hz for mode 1, mode 2 and mode 3, correspondingly.

**TABLE 4. 1.** Measured frequencies and damping ratios  $\xi$

Cable	Mode 1		Mode 2		Mode 3	
	Frequency $f$ (Hz)	Damping ratio $\xi$ (%)	Frequency $f$ (Hz)	Damping ratio $\xi$ (%)	Frequency $f$ (Hz)	Damping ratio $\xi$ (%)
<b>C01E</b>	0.827	0.477	1.640	0.390	2.465	0.352
<b>C02E</b>	0.992	0.578	1.973	0.523	2.960	0.420
<b>C17E</b>	0.674	0.321	1.328	0.394	1.999	0.403
<b>C18E</b>	0.641	0.692	1.259	0.594	1.897	0.524
<b>C17W</b>	0.682	0.428	1.345	0.562	2.022	0.491
<b>C18W</b>	0.674	0.548	1.333	0.616	2.004	0.541

### 4.3. Theoretical damping and damper effectiveness

Cable properties and the characteristics of HDR dampers are shown in Table 4.2, in which cable tensions  $H$  are estimated based on measured frequencies.<sup>5</sup>

**TABLE 4. 2.** Cable properties and damper parameters

Cable No.	Cable properties						HDR Damper		
	$l$ (m)	$m$ (kg/m)	$EI$ (N.m <sup>2</sup> )	$H$ (N)	$EA$ (N)	$\varphi$ (°)	Damper location $a$ (m)	Spring factor $K$ (N/m)	Loss factor $\phi$
<b>C01E</b>	137.82	68.4	$2.73 \times 10^6$	$3.45 \times 10^6$	$2.59 \times 10^9$	34.42	4.54	$6.44 \times 10^5$	0.62
<b>C02E</b>	127.47	68.4	$2.73 \times 10^6$	$4.26 \times 10^6$	$2.59 \times 10^9$	36.02	4.37	$6.44 \times 10^5$	0.62
<b>C17E</b>	167.18	64.3	$2.34 \times 10^6$	$3.10 \times 10^6$	$2.39 \times 10^9$	23.35	5.54	$5.63 \times 10^5$	0.62
<b>C18E</b>	184.72	60.2	$1.98 \times 10^6$	$3.20 \times 10^6$	$2.20 \times 10^9$	21.83	5.85	$4.83 \times 10^5$	0.62
<b>C17W</b>	167.18	64.3	$2.34 \times 10^6$	$3.18 \times 10^6$	$2.39 \times 10^9$	23.35	5.54	$5.63 \times 10^5$	0.62
<b>C18W</b>	184.72	60.2	$1.98 \times 10^6$	$3.67 \times 10^6$	$2.20 \times 10^9$	21.83	5.85	$4.83 \times 10^5$	0.62

Note:  $EA$  = cable axial stiffness; and  $\varphi$  = cable inclination angle.

In addition to Table 4.2, damper support stiffness  $K_{vs}$  was included for a cable C17E since the cross-sectional deformation of a steel tube which supported to the damper was observed during the measurement. The support part of the damper has the length of 110 mm, diameter of 355.6 mm and thickness of 7.9 mm. The value of support stiffness was  $K_{vs} = 1143 \times 10^3$  N/m in cable C17E which was determined based on the ratio of a unit force along the diameter to tube's deformation. Negative stiffness was not included to all cables  $K_{NS} = 0$ . Rotational restraint stiffness at cable ends was also unknown, therefore both hinged-hinged end ( $K_r = 0$ ) and fixed-fixed end ( $K_r \rightarrow \infty$ ) were evaluated.

The theoretical damping ratios  $\xi$  in the cables are computed with two different solutions: the proposed universal damping curve which is presented in Chapter 3 and the Finite Difference Method (FDM). The FDM was originally developed by Tabatabai and Mehrabi<sup>38</sup> for the vibration of a cable with a viscous damper. The FDM method is modified in this present study for the cables with HDR damper types, referring to the Appendix. The results are summarized in Table 4.3.

The results show that damping ratios obtained by the proposed universal damping curve coincide with the FDM, an error of 2.0 % on average. The theoretical damping ratios are around 0.4 % - 0.5 %, except for the cable C17E (less than 3.3%). The discrepancy of damping ratios between hinged-hinged end cables and fixed-fixed end cables is relatively remarkable (15% - 26%), especially in shorter cables (C01E and C02E). It is understandable because short cables trigger a significant difference about cable configurations near cable ends than that of long cables while dampers are often installed near cable ends; therefore, damping of short cables depends heavily on boundary conditions at cable ends than that of long cables. Note that, all cables in this analysis were discretized into  $n = 800$  nodes when using the FDM.

**TABLE 4. 3.** Theoretical damping ratios

Cable No.	by proposed universal damping curve			by Finite Difference Method		
	Fixed ends $\xi_f$ (%)	Hinged ends $\xi_h$ (%)	$\frac{(\xi_h - \xi_f)}{\xi_f} \times 100$	Fixed ends $\xi_f$ (%)	Hinged ends $\xi_h$ (%)	$\frac{(\xi_h - \xi_f)}{\xi_f} \times 100$
C01E	0.416	0.519	24.76	0.419	0.521	24.34
C02E	0.413	0.521	26.15	0.412	0.519	25.97
C17E	0.257	0.312	21.40	0.269	0.323	20.07
C18E	0.419	0.484	15.51	0.422	0.485	14.93
C17W	0.437	0.511	16.93	0.458	0.529	15.50
C18W	0.415	0.478	15.18	0.416	0.478	14.90

The impact of cable sag on the attainable damping is neglected when developing the universal damping curve. In order to take sag effect into account, a reduction factor  $R_{sag}$  of added damping due to cable sag was calculated. The FDM is used in this calculation.

$$R_{sag} = \frac{\xi_s}{\xi_{ws}} \quad (4.2)$$

where  $\xi_s$  and  $\xi_{ws}$  are the damping ratio of a cable with and without cable sag, respectively.

Tables 4.4, 4.5 and 4.6 show the reduction factors  $R_{sag}$  of damping ratios for the mode 1, mode 2 and mode 3, correspondingly. The results show that cable sag causes a notable reduction of the damping ratio for the mode 1 whereas having almost no effect on the mode 2 and a relatively small reduction for the mode 3. In the previous studies<sup>14,18</sup>, the reductions of the added damping due to cable sag were analytically investigated by an asymptotic solution; these two papers have come out the same result that cable sag only significantly reduces attainable damping for mode 1; however, in their works, cable sag was approximated by a parabolic formulation without considering bending stiffness of cable in the sag profile. Hence, the reduction of damping<sup>14,18</sup> is independent of boundary condition types at cable ends (hinged, fixed or restraint ends). The results in Tables 4.4, 4.5 and 4.6, on the other hand, illustrate that the reduction of damping  $R_{sag}$  of the fixed-fixed end cables is more significant than hinged-hinged end cables, especially for long cables (C17 and C18).

**TABLE 4. 4.** Reduction factors of damping due to cable sag for Mode 1

Mode 1						
Cable No.	Fixed-Fixed end cable			Hinged-Hinged end cable		
	Without sag $\xi_{ws}$ (%)	With sag $\xi_s$ (%)	Reduction factor $R_{sag}$	Without sag $\xi_{ws}$ (%)	With sag $\xi_s$ (%)	Reduction factor $R_{sag}$
<b>C01E</b>	0.419	0.382	0.91	0.520	0.499	0.96
<b>C02E</b>	0.412	0.396	0.96	0.519	0.509	0.98
<b>C17E</b>	0.269	0.223	0.83	0.323	0.296	0.92
<b>C18E</b>	0.422	0.352	0.83	0.485	0.448	0.92
<b>C17W</b>	0.458	0.386	0.84	0.529	0.488	0.92
<b>C18W</b>	0.416	0.369	0.89	0.478	0.453	0.95

**TABLE 4. 5.** Reduction factors of damping due to cable sag for Mode 2

Mode 2						
Cable No.	Fixed-Fixed end cable			Hinged-Hinged end cable		
	Without sag $\xi_{vs}$ (%)	With sag $\xi_s$ (%)	Reduction factor $R_{sag}$	Without sag $\xi_{vs}$ (%)	With sag $\xi_s$ (%)	Reduction factor $R_{sag}$
C01E	0.420	0.420	1.00	0.522	0.522	1.00
C02E	0.412	0.412	1.00	0.520	0.520	1.00
C17E	0.270	0.270	1.00	0.324	0.324	1.00
C18E	0.423	0.423	1.00	0.487	0.487	1.00
C17W	0.460	0.460	1.00	0.532	0.532	1.00
C18W	0.417	0.417	1.00	0.479	0.479	1.00

**TABLE 4. 6.** Reduction factors of damping due to cable sag for Mode 3

Mode 3						
Cable No.	Fixed-Fixed end cable			Hinged-Hinged end cable		
	Without sag $\xi_{vs}$ (%)	With sag $\xi_s$ (%)	Reduction factor $R_{sag}$	Without sag $\xi_{vs}$ (%)	With sag $\xi_s$ (%)	Reduction factor $R_{sag}$
C01E	0.421	0.419	1.00	0.526	0.526	1.00
C02E	0.413	0.412	1.00	0.523	0.523	1.00
C17E	0.270	0.267	0.99	0.325	0.325	1.00
C18E	0.425	0.419	0.99	0.489	0.489	1.00
C17W	0.462	0.457	0.99	0.535	0.535	1.00
C18W	0.418	0.415	0.99	0.481	0.481	1.00

Theoretical damping ratios by the universal damping curve in Table 4.3 are multiplied by the reduction factor  $R_{sag}$  and compared with the measured damping in Table 4.1. The comparison is presented in Figure 4.7. It is noted that the measured damping ratios appeared in Table 4.1 also consisted of cable inherent damping  $\xi_0$ . This inherent damping is around  $\xi_0 \approx 0.08\%$ .

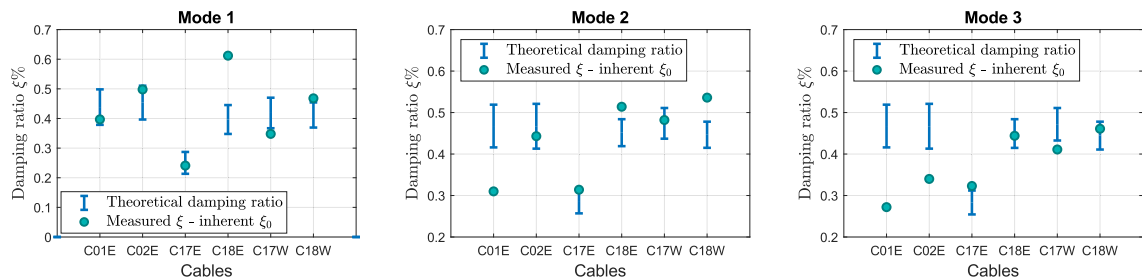


**FIGURE 4. 7.** Comparison between theoretical damping ratios and measured values.

The lower bound of the theoretical damping values means the damping of fixed-fixed end cables while upper bound corresponds to hinged-hinged end cables. Overall, the measured damping values are within or close to the range of theoretical calculations, except for cable C18E mode 1, C01E mode 2 and mode 3. The effectiveness of HDR dampers is evaluated by the ratio between measured damping and the average value of theoretical damping in Figure 4.7; and it shows that the effectiveness is larger than 0.70 for all three modes, except for mode 2 (0.66) and mode 3 (0.58) of cable C01E. It is the fact that the theoretical damping is analytically calculated based on pure conditions whereas measured damping would be under several operational and environmental variations like wind speeds, temperatures, measurement noise. These factors may cause the discrepancy between measured and theoretical damping ratios.

#### 4.4. Discussion on the amplitude dependency of measured damping

The measured damping ratio is computed from two consecutive peaks of the filtered acceleration data of free-decay response, then plotting it over the respective peaks of the accelerations. Acceleration measurement data of cables C17E, C17W, 18W are used in this investigation.

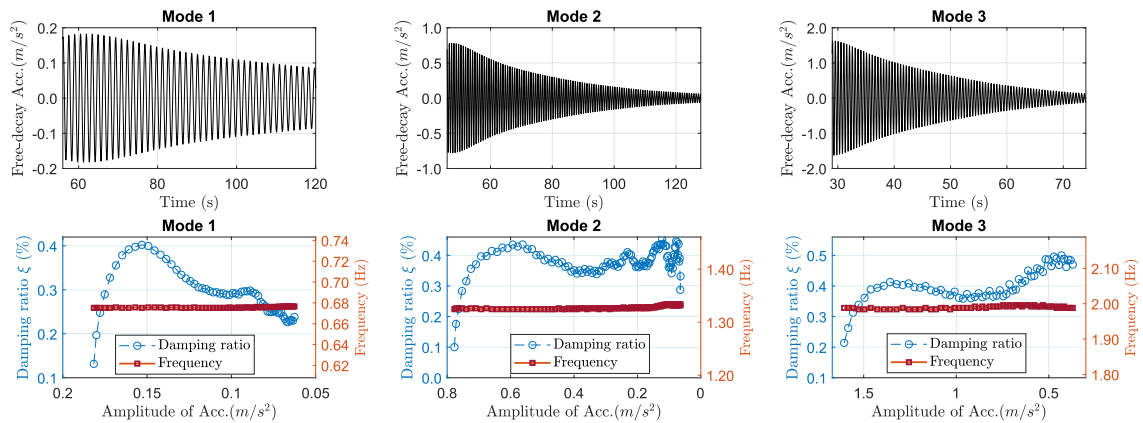


**FIGURE 4. 8.** Amplitude dependency of damping ratios and frequencies of cable C17E.

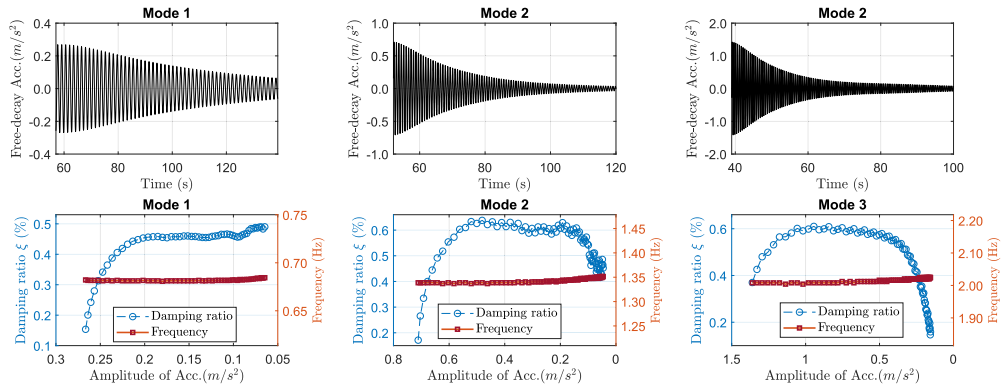


**FIGURE 4. 9.** Amplitude dependency of damping ratios and frequencies of cable C17W.

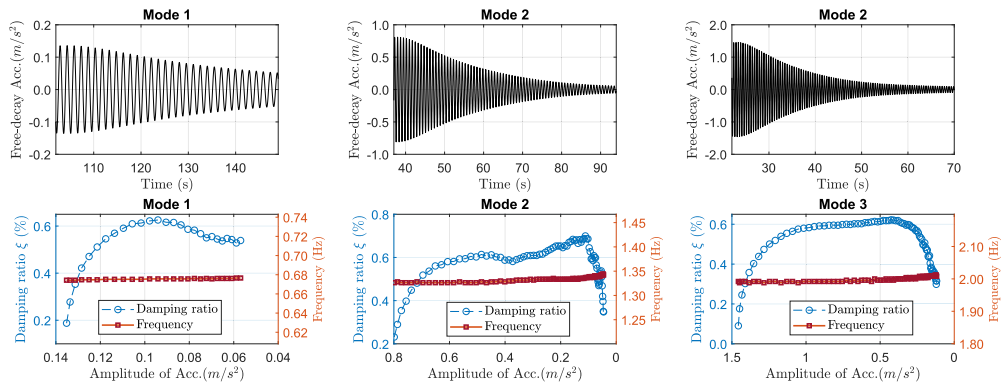


**FIGURE 4. 10.** Amplitude dependency of damping ratios and frequencies of cable C18W.

Figures 4.8, 4.9 and 4.10 illustrate the variation in damping ratios and frequencies versus amplitudes of the free-decay acceleration. Overall, the frequencies are almost unchanged over amplitudes while the amplitude dependency of damping is remarkable. Although the variation in damping is not perfectly consistent, it seems that damping ratios increase first as amplitudes decrease (decay), then damping ratios decrease as amplitudes continuously decrease. To the best knowledge of the authors, this variation in damping can be explained as: the damping generated by High Damping Rubber (HDR) dampers is proportional to dissipated energy and inversely proportional to shear displacement of the rubber in damper<sup>55</sup>; Therefore, when the amplitude is large, the energy is not dissipated anymore (constant), and damping tends to increase as amplitude decreases; on the other hand, when the amplitude is



not large, the dissipation of energy decreases as the amplitude decreases leading to decrease in attainable damping.

#### **4.5. Summary**

In this chapter, the procedure and implementation of damping analysis is performed on full-scale cables of Shinminato Bridge. The cables were installed with HDR damper. Measured damping and measured frequencies were determined based on field measurement data. Theoretical damping is calculated according to the theory presented in Chapter 4. Effect of cable sag was evaluated using Finite Difference Method. The damper effectiveness was computed as a ratio between measured damping and theoretical damping. The conclusions are as follows:

- 1) The reduction of damping ratios due to cable sag was investigated employing the Finite Difference Method (FDM). It showed that cable sag causes a notable reduction of the damping ratio for the mode 1 whereas having almost no effect on the mode 2 and a relatively small reduction for the mode 3. Additionally, cable sag triggered larger reduction of damping in fixed-fixed end cables than that of hinged-hinged end cables.
- 2) The damping analysis of full-scale cables with HDR damper from vibration measurement data was presented. Measured damping ratios were compared to theoretical values, and the results showed that the HDR damper effectiveness was greater than 0.7 for all cables, except for mode 2 (0.66) and mode 3 (0.58) of cable C01E. Moreover, the variation of damping ratios and frequencies versus amplitudes was also investigated. While frequencies were almost unchanged over amplitudes, the damping ratios tended to increase first as amplitudes decreased, then damping ratios decreased as amplitudes continuously decreased.

## Appendix: Finite Difference Method

The Finite Difference Method is modified in this study based on the previous works<sup>16,38</sup>. The original paper<sup>38</sup> presented the vibration of a cable with a viscous damper through FDM. This Appendix shows the FDM modified for a cable with an HDR damper. The schematic diagram is shown in Figure 4.11.

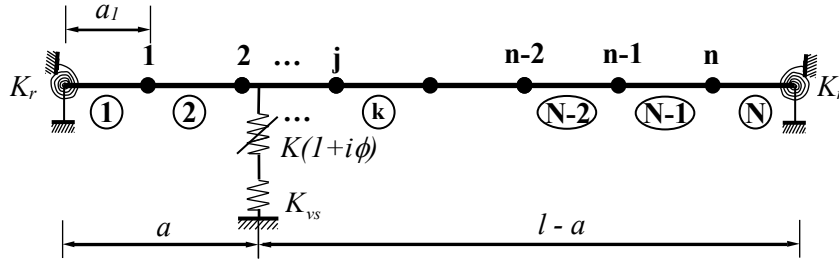


FIGURE 4. 11. Discretized cable with an HDR damper.

A cable is discretized in  $N$  elements with an equal length of  $a_1$  and consists of  $n$  internal nodes ( $n = N - 1$ ). Cable damping ratios and its natural frequencies are determined from the matrix equation<sup>16</sup> of the discretized cable.

$$[K]\{\tilde{v}\} + p[C]\{\tilde{v}\} + p^2[M]\{\tilde{v}\} = 0 \quad (4.3)$$

in which  $[K]$ ,  $[C]$  and  $[M]$  are the stiffness, damping and mass matrices, respectively;  $\{\tilde{v}\}$  is the mode shape vector of the nodal displacements; and  $p = -\xi\omega_0 \pm i\omega_0\sqrt{1 - \xi^2}$  is the complex number related to damping ratio  $\xi$  and undamped natural circular frequency  $\omega_0$ . These matrices have size  $n \times n$ .

The determination of added damping ratios in a cable with an HDR damper is our target and the inherent damping in the cable is neglected. As a result,  $[C]$  is a zero matrix,  $[M]$  is defined as<sup>16</sup>

$$[M] = \begin{bmatrix} m_1 & 0 & 0 & 0 & 0 & 0 \\ 0 & m_2 & 0 & 0 & 0 & 0 \\ 0 & 0 & \dots & 0 & 0 & 0 \\ 0 & 0 & 0 & m_j & 0 & 0 \\ 0 & 0 & 0 & 0 & \dots & 0 \\ 0 & 0 & 0 & 0 & 0 & m_n \end{bmatrix} \quad (4.4)$$

where  $m_j$  is the mass per unit length at node  $j$ .

Stiffness matrix  $[K]$  as

$$[K] = [K_1] + [K_2] + [K_3] \quad (4.5)$$

in which  $[K_1]$  is due to cable bending stiffness  $EI$  and static cable tension  $H$ ;  $[K_2]$  is contributed by a negative stiffness HDR damper; and  $[K_3]$  is due to the additional cable tension which involves with cable sag.

Stiffness matrix  $[K_1]$  as

$$[K_1] = \frac{H}{a_1^2} \left( \frac{1}{\zeta^2} \right) \begin{bmatrix} \alpha n^2 + 2\zeta^2 & -4n^2 - \zeta^2 & n^2 & 0 & 0 & 0 & 0 & 0 & 0 \\ -4n^2 - \zeta^2 & 6n^2 + 2\zeta^2 & -4n^2 - \zeta^2 & n^2 & 0 & 0 & 0 & 0 & 0 \\ n^2 & -4n^2 - \zeta^2 & 6n^2 + 2\zeta^2 & -4n^2 - \zeta^2 & n^2 & 0 & 0 & 0 & 0 \\ 0 & n^2 & -4n^2 - \zeta^2 & 6n^2 + 2\zeta^2 & -4n^2 - \zeta^2 & n^2 & 0 & 0 & 0 \\ 0 & \dots & \dots & \dots & \dots & \dots & \dots & \dots & 0 \\ 0 & 0 & 0 & 0 & n^2 & -4n^2 - \zeta^2 & 6n^2 + 2\zeta^2 & -4n^2 - \zeta^2 & \\ 0 & 0 & 0 & 0 & 0 & n^2 & -4n^2 - \zeta^2 & \alpha n^2 + 2\zeta^2 \end{bmatrix} \quad (4.6)$$

where  $\zeta = l\sqrt{H/EI}$ ; and  $\alpha$  is the boundary condition index which relies on restraint stiffness at cable ends as

$$\alpha = \frac{\lambda^2 (K_r / Ha_1) (a_1 / l)^2 - 2}{\lambda^2 (K_r / Ha_1) (a_1 / l)^2 + 2} + 6 \quad (4.7)$$

For a cable with fixed-fixed ends ( $K_r \rightarrow \infty$ ) or hinged-hinged ends ( $K_r = 0$ ),  $\alpha = 7$  or  $\alpha = 5$ , respectively. Stiffness matrix  $[K_1]$  of these two conventional cases ( $\alpha = 7$  or  $5$ ) was previously introduced by Mehrabi and Tabatabai<sup>16</sup>.

Stiffness matrix  $[K_2]$  as

$$[K_2] = \begin{bmatrix} 0 & 0 & 0 & 0 & 0 & 0 \\ 0 & 0 & 0 & 0 & 0 & 0 \\ 0 & 0 & \dots & 0 & 0 & 0 \\ 0 & 0 & 0 & \left( \frac{K_{vs} K(1+\phi i)}{K_{vs} + K(1+\phi i)} \right) / a_1 & 0 & 0 \\ 0 & 0 & 0 & 0 & \dots & 0 \\ 0 & 0 & 0 & 0 & 0 & 0 \end{bmatrix} \quad (4.8)$$

The matrix  $[K_2]$  contains only one non-zero element with respect to a node where the HDR damper is attached to the cable.

The stiffness matrix  $[K_3]$  is defined as<sup>16</sup>

$$[K_3] = \mathbf{r}\mathbf{s}^T \quad (4.9)$$

where the vector  $\mathbf{r}$  and  $\mathbf{s}$  are obtained as

$$\mathbf{s} = [s_1 \ s_2 \ \dots \ s_i \ \dots \ s_n]^T; s_i = \left( \frac{y_{i+1} - 2y_i + y_{i-1}}{a_1^2} \right) \quad (4.10)$$

$$\mathbf{r} = [r_1 \ r_2 \ \dots \ r_i \ \dots \ r_n]^T; r_i = \frac{s_i}{\sum_{i=1}^n \frac{\left[ \left( \frac{y_{i+1} - y_{i-1}}{2a_1} \right)^2 + 1 \right]^{3/2}}{EA}} \quad (4.11)$$

where  $y$  is the transverse displacement of the cable due to its self-weight; and  $EA$  is the cable axial rigidity.

After solving Eq. (4.3), the complex eigenvalues  $p$  can be found and the damping ratios  $\xi$  can be deduced as

$$\xi = \frac{-\text{Re}(p)}{\sqrt{\text{Re}(p)^2 + \text{Im}(p)^2}} \quad (4.12)$$

## CHAPTER 5. FRAMEWORK FOR ESTIMATION OF CABLE TENSION UNDER LIMITED INFORMATION OF CABLE PROPERTIES BY APPLICATION OF ARTIFICIAL NEURAL NETWORKS (ANNS)

Damping and tension are two important engineering values of stay cables. Studies on damping was illustrated in Chapters 2, 3 and 4. This chapter proposes a framework for estimating tension of stay cables with and without lateral attachments (dampers, crossties) under limited information of cable properties. For a vibration-based cable tension estimation method, cable length, mass per unit length and the first few natural frequencies are most likely available. But the other parameters such as bending stiffness, axial stiffness, cable inclination, rotational restraint stiffness at the cable ends, and lateral components (if any) are often unknown or uncertain. Under limited information of cable parameters, the formulations of cable tension developed in the past seem to fail to estimate tension. Hence, it raises the question of how to identify tension utilizing some available parameters but still accounting for unavailable information. With that concern, this chapter proposes a framework for cable tension estimation via an application of artificial neural networks (ANNs), in which tension is determined using just three parameters (cable length, mass per unit length and measured natural frequencies) in conjunction with unknown parameters mentioned above. The feasibility and robustness of the proposed framework were confirmed through numerical verifications. The proposed framework was applied to estimate tensions in stay cables of Tatara Bridge as a case study of full-scale engineering application. The content written in this chapter has been published by the authors as<sup>56</sup> “Le LX, Siringoringo DM, Katsuchi H, Fujino Y. *Stay cable tension estimation of cable - stayed bridge under limited information on cable properties using artificial neural networks*. Structural Control and Health Monitoring.e3015.”

**Keywords:** Vibration-based cable tension estimation, cable-stayed bridge, artificial neural networks, stay cable lateral attachment, dampers, crossties, finite difference method.

### 5.1. Introduction

Tension and damping of stay cables are usually measured during the construction, regular assessments, and long-term health monitoring<sup>5</sup>. These indicators

would provide owner with useful information about bridge safety, possible damages, structural changes, and deterioration<sup>3,57</sup>. Several methods have been adopted to determine cable tension which can be broadly categorized into the directly and indirectly method. The direct measurement like lift-off test would yield consistent tension values and obtain high accuracy but require massive devices, skillful labor as well as high cost<sup>8</sup>. The indirect measurement by a vibration method<sup>5,8,58,59</sup>, on the other hand, has been widely used to estimate cable force owing to various merits such as simplicity, non-destructive implementations, and relatively inexpensive cost. This makes the indirect measurement by vibration testing favorable for frequent application of stay cable tension estimation.

The reliability of the vibration-based tension estimation method depends highly not only on measured frequencies but also on the analytical relationship between tension and measured frequencies. Numerous studies have been conducted to propose the formulation of cable tension. Tension estimated based on taut string theory<sup>60</sup> is the simplest one where cable tension is estimated using a relationship that includes parameters of cable length, mass per unit length, and the measured natural frequency. Taut-string theory, however, neglects the effect of cable bending stiffness and cable sag. To alleviate that, Irvine & Caughey<sup>15</sup> developed a cable model with sag extensibility but still overlooking cable bending stiffness. In addition, some researchers<sup>5,16,61</sup> have emphasized on the combined effects of the sag and bending stiffness on cable tension. Others have considered restrained boundary conditions at cable ends rather than purely fixed or hinged ends<sup>62,63</sup>. Another point to consider is the lateral attachments like dampers or cross ties attached to cables; stay cables have shown very low inherent damping<sup>26</sup>, thus cross ties<sup>2,27,28</sup> or dampers<sup>18,23,29-31</sup> are often mounted to cables to suppress wind-induced vibration. The presence of the lateral components has made estimation of cable force even more challenging.

Recently, some of emerging optimization algorithms have been adopted to identify not only cable tension but also other parameters like cable bending stiffness, restraint stiffness at cable ends as well as the lateral components (e.g., damper characteristics). The main purpose of the optimization is to minimize the errors between measured and analytical cable frequencies. Kim and Park<sup>32</sup> used the frequency-based sensitivity-updating algorithm (FBSU) to determine tension, bending stiffness and axial stiffness. Ma<sup>33</sup> extended the FBSU for a cable with rotational restraint ends. Zarbaf et al.<sup>34</sup> used Genetic Algorithm (GA) and Particle Swarm Optimization (PSO). Dan et al.<sup>35</sup> also used PSO for the identification of

tension and lateral force components (e.g., additional mass, dampers); however, only tension and damping coefficient were successfully identified with acceptable accuracy. Apart from the above optimization solutions, Zarbaf et al.<sup>36</sup> was among the first to introduce an application of Artificial Neural Networks (ANNs) in estimating tension. In this work, however, cable inclination, restraints at cable ends and lateral components like dampers and cross ties were not incorporated into the cable model.

For a vibration-based cable tension estimation method, cable length, mass per unit length and the first few natural frequencies are most likely available. But the other parameters such as bending stiffness, axial stiffness, cable inclination, rotational restraint stiffness at the cable ends, and lateral components (if any) are often unknown or uncertain. Under limited information of cable parameters, the formulations of cable tension developed in the past seem to fail to estimate tension except for taut-string-theory-based tension formula; the use of this formula, however, oversimplifies cable analysis, triggering the overestimation of tension. It raises the question of how to identify tension utilizing some available parameters but still accounting for unavailable information.

This chapter proposes a framework for estimating tension of stay cables with/without lateral attachments under limited information of cable properties. For stay cables without lateral attachments, tension is estimated using three known parameters, namely cable length, mass per unit length, and measured frequency while still accounting for unknown features like cable bending stiffness, axial stiffness, cable inclination and restraint boundary conditions at the cable ends. The methodology is then extended to stay cables with lateral attachments (dampers, cross ties), whose properties are also considered as unknown parameters. The framework is proposed via the application of back-propagation artificial neural networks (ANNs). The finite difference formulation of the cable model is derived to create datasets for training, validation, and testing in the ANNs scheme. The feasibility and robustness of the proposed framework were confirmed through numerical verifications. Overall, the results indicated that tension in cables without lateral attachments was successfully evaluated using at least two measured frequencies whereas cables with lateral attachments needed at least three measured frequencies to achieve high accuracy. The proposed framework was applied to estimate tensions in stay cables of Tatara Bridge; the results demonstrated that the proposed method could estimate the cable tension with acceptable accuracy.

## 5.2. Methodology and modeling of the stay cable

### 5.2.1. Cable model

Schematic diagram of an inclined cable used in this study is shown in Figure 5.1 with some modifications from the original figure introduced by Fujino and Hoang (2008)<sup>18</sup>. The original one presents an inclined cable with fixed-fixed end, and a single damper is attached to the cable. However, the fixed-fixed or hinged-hinged end conditions are rarely achieved in practice due to finite stiffness of attached components at the cable anchorages (e.g., bearing plates, ring nuts, neoprene rubber bushings). Also, the cable is sometimes installed with more than one damper like stay cables of Tsurumi Tsubasa Bridge in Japan<sup>47</sup>. Therefore, in this study, the modification of the cable mode is made by considering rotational restraints at cable ends as well as several lateral forces. Figure 5.1a shows a cable without lateral supports and Figure 5.1b depicts a complex cable with the existence of lateral forces. The coordinate system is established with  $x$  along the cable chord and  $y$  in the transverse direction.

Cable properties consist of mass per unit length  $m$ , chord length  $l$ , chord tension  $H$ , inclination  $\varphi$ , bending stiffness  $EI$ , axial stiffness  $EA$ , rotational restraint stiffness at cable ends  $K_r$ , and transverse sag at midspan  $d$ . The lateral supports are mounted to the cable at location  $x_d = (x_1, x_2, \dots, x_i)$  and their respective lateral forces are denoted by  $f(t) = (f_1(t), f_2(t), \dots, f_i(t))$ .

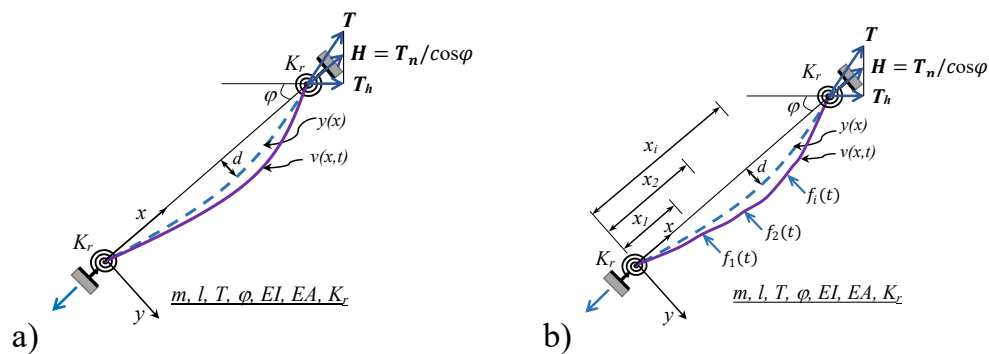


**FIGURE 5. 1.** Schematic diagram: a) cable without lateral components; and b) cable with lateral components (Note: lateral components are dampers and/or cross ties).



### 5.2.2. Case 1: Equation of motion and eigenvalue analysis of cable without lateral attachments

The general form of equation for cable in-plane motion is expressed as<sup>5,18</sup>

$$H \frac{\partial^2 v(x,t)}{\partial x^2} - m \frac{\partial^2 v(x,t)}{\partial t^2} + h(t) \frac{d^2 y(x)}{dx^2} - EI \frac{\partial^4 v(x,t)}{\partial x^4} = 0 \quad (5.1)$$

where  $v(x,t)$  denotes the cable transverse displacement;  $y(x)$  is the cable static profile; and  $h(t)$  denotes the time-dependent additional chord tension due to vibration. For free vibration of cable, the transverse displacement  $v(x,t)$  and the additional tension  $h(t)$  can be described in terms of time-independent and time-dependent parts as

$$v(x,t) = \tilde{v}(x)e^{pt} \quad (5.2)$$

and

$$h(t) = \tilde{h}e^{pt} \quad (5.3)$$

in which  $\tilde{v}(x)$  is the cable mode shape and  $\tilde{h}$  is the time-independent additional chord tension. Note that  $p$  in Eq. (5.2) and Eq. (5.3) is defined as

$$p = i\omega \quad (5.4)$$

where  $\omega$  characterizes undamped natural circular frequency; and  $i^2 = -1$ .

The component  $h(t)$  in Eq. (5.1) can be derived from the elastic and geometric compatibility of a cable element<sup>64</sup>.

$$h(t) = \frac{\int_0^l \frac{\partial u(x,t)}{\partial x} dx + \int_0^l \frac{dy(x)}{dx} \frac{\partial v(x,t)}{\partial x} dx}{\int_0^l \frac{(ds/dx)^3}{EA} dx} \quad (5.5)$$

where  $u(x,t)$  is the longitudinal displacement of cable due to vibration; and  $ds = \sqrt{dx^2 + dy^2}$  is the tangential length of a cable element.

Since cable ends are immovable, the first component in the numerator of Eq. (5.5) is vanished. By inserting  $v(x,t)$  from Eq. (5.2) into Eq. (5.5) and taking the integration by parts of its numerator, Eq. (5.5) becomes

$$h(t) = \frac{-\int_0^l \frac{d^2 y(x)}{dx^2} \tilde{v}(x) dx}{\int_0^l \left[ \left( \frac{dy}{dx} \right)^2 + 1 \right]^{3/2} \frac{dx}{EA}} e^{pt} \quad (5.6)$$

Substitution of Eq. (5.2) and Eq. (5.6) into Eq. (5.1) yields the mode shape equation as

$$EI \frac{d^4 \tilde{v}(x)}{dx^4} - H \frac{d^2 \tilde{v}(x)}{dx^2} + \frac{\int_0^l \frac{d^2 y(x)}{dx^2} \tilde{v}(x) dx}{\int_0^l \left[ \left( \frac{dy}{dx} \right)^2 + 1 \right]^{3/2} \frac{dx}{EA}} \frac{d^2 y(x)}{dx^2} + mp^2 \tilde{v}(x) = 0 \quad (5.7)$$

To solve Eq. (5.7), the modification of the Finite Difference Method (FDM) originally proposed by Mehrabi & Tabatabai<sup>16</sup> is employed. While the original work put forward the vibration of a cable with fixed or hinged end boundary conditions, in this study, we made the modification by adding rotational restraint at cable ends in accordance with the cable model in Figure 5.1. A cable is discretized into  $n$  interior nodes along the chord length with grid size  $a_l$ . The derivatives in the differential equation Eq. (5.7) are replaced by the difference quotients as shown in Figure 5.2.

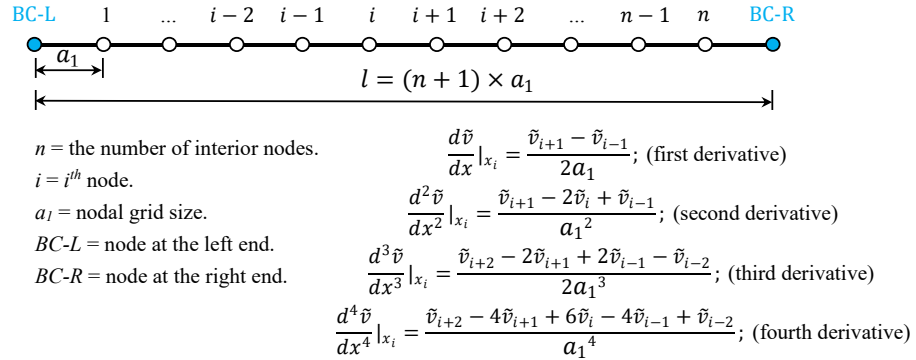


**FIGURE 5. 2.** Finite difference scheme for discretized cable.

The difference quotients are accordingly substituted into Eq. (5.7) to approximate the derivatives, then applying the finite difference approximation with respect to each

interior node (from node 1 to node  $n$ ). As a result, the discretized version of Eq. (5.7) is obtained in the matrix form as

$$[K]_{n \times n} \{\tilde{v}\}_{n \times 1} + p^2 [M]_{n \times n} \{\tilde{v}\}_{n \times 1} = 0 \quad (5.8)$$

where  $[K]_{n \times n}$  is the stiffness matrix;  $[M]_{n \times n}$  is the mass matrix; and  $\{\tilde{v}\}_{n \times 1}$  is the vector of nodal displacements. Inserting  $p$  from Eq. (5.4) into Eq. (5.8) leads to

$$[K]_{n \times n} \{\tilde{v}\}_{n \times 1} - \omega^2 [M]_{n \times n} \{\tilde{v}\}_{n \times 1} = 0 \quad (5.9)$$

Mass matrix  $[M]_{n \times n}$  is derived from the last part of Eq. (5.7)

$$[M]_{n \times n} = \text{diag}\{m_1, m_2, \dots, m_n\} \quad (5.10)$$

where  $m_i$  ( $i$  from 1 to  $n$ ) denotes mass per unit length at node  $i$ . Stiffness matrix  $[K]_{n \times n}$  is defined as

$$[K]_{n \times n} = [K_1]_{n \times n} + [K_2]_{n \times n} \quad (5.11)$$

where  $[K_1]_{n \times n}$  is obtained from the first two parts of Eq. (5.7), and  $[K_2]_{n \times n}$  is determined from the third part of Eq. (5.7). The stiffness matrix  $[K_1]_{n \times n}$  is defined as

$$[K_1]_{n \times n} = \frac{H}{a_1^2} \left( \frac{1}{\zeta^2} \right) \begin{bmatrix} \alpha n^2 + 2\zeta^2 & -4n^2 - \zeta^2 & n^2 & 0 & 0 & 0 & 0 & 0 & 0 \\ -4n^2 - \zeta^2 & 6n^2 + 2\zeta^2 & -4n^2 - \zeta^2 & n^2 & 0 & 0 & 0 & 0 & 0 \\ n^2 & -4n^2 - \zeta^2 & 6n^2 + 2\zeta^2 & -4n^2 - \zeta^2 & n^2 & 0 & 0 & 0 & 0 \\ 0 & n^2 & -4n^2 - \zeta^2 & 6n^2 + 2\zeta^2 & -4n^2 - \zeta^2 & n^2 & 0 & 0 & 0 \\ 0 & \dots & \dots & \dots & \dots & \dots & \dots & \dots & 0 \\ 0 & 0 & 0 & 0 & n^2 & -4n^2 - \zeta^2 & 6n^2 + 2\zeta^2 & -4n^2 - \zeta^2 & \\ 0 & 0 & 0 & 0 & 0 & n^2 & -4n^2 - \zeta^2 & \alpha n^2 + 2\zeta^2 \end{bmatrix}_{n \times n} \quad (5.12)$$

where  $\zeta = l\sqrt{H/EI}$  is the nondimensional parameter of cable bending stiffness; and  $\alpha$  is the index of boundary conditions. Note that each row of the matrix corresponds to each node, such that row one is written for node 1.

$$\alpha = \frac{\zeta^2 (K_r / Ta_1)(a_1 / l)^2 - 2}{\zeta^2 (K_r / Ta_1)(a_1 / l)^2 + 2} + 6 \quad (5.13)$$

The derivation of the stiffness matrix  $[K_1]_{n \times n}$  and the index of boundary conditions  $\alpha$  is detailed in the Appendix. It can be easily verified that the index of boundary condition  $\alpha = 5$  or  $7$  when  $K_r = 0$  (hinged ends) or  $K_r \rightarrow \infty$  (fixed ends), respectively. For these conventional cases ( $\alpha = 5$  or  $7$ ), matrix  $[K_1]_{n \times n}$  is the same as the stiffness matrix derived in the original paper by Mehrabi & Tabatabai<sup>16</sup>.

Stiffness matrix  $[K_2]_{n \times n}$  due to cable sag is obtained as<sup>16</sup>

$$[K_2]_{n \times n} = \mathbf{r} \mathbf{s}^T \quad (5.14)$$

where

$$\mathbf{s} = \{s_1 \ s_2 \dots \ s_i \dots \ s_n\}^T; s_i = \left( \frac{y_{i+1} - 2y_i + y_{i-1}}{a_1^2} \right) \quad (5.15)$$

$$\mathbf{r} = \{r_1 \ r_2 \dots \ r_i \dots \ r_n\}^T; r_i = \frac{s_i}{\sum_{i=1}^n \left[ \left( \frac{y_{i+1} - y_{i-1}}{2a_1} \right)^2 + 1 \right]^{3/2}} EA \quad (5.16)$$

in which  $y_i$  represents the static profile of cable at node  $i$ ; static profile of cable  $y$  is obtained from the differential equation of cable under its self-weight.

$$[K_s]_{n \times n} \{y_s\}_{n \times 1} = \{M_s\}_{n \times 1} \quad (5.17)$$

In Eq. (5.17),  $\{M_s\}_{n \times 1} = \{m_1 g \cos \varphi \ m_2 g \cos \varphi \dots \ m_n g \cos \varphi\}^T$  is the vector of cable self-weight in the in-plane transverse direction. After completing the matrices ( $[K]_{n \times n}$  and  $[M]_{n \times n}$ ), Eq. (5.9) can be solved to determine the  $k^{th}$  circular natural frequency  $\omega_k$ ; the natural frequency  $f_k$  of the cable then can be deduced as  $f_k = \omega_k / (2\pi)$ .

### 5.2.3. Case 2: Equation of motion and eigenvalue analysis of cable with lateral attachments

Dampers and cross ties are considered as the lateral attachments of the cable, installed at locations  $x_d = \{x_1, x_2, \dots, x_i\}$  as shown in Figure 5.1b. In this study, two types of dampers, namely viscous damper and High Damping Rubber (HDR) damper are selected because they are widely used for the vibration control of cables, especially in Japan<sup>9</sup>. The performance characteristic of a viscous damper is defined by damper coefficient  $c$  while an HDR damper is characterized by the spring stiffness factor  $K$  and loss factor of rubber material  $\phi$ . Figure 5.3 displays the schematic diagram of viscous and HDR dampers;  $v(x_d, t)$  is the displacement of the cable at the damper location  $x_d$ . The cable-crosstie system is more complicated than the cable-damper system, and they are often modelled as rigid links<sup>65,66</sup> or non-rigid connections<sup>66,67</sup> like elastic springs. Because the latter is more realistic, the cross tie in this study is also simplified as a non-rigid lateral support with elastic stiffness  $K_{cr}$ .

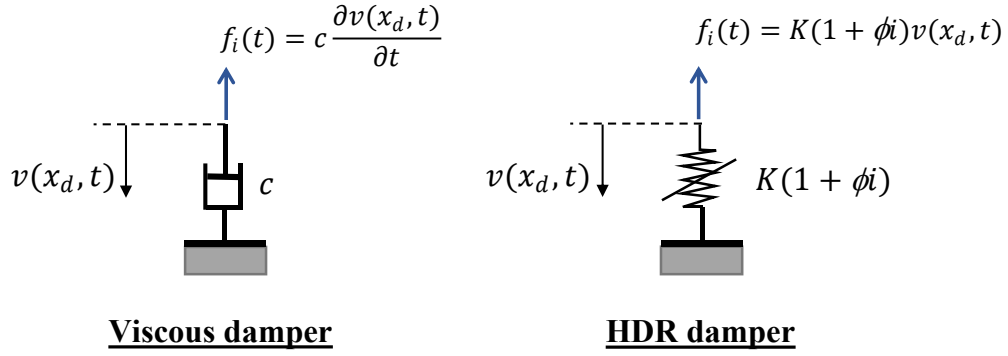


**FIGURE 5.3.** Viscous damper and HDR damper.

In the presence of the damper forces  $f_i(t)$ , the cable's equation of motion Eq. (5.1) is re-written in accordance with the cable model in Figure 5.1b.

$$H \frac{\partial^2 v(x,t)}{\partial x^2} - m \frac{\partial^2 v(x,t)}{\partial t^2} + h(t) \frac{d^2 y(x)}{dx^2} - EI \frac{\partial^4 v(x,t)}{\partial x^4} = f_i(t) \delta(x - x_d) \quad (5.18)$$

where  $\delta(x - x_d)$  denotes the Dirac delta function; and  $f_i(t)$  denotes concentrated damper forces. Note that the concentrated loads at damper locations create discontinuity in Eq. (5.1) at the damper locations. By using Dirac delta function to represent the concentrated load, Eq. (5.18) is valid throughout the entire length of the cable and its solution still has the same form as the Eq. (5.2), such that  $v(x, t) = \tilde{v}(x)e^{pt}$  and  $h(t) = \tilde{h}e^{pt}$ . However, the complex number  $p$  is now re-written for damped system instead of undamped cable:

$$p = -\xi\omega \pm i\omega\sqrt{1 - \xi^2} \quad (5.19)$$

where  $\xi$  characterizes the damping ratio; and  $\omega\sqrt{1 - \xi^2}$  is the damped natural angular frequency.

Substitution of damper forces into Eq. (5.18) gives

$$H \frac{\partial^2 v(x,t)}{\partial x^2} - m \frac{\partial^2 v(x,t)}{\partial t^2} + h(t) \frac{d^2 y(x)}{dx^2} - EI \frac{\partial^4 v(x,t)}{\partial x^4} = \left[ c \frac{\partial v(x_d, t)}{\partial t} \delta(x - x_d) + K(1 + \phi i)v(x_d, t) \delta(x - x_d) \right] \quad (5.20)$$

Making use of  $v(x, t) = \tilde{v}(x)e^{pt}$  and  $h(t)$  from Eq. (5.6), Eq. (5.20) becomes

$$EI \frac{d^4 \tilde{v}(x)}{dx^4} - H \frac{d^2 \tilde{v}(x)}{dx^2} + \frac{\int_0^l \frac{d^2 y(x)}{dx^2} \tilde{v}(x) dx}{\int_0^l \left[ \left( \frac{dy}{dx} \right)^2 + 1 \right]^{3/2} dx} \frac{d^2 y(x)}{dx^2} + mp^2 \tilde{v}(x) + \left[ cp \tilde{v}(x_d) \delta(x - x_d) + K(1 + \phi i) \tilde{v}(x_d) \delta(x - x_d) \right] = 0 \quad (5.21)$$

The concentrated elements  $c\delta(x - x_d)$  and  $K(1 + \phi i)\delta(x - x_d)$  are transformed into distributed parts before writing the finite difference approximations for Eq. (5.21). Dirac delta function can be presented by a cosine approximation, a piecewise cubic function, a linear hat function hat<sup>68</sup>, etc. For the simplicity, the piecewise linear hat function is adopted in this study to distribute the concentrated  $c$  and  $K(1 + \phi i)$  over the cable length. Figure 5.4 shows the distributed damper coefficients.

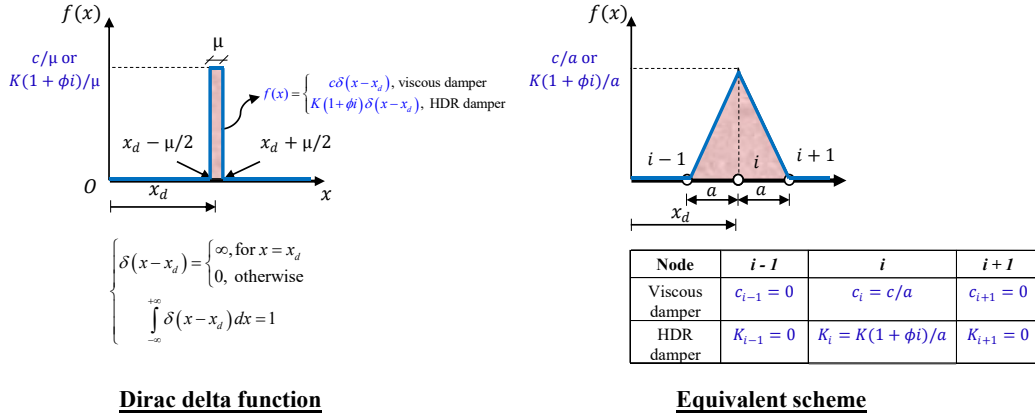


**FIGURE 5.4.** Distributed damper coefficient over cable length.

After distributing damper coefficients over the cable's length, Eq. (5.21) can be discretized using the finite difference method as in the case 1. The matrix form of Eq. (5.21) is

$$[K]_{n \times n} \{\tilde{v}\}_{n \times 1} + p[C]_{n \times n} \{\tilde{v}\}_{n \times 1} + p^2[M]_{n \times n} \{\tilde{v}\}_{n \times 1} = 0 \quad (5.22)$$

where

$$[K]_{n \times n} = [K_1]_{n \times n} + [K_2]_{n \times n} + [K_3]_{n \times n} \quad (5.23)$$

It is noted that  $[M]_{n \times n}$ ,  $[K_1]_{n \times n}$ , and  $[K_2]_{n \times n}$  are the same as in Eq. (5.10), Eq. (5.12), and Eq. (5.14), respectively. Stiffness matrix  $[K_3]_{n \times n}$  is the additional

stiffness due to the presence of HDR damper, which is derived from the second part inside the square brackets in Eq. (5.21). Based on the equivalent scheme of the distributed HDR damper coefficient in Figure 5.4, the diagonal stiffness matrix  $[K_3]_{n \times n}$  contains only one non-zero element at the node where the HDR damper is attached to, and the matrix  $[K_3]_{n \times n}$  can be defined as:

$$[K_3]_{n \times n} = \text{diag}\{0, 0, \dots, K(1 + \phi i) / a_1, \dots, 0\} \quad (5.24)$$

The damping matrix  $[C]_{n \times n}$  is derived from the first component inside the square brackets of Eq. (5.21), which is related to viscous damper. Similarly, matrix  $[C]_{n \times n}$  will have only one non-zero component at the node of the viscous damper location and zeros elsewhere, so that:

$$[C]_{n \times n} = \text{diag}\{0, 0, \dots, c / a_1, \dots, 0\} \quad (5.25)$$

Noting that if several viscous dampers or HDR dampers are installed, Eq. (5.24) and Eq. (5.25) can be further modified by adding distributed damper coefficients  $c/a_1$  or  $K(1 + \phi i)/a_1$  to the nodes where dampers are attached to.

If the cable is equipped with the cross ties (stiffness  $K_{cr}$ ), an additional stiffness matrix  $[K_4]_{n \times n}$  due to cross ties will be added to Eq. (5.23). Stiffness matrix  $[K_4]_{n \times n}$  takes the same form as  $[K_3]_{n \times n}$  in Eq. (5.24), just replacing  $K(1 + \phi i)$  by  $K_{cr}$ . To solve the eigenfrequencies, Eq. (5.22) is re-formed as

$$\begin{bmatrix} [K]_{n \times n} & 0 \\ 0 & [I]_{n \times n} \end{bmatrix}_{2n \times 2n} \begin{Bmatrix} \{\tilde{v}\}_{n \times 1} \\ p\{\tilde{v}\}_{n \times 1} \end{Bmatrix}_{2n \times 1} + p \begin{bmatrix} [C]_{n \times n} & [M]_{n \times n} \\ -[I]_{n \times n} & 0 \end{bmatrix} \begin{Bmatrix} \{\tilde{v}\}_{n \times 1} \\ p\{\tilde{v}\}_{n \times 1} \end{Bmatrix}_{2n \times 1} = 0 \quad (5.26)$$

in which  $[I]_{n \times n}$  is the identity matrix. By solving Eq. (5.26) the complex eigenfrequencies  $p_k$  at mode  $k$  can be found. The cable natural circular frequencies then can be accordingly deduced using Eq. (5.19)

$$\omega_k = \sqrt{(\text{Re}[p_k])^2 + (\text{Im}[p_k])^2} \quad (5.27)$$

Natural frequency  $f_k$  at mode  $k$  is  $f_k = \omega_k / (2\pi)$ .

### 5.3. Application of ANNs for cable tension estimation with unknown cable parameters

A framework for the vibration-based cable tension estimation, which accounts for cable unknown parameters, is proposed in this section using an application of Artificial Neural Networks (ANNs). ANNs are a computational modelling tools with

the utilization in solving many real-world problems, of which the models are complex and difficult to be traditionally addressed<sup>69</sup>. There have been many applications of the neural networks in civil engineering, e.g., optimization<sup>70</sup>, structural system identification<sup>71</sup>, etc. In fact, the ANNs are the architecture of fully connected neural networks which are composed of an input layer, an output layer, and hidden layers. Information from the input layer will pass through neurons in hidden layers to the output layer via an activation function and weights. In this study, the user interface of MATLAB's Neural Network Toolbox (R2019a), namely neural net fitting is used for implementing ANNs; the Levenberg-Marquardt backpropagation training algorithm is used; the Levenberg-Marquardt algorithm is known as a solver to tackle the least squares problems by minimizing the square of errors of data points<sup>72</sup>, and it results in faster and better performance in training than others<sup>73</sup>. Figure 5.5 describes three steps of the proposed framework.

**Step 1. Generate datasets:** Cable length  $l$  and mass per unit length  $m$  are set to be known parameters. Other parameters including cable tension  $H$ , bending stiffness  $EI$ , axial stiffness  $EA$ , cable inclination  $\varphi$ , rotational restraints at cable ends  $K_r$ , and information of lateral components  $(x_d, c, K, \phi, K_{cr})$  are considered as the unknowns. Each of these unknown elements will be randomly generated into  $\gamma$  datapoints from lower bound (LB) to upper bound (UB). Afterwards, the known and unknown parameters are combined to create  $\gamma$  sets of data, where each set of data will contain a full description of the cable parameters  $(l, m, H, EI, EA, \varphi, K_r, x_d, c, K, \phi, K_{cr})$ . The natural frequencies  $f_k$  of the cable with respect to each dataset are computed using Eq. (5.9) or Eq. (5.22) depending on whether the cable has lateral attachments or not.

**Step 2. Training, validation and testing of datasets with ANNs:** Cable length  $l$ , mass per unit length  $m$ , generated tension  $H$  and computed natural frequencies  $f_k$  from step 1 are grouped into matrices of numeric input and numeric output as Eq. (5.28a) and Eq. (5.28b), respectively. The input matrix has  $l$ ,  $m$ , and  $f_k$ , while the output contains  $H$ .

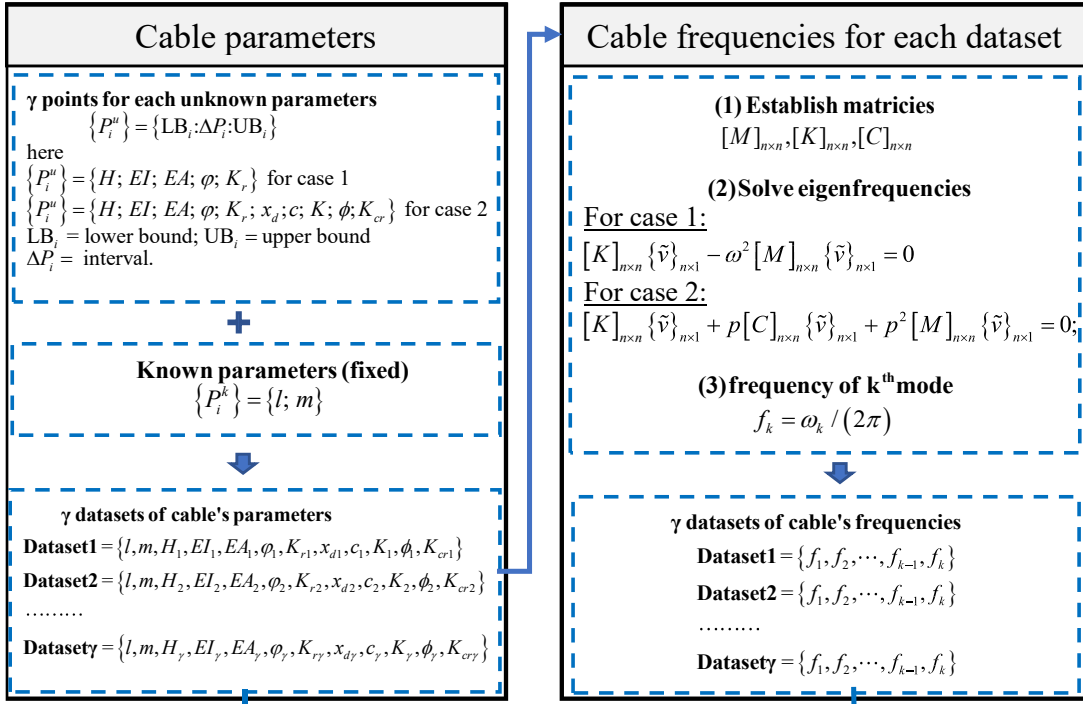
It is noted that other parameters of cable and lateral attachments do not appear in the input layer because these components are considered as the unknowns. It is worth mentioning again that natural frequencies embedded in the input matrix are computed from a full description of cable parameters.



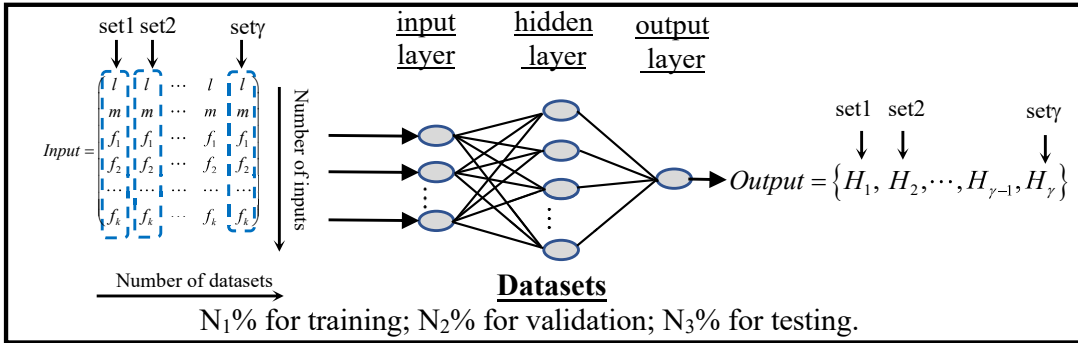
$$Input = \begin{pmatrix} l & l & \cdots & l & l \\ m & m & \cdots & m & m \\ f_1 & f_1 & \cdots & f_1 & f_1 \\ f_2 & f_2 & \cdots & f_2 & f_2 \\ \cdots & \cdots & \cdots & \cdots & \cdots \\ f_k & f_k & \cdots & f_k & f_k \end{pmatrix}_{(k+2) \times \gamma} ; Output = (H_1, H_2, \cdots, H_{\gamma-1}, H_\gamma)_{1 \times \gamma} \quad (5.28a,b)$$

ANNs are utilized to map datasets from input to output. What lies at the root of this mapping is to pinpoint the relationship between input and output. In other words, to find a roadmap between input and output. After successfully mapped, the trained mode is ready to use to estimate cable tension (output). The datasets are divided into  $N_1\%$  for training,  $N_2\%$  for validation, and  $N_3\%$  for testing. Again, the procedures of training, validation and testing in this study are implemented in the MATLAB's Neural Network Toolbox (R2019a).

### Step 1: Generate Datasets



### Step 2: Training, Validation and Testing in ANNs



### Step 3: Use Trained ANNs to Estimate Cable Tension

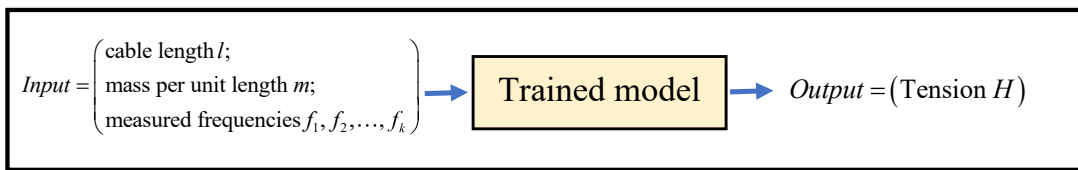


**FIGURE 5. 5.** Framework of vibration-based cable tension estimation with ANNs.

To evaluate the performance of training a network, three assessment indicators are used, namely correlation coefficient ( $R < 1$ ), Mean Absolute Percentage Error (MAPE), and Root Mean Square Error (RMSE) and they are defined respectively as:

$$R = \left( \frac{\sum_{i=1}^N (H_{pred,i} - \bar{H}_{pred})(H_{targ,i} - \bar{H}_{targ})}{\sqrt{\sum_{i=1}^N (H_{pred,i} - \bar{H}_{pred})^2 \sum_{i=1}^N (H_{targ,i} - \bar{H}_{targ})^2}} \right) \quad (5.29)$$

$$MAPE = \left[ \frac{1}{N} \sum_{i=1}^N \left| \frac{H_{targ,i} - H_{pred,i}}{H_{targ,i}} \right| \right] \times 100 \quad (5.30)$$

$$RMSE = \sqrt{\frac{1}{N} \sum_{i=1}^N (H_{targ,i} - H_{pred,i})^2} \quad (5.31)$$

In the above equations,  $N$  is the number of data points;  $H_{pred,i}$  and  $H_{targ,i}$  are the predicted and targeted tensions of the  $i^{th}$  data point, respectively; and  $\bar{H}_{pred}$ ,  $\bar{H}_{targ}$  are their respective averages. It is noted that the targeted tensions  $H_{targ,i}$  are the values in Eq. (5.28b) while the predicted tensions  $H_{pred,i}$  are obtained by training networks with datasets in the input.

**Step 3. Use trained ANNs model to estimate cable tension:** After completing step 2, a well-trained model is created. In other words, a relationship between the input and output is created. Therefore, one can obtain the cable tension  $H$  by importing three available features (length, mass per unit length and measured frequencies) into the trained model.

#### 5.4. Numerical verifications

Four cables are selected in the verifications. The selection of the cables was based on the sag-extensibility  $\lambda^2$  parameter (Irvine & Caughey<sup>15</sup>) and the bending stiffness parameter  $\zeta = l\sqrt{H/EI}$  (Zui et al.<sup>5</sup>).

$$\lambda^2 = \left( \frac{mgl \cos \varphi}{H} \right)^2 \frac{l}{HL_e / EA}; L_e \approx l \left[ 1 + \frac{1}{8} \left( \frac{mgl \cos \varphi}{H} \right)^2 \right] \quad (5.32)$$

Large  $\lambda^2$  means large sag effect, and vice versa; large  $\zeta$  means small effect of bending stiffness, and vice versa. Mehrabi & Tabatabai<sup>16</sup> stated that stay cables with  $\lambda^2 < 3.1$  and  $\zeta > 50$  cover 95% of cables in the cable-stayed bridges around the world. With that, four typical cables were selected as: cable C01 (small sag  $\lambda^2 = 0.1$ , and small bending stiffness  $\zeta = 605$ ); cable C02 (small sag  $\lambda^2 = 0.1$  and large

bending stiffness  $\zeta = 50$ ); cable C03 (moderate sag  $\lambda^2 = 1.41$  and moderate bending stiffness  $\zeta = 100$ ); and cable C04 (large sag  $\lambda^2 = 3.1$  and large bending stiffness  $\zeta = 50$ ). Table 5.1 summarizes properties of the four selected cables in the verifications.

**TABLE 5. 1.** Cable properties

No.	$l$ (m)	$H$ (kN)	$m$ (kg/m)	$\varphi$ (°)	$EA$ (N)	$EI$ (N.m <sup>2</sup> )	$K_r$ (N.m/rad)	$\lambda^2$	$\zeta$
C01	100	1069.76	78.30	30	2.77E+07	2.92E+04	1.00E+04	0.10	605
C02	100	12947.14	78.30	30	4.90E+10	5.18E+07	1.00E+05	0.10	50
C03	100	1723.83	78.30	30	1.63E+09	1.72E+06	1.00E+06	1.41	100
C04	100	2325.26	78.30	30	8.81E+09	9.30E+06	1.00E+07	3.10	50

#### 5.4.1. Verification 1: Cable without lateral attachments

The natural frequencies of the cables in Table 5.1 are calculated using Eq. (5.9) and shown in Table 5.2. Each cable is discretized into 200 interior nodes. This number of nodes is chosen based on the frequency convergence against number of nodes as can be seen in Figure 5.6.

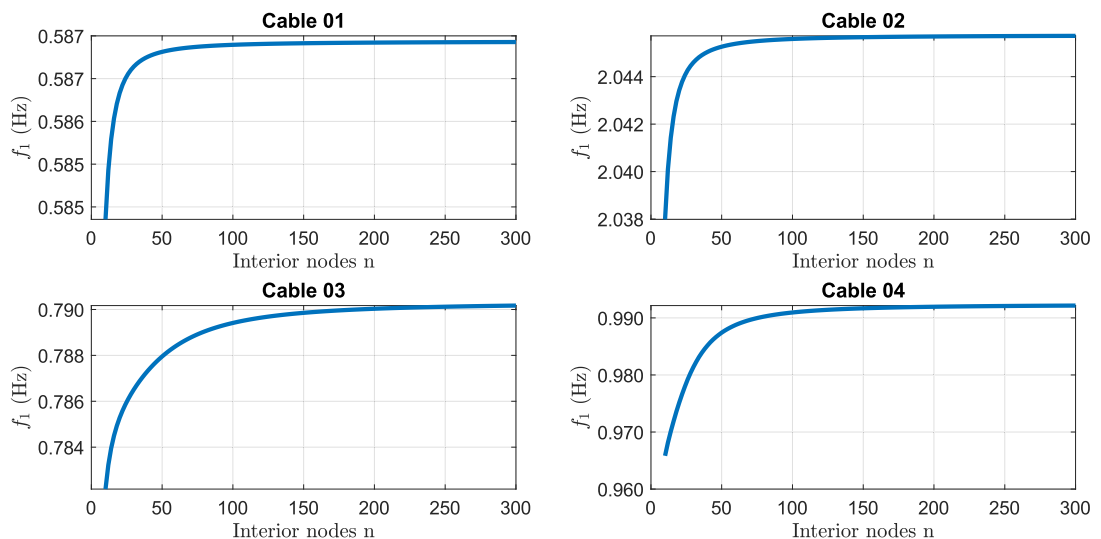


**FIGURE 5. 6.** Convergence of cable fundamental frequency versus the number of interior nodes.

**TABLE 5. 2.** Natural frequencies of the cables without lateral supports

No.	Natural frequencies of cables from Mode 1 to Mode 8							
	$f_1$ (Hz)	$f_2$ (Hz)	$f_3$ (Hz)	$f_4$ (Hz)	$f_5$ (Hz)	$f_6$ (Hz)	$f_7$ (Hz)	$f_8$ (Hz)
<b>C01</b>	0.587	1.169	1.754	2.338	2.923	3.508	4.092	4.677
<b>C02</b>	2.046	4.099	6.207	8.383	10.65	13.026	15.529	18.174
<b>C03</b>	0.790	1.497	2.253	3.012	3.781	4.559	5.351	6.156
<b>C04</b>	0.992	1.785	2.709	3.649	4.637	5.667	6.755	7.900

In the verification, we assumed that the four cables in Table 5.1 were existing cables, and we only know cable length  $l$ , mass per unit length  $m$  with values shown in Table 5.1. In addition, we assumed that the frequencies of the cables  $f_k$  were available from measurement as listed in Table 5.2. Other parameters ( $EI$ ,  $EA$ ,  $\varphi$ ,  $K_r$ ) were unknown. Cable tensions  $H$  were estimated using the three known parameters and regardless of the other unknown components. The estimated tensions by ANNs then compared with exact tensions  $H$  in Table 5.1 for the verification.

As mentioned in Section 5.3, the first step was to generate datasets.  $EI$ ,  $EA$ ,  $\varphi$ ,  $K_r$  and  $H$  were generated from lower bound to upper bound [ $LB$ :  $UB$ ] and then combined with the known features ( $l$ ,  $m$ ). In this verification,  $LB$  and  $UB$  were set to be 50% lower and 50% higher than their exact values, respectively. The ranges of datasets are presented in Table 5.3.

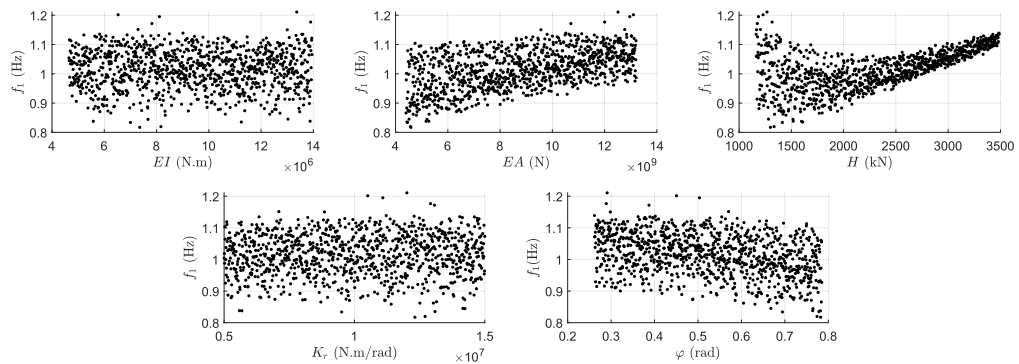
**TABLE 5. 3.** Ranges of cable parameters used in generating datasets

No.	Unknown parameters										Known parameters	
	$EI$ (N.m <sup>2</sup> )		$EA$ (N)		$K_r$ (N.m/rad)		$H$ (kN)		$\varphi$ (°)		$l$ (m)	$m$ (kg/m)
	LB	UB	LB	UB	LB	UB	LB	UB	LB	UB		
<b>C01</b>	1.46E+4	4.38E+4	1.38E+7	4.15E+7	5.00E+3	1.50E+4	5.35E+2	1.60E+3	15.0	45.0	100.0	78.30
<b>C02</b>	2.59E+7	7.77E+7	2.5E+10	7.4E+10	5.00E+4	1.50E+5	6.47E+3	1.94E+4	15.0	45.0	100.0	78.30
<b>C03</b>	8.62E+5	2.59E+6	8.16E+8	2.45E+9	5.00E+5	1.50E+6	8.62E+2	2.59E+3	15.0	45.0	100.0	78.30
<b>C04</b>	4.65E+6	1.40E+7	4.40E+9	1.32E+10	5.00E+06	1.50E+7	1.16E+3	3.49E+3	15.0	45.0	100.0	78.30

Note: LB = lower bound; UB = upper bound.

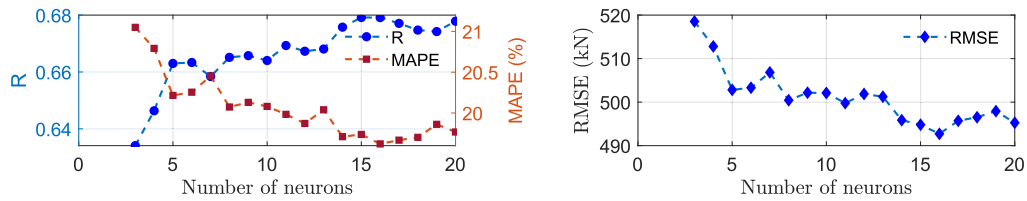
Range of each unknown parameter in Table 5.3 was generated into 1000 data points (interval of 0.1% of exact value), randomly shuffled, then combined with  $l$  and  $m$  to establish 1000 complete sets of data. Each set had a full description of cable parameters ( $EI$ ,  $EA$ ,  $K_r$ ,  $H$ ,  $\varphi$ ,  $l$ ,  $m$ ). Natural frequencies of cable in each set were then determined using Eq. (5.9).

Figure 5.7, as an example, plots the scatters of the fundamental frequency of 1000 data points against the cable properties for cable C04. It is noted that although some data points are unrealistic owing to the random combinations of the cable parameters, they are not faulty.



**FIGURE 5. 7.** Fundamental frequencies of cable C04 against cable properties.

The second step is training, validating, and testing in ANNs. Input and output were prepared before training, validation, and testing. Input composed of known parameters ( $l$ ,  $m$ ,  $f_1$ ,  $f_2$ , ...,  $f_k$ ). Output presented targeted tensions  $H$ . The input was then mapped to the output using the ANNs. Noting that, the input and output were prepared in the form of numeric matrices as Eq. (5.28a) and (5.28b), respectively. Datasets were then separated into three packages: for training (70% datasets), validation (15% datasets) and testing (15% datasets). In this study, the number of neurons in the hidden layer was set to be 15; using more than 15 neurons did not noticeably increase the training performance (R, MAPE, RMSE) as can be seen in Figure 5.8 which is plotted for the cable C04 as an example.



**FIGURE 5. 8.** Performance of training in ANNs versus number of neurons.

Because the training in ANNs was a random process, they were conducted 30 times independently, and the results were the average of 30 times. Figure 5.9 displays the mapping performance (R, MAPE, RMSE) between the input and the output. Overall, the increase in the number of used frequencies (more features in input) results in higher performance of training a network. Interestingly, the mapping became consistently good when at least two natural frequencies were simultaneously used for training. For instance,  $R > 0.999$  and  $MAPE < 1.5\%$  for all cables when two frequencies were used. In addition, using more than two frequencies did not significantly raise the training performance.

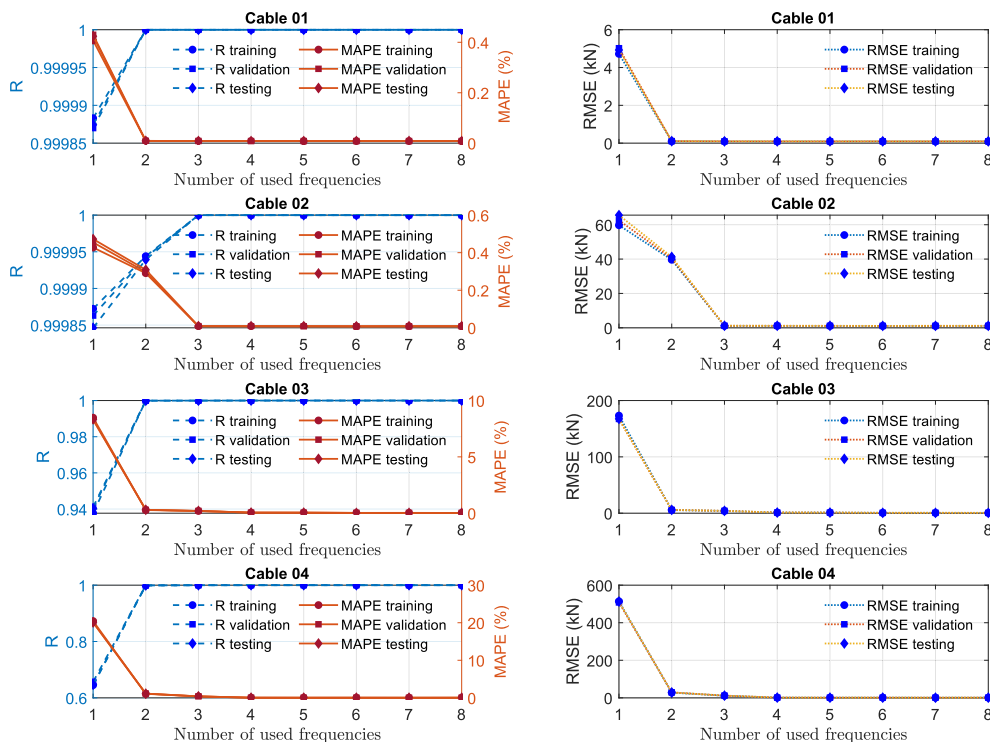


**FIGURE 5. 9.** R, MAPE and RMSE of training, validation and testing in ANNs for cables without lateral attachments.

When only the fundamental frequency  $f_1$  was utilized, cables C01 and C02 still achieved relatively good performance ( $R > 0.99$  and  $MAPE < 0.5\%$ ) whereas cable C03 ( $R \approx 0.94$  and  $MAPE \approx 9\%$ ) resulted in lower training quality and even worse for cable C04 ( $R \approx 0.65$  and  $MAPE \approx 20\%$ ). This happened because cables C01 and C02 have small sag parameter while cables C03 and C04 have moderate and large sag parameters, respectively; cable sag has been proved to have significant influence on the first cable vibration mode<sup>1</sup>.

Figure 5.10 illustrates the scatters between estimated tensions and the targeted tensions for cable C04 as an example with respect to three scenarios of the input: scenario 1 ( $l, m, f_1$ ), scenario 2 ( $l, m, f_1, f_2$ ), and scenario 3 ( $l, m, f_1, f_2, f_3$ ). It is evident that cable C04 had poor training quality when input contained only 3 features like in the scenario 1, this performance was greatly improved with the increase in the number of used frequencies. Recall that the estimated tensions in Figure 5.10 were the values determined from training in ANNs with the given input whereas targeted tensions were the values that the input headed to. After successfully trained, the trained ANN model is used for estimating tension with the measured frequencies.

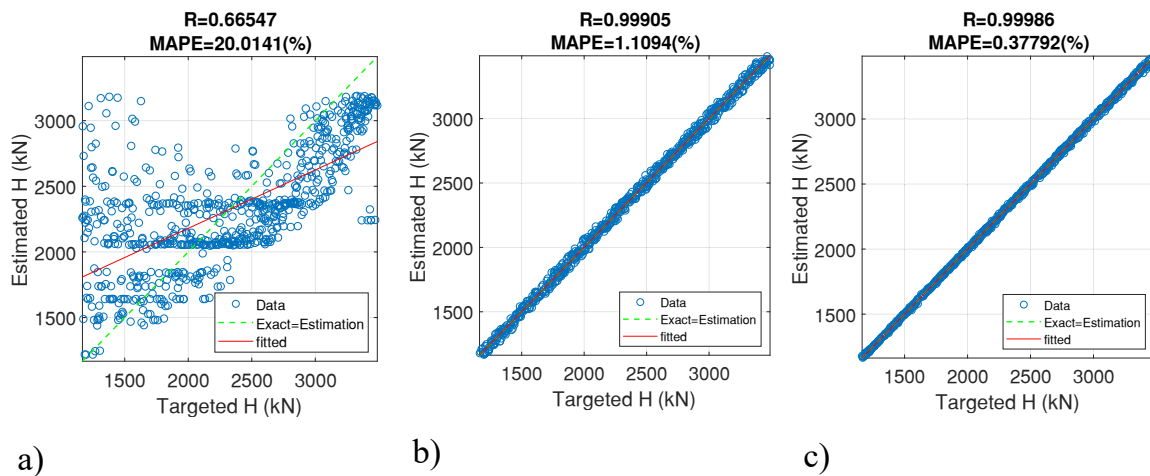


**FIGURE 5. 10.** Scatters between estimated and targeted tensions with different input scenarios: a) scenario 1 ( $l, m, f_1$ ); b) scenario 2 ( $l, m, f_1, f_2$ ); and, c) scenario 3 ( $l, m, f_1, f_2, f_3$ ).

In step 3, the trained model was employed to estimate cable tension. Importing two cable properties ( $l, m$ ) in Table 6.1 and frequencies  $f_k$  in Table 5.2 into the trained ANN model, tension in each cable is estimated and compared with exact tension  $H$ . The results are shown in Table 5.4. When only natural frequency  $f_1$  was available, the



absolute errors of tension were large, namely 5.17% and 10.8% for cables C03 and C04, respectively. In contrast, cable C01 and C02 still obtained a high accuracy. On condition that natural frequencies of the higher modes are available, the errors between the exact and estimated tensions were relatively small, less than 0.2% for all cables.

**TABLE 5. 4.** Estimated tension by ANNs for cables without lateral attachments

No.	Exact <i>H</i> (kN)	Tension <i>H</i> based on trained ANN model (kN)							
		Increasing number of used frequencies							
		1	2	3	4	5	6	7	8
C01	1069.75	1069.94 (0.02%)	1069.84 (0.01%)	1069.91 (0.01%)	1070.14 (0.04%)	1069.93 (0.02%)	1070.12 (0.03%)	1070.11 (0.03%)	1069.94 (0.02%)
C02	12947.14	12952.11 (0.04%)	12950.80 (0.03%)	12947.50 (0.00%)	12947.03 (0.00%)	12946.50 (0.00%)	12944.88 (-0.02%)	12945.90 (-0.01%)	12945.71 (-0.01%)
C03	1723.83	1634.67 (-5.17%)	1725.43 (0.09%)	1725.63 (0.10%)	1724.99 (0.07%)	1724.96 (0.07%)	1725.13 (0.08%)	1725.05 (0.07%)	1725.18 (0.08%)
C04	2325.26	2074.68 (-10.8%)	2328.35 (0.13%)	2327.42 (0.09%)	2323.10 (-0.09%)	2323.15 (-0.09%)	2323.36 (-0.08%)	2323.45 (-0.08%)	2323.59 (-0.07%)

Note: (·) denotes the error between estimated and exact tensions.

Usually, when only information on the length, mass per unit length and measured frequencies available, tension identified by taut-string theory<sup>60</sup>.

$$H = \frac{1}{N} \sum_{k=1}^N 4ml^2 \left( \frac{f_k}{k} \right)^2 \quad (5.33)$$

where  $f_k$  is the natural frequency of cable at mode  $k$ ; and  $N$  is the number of consecutive vibration modes. The results are shown in Table 5.5.

The results in Table 5.5 demonstrate that for a cable with small bending stiffness and small sag parameters like cable C01, tension was successfully calculated with relatively small errors, less than 1.0%. This is understandable because sag and bending stiffness are neglected in string theory. However, taut-string theory failed to accurately estimate tension of cables with either moderate or significant influences of sag/bending stiffness such as cable C02, C03, and C04, that resulted in unaccepted errors. Furthermore, bending stiffness caused larger errors in higher modes (e.g., C02) whereas significant sag extensibility triggered large errors in the lower modes

(e.g., C03 and C04). By comparing the results in Tables 5.4 and 5.5, it is fair to say that with the same amount of information about cable ( $l, m, f_k$ ), tension estimated by the proposed approach is far better than that of the simple taut-string formula.

**TABLE 5. 5.** Estimated cable tension based on taut-string theory Eq. (5.33)

No.	Exact $H$ (kN)	Tension $H$ based on taut-string formulation (kN) Eq. (5.33)							
		Increasing number of used frequencies							
		1	2	3	4	5	6	7	8
C01	1069.75	1078.90 (0.85%)	1074.52 (0.45%)	1073.11 (0.31%)	1072.39 (0.25%)	1071.97 (0.21%)	1071.70 (0.18%)	1071.52 (0.17%)	1071.40 (0.15%)
C02	12947.14	13106.98 (1.23%)	13129.70 (1.41%)	13221.54 (2.12%)	13355.17 (3.15%)	13525.83 (4.47%)	13731.65 (6.06%)	13971.83 (7.91%)	14245.92 (10.03%)
C03	1723.83	1954.84 (13.40%)	1855.20 (7.62%)	1825.83 (5.92%)	1813.24 (5.19%)	1808.78 (4.93%)	1808.74 (4.93%)	1811.81 (5.10%)	1817.18 (5.24%)
C04	2325.26	3081.80 (32.54%)	2787.77 (19.89%)	2709.72 (16.53%)	2683.95 (15.43%)	2685.98 (15.51%)	2703.96 (16.29%)	2734.31 (17.59%)	2774.30 (19.30%)

Note: (·) is the error of tension by string theory compared to exact value.

#### 5.4.2. Verification 2: Cable with lateral attachments

Four cables with the properties shown in Table 5.1 are re-used in this section. Additionally, a High Damping Rubber (HDR) damper, a viscous damper, and a cross tie are assumed to be mounted to each cable at locations 2%, 5% and 50% of the cable length, respectively. In practice, the damper locations are often restricted due to aesthetic and technical issues; de Sá Caetano<sup>1</sup> reported that the damper location is around 1% to 6% of cable length. Also, the cross tie is considered as a lateral elastic spring. The information of these lateral attachments is given in Table 5.6. Based on the cable properties and parameters of attachments, the analytically natural frequencies and cable mode shapes are solved using Eq. (5.22).

Table 5.7 shows the calculated natural frequencies of the cables with the lateral attachments, and Figure 5.11 accordingly displays their normalized mode shapes over the cable length from mode 1 to mode 4. In fact, the natural frequencies of the cables with these lateral attachments were higher than that of the cables without any lateral attachment. This is attributed to the additional stiffness provided from the lateral supports, mainly by the cross tie. The increase ratios of frequencies due to the added attachments are put in the round brackets in Table 5.7. Overall, the affected modes

are heavily dependent on the locations and stiffnesses of the lateral attachments. In this verification example, because the cross tie was transversely attached to the cables at mid length, the natural frequencies and mode shapes of the odd modes were noticeably affected, especially the fundamental mode.

**TABLE 5. 6.** Information of lateral attachments

No.	HDR damper			Viscous damper		Cross tie	
	Location $x_1$ (m)	Loss factor $\phi$	Spring stiffness factor $K$ (N/m)	Location $x_2$ (m)	Viscous coefficient $c$ (N.s.m <sup>-1</sup> )	Location $x_3$ (m)	Stiffness $K_{cr}$ (N/m)
<b>C01</b>	2.0	0.6	4.59E+05	5.0	5.83E+04	50.0	5.00E+05
<b>C02</b>	2.0	0.6	5.55E+06	5.0	2.03E+05	50.0	5.00E+05
<b>C03</b>	2.0	0.6	7.39E+05	5.0	7.40E+04	50.0	5.00E+05
<b>C04</b>	2.0	0.6	9.97E+05	5.0	8.59E+04	50.0	5.00E+05

**TABLE 5. 7.** Analytically derived natural frequencies of cables with lateral supports

No.	Natural frequencies of cables from Mode 1 to mode 8							
	$f_1$ (Hz)	$f_2$ (Hz)	$f_3$ (Hz)	$f_4$ (Hz)	$f_5$ (Hz)	$f_6$ (Hz)	$f_7$ (Hz)	$f_8$ (Hz)
<b>C01</b>	1.1105 (1.89)	1.2288 (1.05)	2.2322 (1.27)	2.4976 (1.07)	3.3698 (1.15)	3.7592 (1.07)	4.5234 (1.11)	5.0163 (1.07)
<b>C02</b>	2.7128 (1.33)	4.2924 (1.05)	6.7992 (1.10)	8.9223 (1.06)	11.4817 (1.08)	13.9619 (1.07)	16.7220 (1.08)	19.5756 (1.08)
<b>C03</b>	1.4028 (1.78)	1.5627 (1.04)	2.8070 (1.25)	3.2064 (1.06)	4.2976 (1.14)	4.8783 (1.07)	5.8652 (1.10)	6.5997 (1.07)
<b>C04</b>	1.6549 (1.67)	1.8410 (1.03)	3.2985 (1.22)	3.8472 (1.05)	5.1952 (1.12)	6.0331 (1.06)	7.3503 (1.09)	8.4567 (1.07)

Note: (·) denotes the frequency ratio between cable with and cable without lateral attachments.

The same verification process is repeated for the cable with attachments. The verification was conducted with a scenario that locations and characteristics of dampers and cross tie were treated as unknown parameters. Tensions were determined with three parameters ( $l, m, f_k$ ), in which  $l$  and  $m$  are shown in Table 5.1

and frequencies  $f_k$  are listed in Table 5.7. Estimated tensions were then confirmed with the exact tensions in Table 5.1.

In this verification, we consider all information of lateral supports as unknowns. These unknowns were generated into 1000 data points from 0.5 to 1.5 times their exact values, shuffled, and combined with other cable parameters in Table 5.3 to create 1000 complete sets of data. The natural frequencies correspond to each set were computed using Eq. (5.22). The procedures for training, validation and testing in ANNs in this verification were the same as in the first case of the verification. The performance (R, MAPE, and RMSE) of training, validation, and testing was evaluated with respect to the increasing number of used frequencies. After successfully trained, the model was employed to estimate the tensions. Figure 5.12 plots R, MAPE, and RMSE of training, validation, and testing. Table 5.8 illustrates the estimated tensions; the errors of tensions compared with exact values are denoted by the round brackets.

It can be seen from Figure 5.12 and Table 5.8 that when only the first natural frequency  $f_1$  was used, the method failed to accurately estimate cable tension; correlation factor  $R < 0.89$  and error of tension  $> 17\%$  compared to exact tensions; these errors were significantly higher than those of the cables without lateral attachments (verification 1). A better accuracy was achieved if more than two frequency was used.

**TABLE 5. 8.** Estimated tensions by ANNs with unknown information of lateral attachments

No.	Exact $H$ (kN)	Tension $H$ based on trained ANN model (kN)							
		Increasing number of used frequencies							
		1	2	3	4	5	6	7	8
C01	1069.75	1298.50 (21.38)	1076.39 (0.62)	1063.78 (-0.56)	1066.03 (-0.35)	1061.39 (-0.78)	1060.85 (-0.83)	1056.56 (-1.23)	1054.90 (-1.39)
C02	12947.14	15185.13 (17.29)	12499.02 (-3.46)	12852.01 (-0.73)	12832.37 (-0.89)	12842.13 (-0.81)	12843.40 (-0.80)	12899.71 (-0.37)	12945.93 (-0.01)
C03	1723.83	2098.94 (21.76)	1717.96 (-0.34)	1692.75 (-1.80)	1714.18 (-0.56)	1709.83 (-0.81)	1718.59 (-0.30)	1714.06 (-0.57)	1719.79 (-0.23)
C04	2325.26	2754.28 (18.45)	2252.50 (-3.13)	2270.12 (-2.37)	2264.69 (-2.60)	2273.30 (-2.23)	2294.54 (-1.32)	2301.19 (-1.04)	2285.64 (-1.70)

Note: (·) denotes the error between estimated and exact tensions.

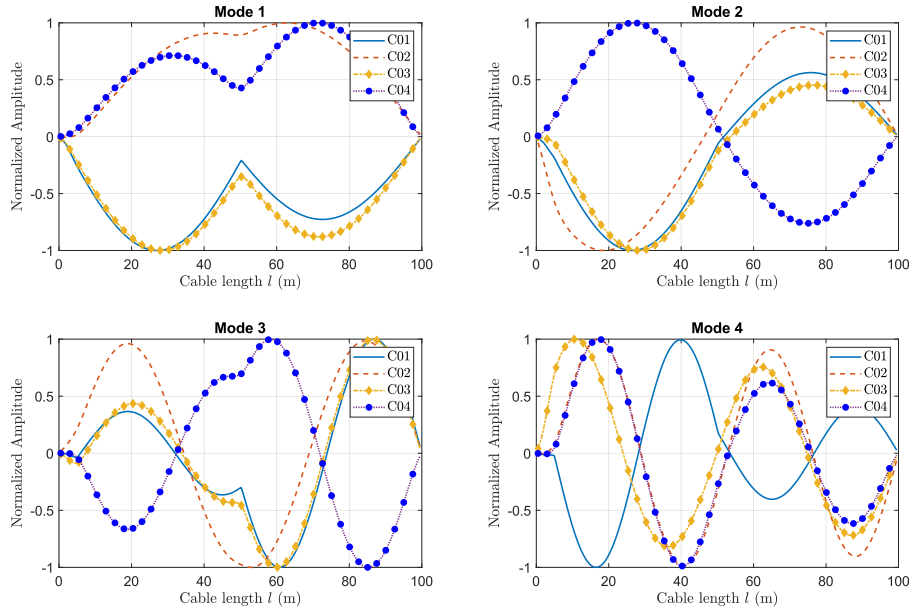


FIGURE 5. 11. Normalized mode shapes of cables with lateral attachments.

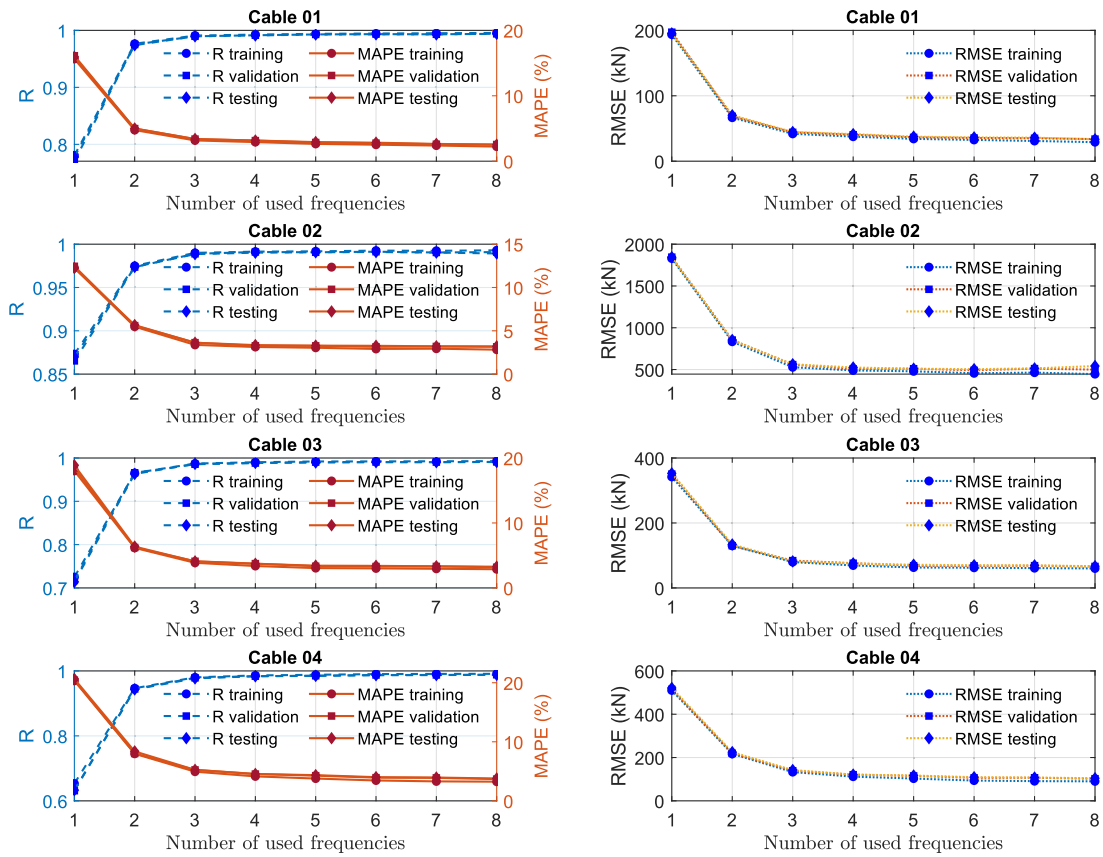


FIGURE 5. 12. R, MAPE and RMSE of training, validation and testing in ANNs for cables with lateral attachments.

## 5.5. Discussion on the ranges of unknown parameters for training, validation and testing in ANNs

This section shall describe how the ranges of unknown parameters are selected when generating datasets. The unknown components are  $EI$ ,  $EA$ ,  $H$ , cable inclination  $\phi$ , restraint at cable ends  $K_r$ , and parameters of lateral attachments ( $x_d$ ,  $c$ ,  $K$ ,  $\phi$ ,  $K_{cr}$ ) if any. The selection of the ranges for these components should be based on an actual situation. For example, the technical reports/drawings of cables in the design or construction stages would provide undoubtedly useful information of these unknowns. Based on that, the lower bound and upper bound of unknown parameters can be set. It is worth noting that narrowing ranges will result in a smaller number of generated data points and vice versa. The following discussions are made to some parameters which are almost undocumented.

### 5.5.1. Range of cable tension

Since cable length  $l$ , mass per unit length  $m$  and measured frequencies  $f_k$  are known, the tension  $H$  would be pre-estimated using the formulation of taut-string theory Eq. (5.33). The error between taut-string tension and the exact one would be less than 20% for most of stay cables. However, this error is, in some cases, higher than 30% for some cables with extremely large sag and bending stiffness parameters, like cable C04 in Table 5.1. For generating datasets, tension  $H$  can be generated based on taut-string tension.

It is worth noting that tension by Eq. (5.33) is derived for taut string without lateral attachments. For cables with dampers, dampers are often mounted near cable ends leading to small perturbation of frequencies between cables with and without dampers<sup>13</sup>. As a result, Eq. (5.33) can be still acceptable for cable with dampers. For cables with cross ties, Eq. (5.33) can lead to unaccepted errors in estimation of cable tension. However, this difficult issue can be tackled by identifying the unaffected vibration modes. For example, Eq. (5.33) can be used for mode 2 of cables which have a cross tie located at mid length.

### 5.5.2. Range of cable bending stiffness, axial stiffness and cable inclination angle

If multiple measured frequencies  $f_k$  of cables are available, the linear regression of  $(f_k/k)^2$  versus square of mode  $k^2$  can be established<sup>8</sup> as

$$\left(\frac{f_k}{k}\right)^2 = Ak^2 + B \quad (5.34)$$

where  $A$  and  $B$  denote the slope and a constant of the regression graph, respectively. By modelling a cable as an axially loaded beam with hinged end boundary conditions, the frequency formulation is<sup>8</sup>

$$\left(\frac{f_k}{k}\right)^2 = \frac{EI\pi^2}{4ml^4}k^2 + \frac{H}{4ml^2} \quad (5.35)$$

Introducing Eq. (5.34) into Eq. (5.35) yields  $EI = 4ml^4A/\pi^2$ . Based on this value, a range of  $EI$  can be approximately selected. However, Cho et al.<sup>8</sup> reported from their measurement of cable vibrations that a negative slope in the relationship between  $(f_k/k)^2$  and  $k^2$  could occur leading to negative bending stiffness; they pointed some possible sources of this negative linearity such as measurement noise. On condition that Eq. (5.34) fails to give information of bending stiffness due to a small number of recorded modes or some source of measurement errors,  $EI$  can be generated based on the common range of bending stiffness parameter  $\zeta$  ( $50 < \zeta < 605$ ) as suggested by Mehrabi & Tabatabai<sup>16</sup>. The determination of axial stiffness  $EA$  would refer to the common range of sag-extensibility parameter  $\lambda^2$  ( $0 < \lambda^2 < 3.1$ )<sup>16</sup>. Using Eq. (5.32), a range of  $EA$  would be obtained. Also, the inclination angle  $\varphi$  of the cables would be selected based on the observation at field.

### 5.5.3. Range of rotational restraint stiffness at cable ends

In this study, the parametric analysis was conducted to observe the influence of restraint stiffness on natural frequencies. For that purpose, 19 cables were used including 4 cables in Table 5.1 except for parameter  $K_r$  and 15 cables in Table 5.9. Table 5.9 shows the properties of 15 cables which were introduced in the paper of Javanbakht et al.<sup>74</sup> The authors cited from a report of Tabatabai et al.<sup>75</sup>, and mentioned that these 15 typical cables represented the engineering specifications of 1406 stay cables of 16 cable-stayed bridges. Briefly, the cables in Table 5.9 have length  $l$  (43.7 m – 460.1 m), inclination angle  $\varphi$  ( $22.6^0 - 58.9^0$ ), mass per unit length  $m$  (52.8 kg/m – 214 kg/m), tension  $H$  ( $2.24 \times 10^3$  kN –  $9.49 \times 10^3$  kN), bending stiffness parameter  $\zeta$  (57.4 – 595.2), and sag-extensibility parameter  $\lambda^2$  (0.01 – 2.70).

**TABLE 5. 9.** Cable properties used in parametric analysis

No.	$l$ (m)	$H$ (kN)	$m$ (kg/m)	$\varphi$ (°)	$EA$ (N)	$EI$ (N.m <sup>2</sup> )	$\lambda^2$	$\zeta$
C05	43.7	2240.20	72.3	49.4	1.23E+09	1.23E+06	0.04	59.0
C06	61.7	5738.00	103.0	58.9	1.97E+09	2.78E+06	0.01	88.7
C07	83.0	8554.90	214.7	27.0	4.73E+09	1.79E+07	0.18	57.4
C08	101.8	2813.00	52.8	27.8	1.06E+09	5.55E+05	0.10	229.2
C09	135.9	5081.30	89.2	24.4	1.94E+09	1.70E+06	0.17	234.8
C10	168.7	8346.20	167.1	25.5	3.51E+09	9.50E+06	0.38	158.1
C11	200.5	7772.00	136.3	25.3	2.69E+09	4.01E+06	0.34	279.0
C12	245.0	9493.80	188.3	23.6	3.47E+09	9.01E+06	0.70	251.5
C13	276.6	5062.90	94.8	35.2	2.23E+09	2.41E+06	0.76	400.8
C14	293.0	5335.70	100.7	33.7	2.36E+09	2.71E+06	0.90	410.9
C15	327.1	4916.80	94.8	34.4	2.23E+09	2.41E+06	1.18	467.1
C16	363.0	4537.10	89.3	26.9	2.14E+09	2.23E+06	1.84	517.7
C17	401.6	4774.50	93.0	25.0	2.23E+09	2.41E+06	2.25	565.1
C18	421.1	4947.20	98.6	24.1	2.36E+09	2.71E+06	2.70	568.7
C19	460.1	6665.90	118.9	22.6	2.86E+09	3.98E+06	2.37	595.2

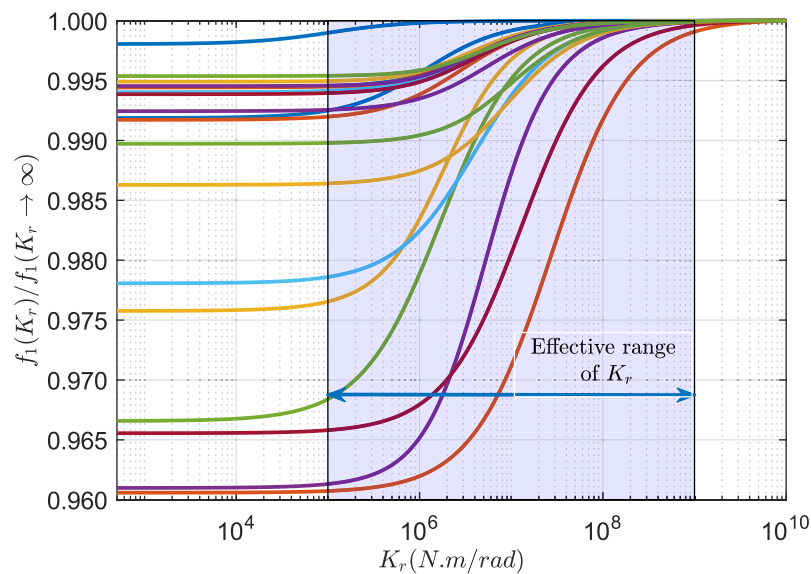


**FIGURE 5. 13.** Normalized fundamental frequency of 19 cables over a wide range of  $K_r$ .



Figure 5.13 presents the normalized fundamental frequency over a wide range of rotational stiffness value  $K_r$ . Normalization  $f_1(K_r)/f_1(K_r \rightarrow \infty)$  means normalizing to the frequency of corresponding fixed-fixed end cable ( $K_r \rightarrow \infty$ ). Based on the parametric results of 19 cables which cover a relatively broad range of cable properties, it is recommended that rotational stiffness with a range from  $1 \times 10^5$  N.m/rad to  $1 \times 10^9$  N.m/rad would be used for generating datasets because  $K_r$  within this range poses the pivotal changes in the cable frequencies, as can be seen in the shadow area in Figure 5.13. In other words, cables with  $K_r < 1 \times 10^5$  can be considered as hinged-hinged end whereas  $K_r > 1 \times 10^9$  N.m/rad can be treated as fixed-fixed end.

#### 5.5.4. Range of the parameters of lateral attachments

Location of damper or cross tie  $x_d$  is measured from a cable end. The range of this location can be approximately made by the observation at field. For cable with viscous dampers, damper coefficient  $c$  is usually designed to maximize added damping. This value of  $c$  is so-called optimal damper coefficient  $c_{opt}$  as<sup>13</sup>. The range of  $c$  then can be set based on  $c_{opt}$ .

$$c_{opt} = \sqrt{Hm} / (\pi k x_d / l) \quad (5.36)$$

where  $k$  is the assigned mode; and  $x_d$  is the location of damper.

For cable with HDR dampers, there are two damper characteristics: loss factor of rubber material  $\phi$  and spring stiffness factor  $K$ . According to some test results,  $\phi$  ranges from 0.12 to 0.18 for natural rubber (NR60)<sup>52</sup>, from 0.30 to 0.41 for butyl rubber (BR60)<sup>52</sup>, and around 0.67 for neoprene rubber<sup>53</sup>. The loss factor  $\phi$  of HDR dampers for the vibration control of the stay cables in Shinminato Bridge in Japan was 0.62. To the best of our knowledge, commercial rubbers with the range  $0 < \phi < 1$  are widely manufactured and used. The range of spring stiffness factor  $K$  can be selected by referring to the its optimal value<sup>30</sup>.

$$K_{opt} = H / \left( x_d \sqrt{1 + \phi^2} \right) \quad (5.37)$$

For cable with cross ties, the equivalent stiffness of each cross tie can be expressed as  $(K_{cr})_i = (EA_{cr})_i / (l_{cr})_i$ , in which  $(EA_{cr})_i$  is the axial stiffness of  $i^{th}$  cross tie, and  $(l_{cr})_i$  is its respective length. This could be useful to set the range of the crosstie stiffness  $K_{cr}$ .

## 5.6. Application of the proposed framework for the estimation of tensions in stay cables of Tatara Bridge

In this section, a full-scale application of the proposed method to a long-span cable-stayed bridge is presented. The object bridge is Tatara Bridge connecting the Ikuchi Island of Hiroshima prefecture and Omishima Island of Ehime prefecture, in Japan. When completed in 1999, it was the longest cable-stay bridge in the world. The bridge has three spans with a total length of 1480 m, in which the main span is 890 m; the bridge is supported by 168 stay cables. Cable length  $l$  of Tatara Bridge varies from 107 m to 470 m; cable diameter varies from 110 mm to 170 mm; and mass per unit length  $m$  stays between 94.8 kg/m and 121.8 kg/m. High Damping Rubber (HDR) dampers were installed to some cables to provide additional damping. Figure 5.14 shows the profile of Tatara Bridge.

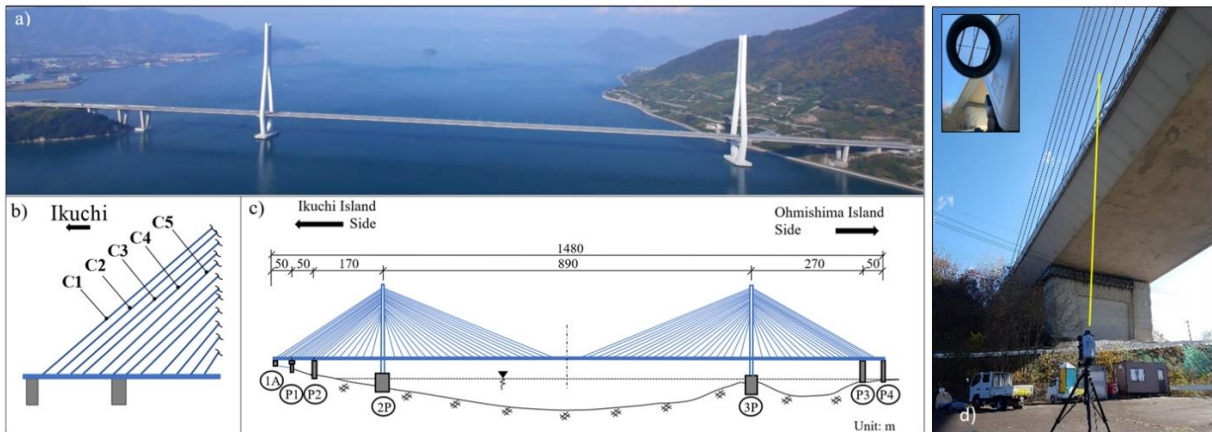


**FIGURE 5. 14.** Tatara Bridge: a) general view; b) selected cables for the identification of tensions; c) span arrangement, and d) stay cables vibration measurement by LDV.

In this study, the vibrations of four typical cables from C1 to C4 on the side span of Ikuchijima island were measured and used for tension identification. Laser Doppler Vibrometer (Polytec's RSV-150) was used to capture the in-plane cable ambient vibrations of the stay cables. Figure 5.15 shows the displacement ambient responses measured by LDV. These time history responses were converted into frequency domain and the displacement spectra are shown in Figure 5.15. From the spectra peaks, natural frequencies of the cables are extracted.

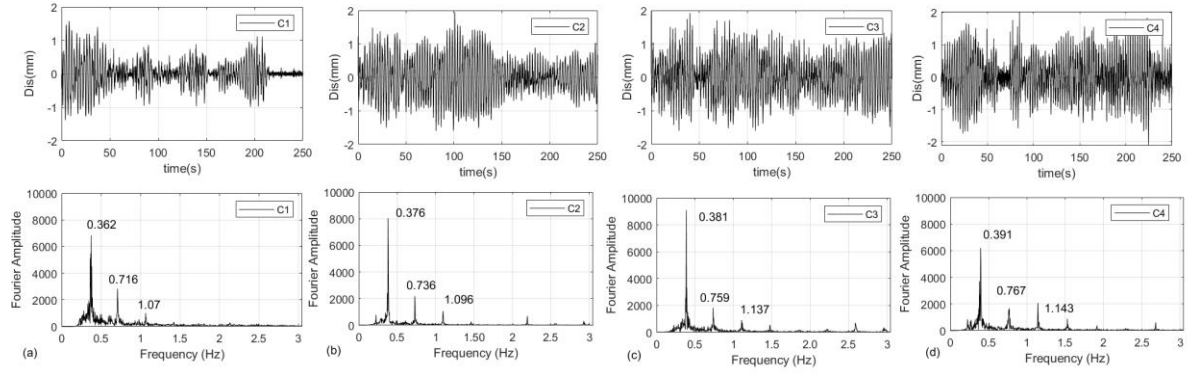


**FIGURE 5. 15.** Ambient vibration of Tatara Bridge stay cables and their frequency spectra measured by LDV: a) cable C1; b) cable C2; c) cable C3; and d) cable C4.

For the identification of cable tensions, cable length  $l$ , mass per unit length  $m$ , and three measured natural frequencies are available as shown in Table 5.10. Others unknown information of cables are cable bending stiffness  $EI$ , axial stiffness  $EA$ , rotational restraint stiffness at cable ends  $K_r$ , cable tension  $H$ , cable inclination  $\varphi$ . Also, the HDR dampers were mounted to cables at location  $x_d$  from one cable end. Because the dampers were sealed into the cable protective tube, this location  $x_d$  was not exactly measured and became an unknown parameter. Characteristics of HDR damper with spring stiffness factor  $K$  and loss factor  $\phi$  of rubber material were also treated as unknown parameters.

**TABLE 5. 10.** Known parameters of cable properties and measured frequencies

No.	$l$ (m)	$m$ (kg/m)	Measured natural frequencies $f$ (Hz)		
			$f_1$ (Hz)	$f_2$ (Hz)	$f_3$ (Hz)
C1	317.72	121.80	0.362	0.716	1.070
C2	309.94	112.60	0.376	0.736	1.096
C3	301.20	108.20	0.381	0.759	1.137
C4	292.93	100.70	0.391	0.767	1.143

To generate datasets, unknown properties of cable and damper were set within appropriate ranges. Referring to the previous discussion,  $EI$  and  $EA$  were chosen based on the common ranges of bending stiffness parameter  $\zeta$  ( $50 < \zeta < 605$ ) and

sag-extensibility parameter  $\lambda^2$  ( $0 < \lambda^2 < 3.1$ ), respectively; rotational stiffness  $1 \times 10^5 < K_r < 1 \times 10^9$  (N.m/rad); tension  $H$  was from 0.5 to 1.2 times the value of string theory Eq. (5.33); inclination of cable varied from 20 to 80 degrees based on our observation at field; damper location  $x_d$  was from 1% to 5% of cable length; loss factor of damper material  $0.1 < \phi < 0.99$ ; and spring stiffness factor  $K$  was set based on optimal value (Eq. 5.37). Tables 5.11 and 5.12 summarize the ranges of unknown cable parameters and the unknown damper information, respectively.

Each parameter in Tables 5.11 and 5.12 were randomly generated into 1000 data points started from lower bound (LB) value to upper bound (UB) value. They were then combined with cable length  $l$  and mass per unit length  $m$  in Table 5.10 to create 1000 datasets of cable-damper properties. Cable natural frequencies  $f_k$  of each set were determined by the Finite Difference Method (200 interior nodes) using Eq. (5.22).

**TABLE 5. 11.** Unknown cable properties

No.	$EI$ (N.m <sup>2</sup> )		$EA$ (N)		$K_r$ (N.m/rad)		$H$ (kN)		$\phi$ (°)	
	LB	UB	LB	UB	LB	UB	LB	UB	LB	UB
<b>C1</b>	1.75E+06	2.56E+08	4.27E+08	1.32E+10	1.00E+05	1.00E+09	3.17E+03	7.60E+03	20.00	80.00
<b>C2</b>	1.55E+06	2.27E+08	4.27E+08	1.32E+10	1.00E+05	1.00E+09	2.96E+03	7.10E+03	20.00	80.00
<b>C3</b>	1.40E+06	2.06E+08	4.30E+08	1.33E+10	1.00E+05	1.00E+09	2.83E+03	6.80E+03	20.00	80.00
<b>C4</b>	1.20E+06	1.76E+08	3.89E+08	1.21E+10	1.00E+05	1.00E+09	2.56E+03	6.15E+03	20.00	80.00

Note: LB = lower bound; UB = upper bound.

**TABLE 5. 12.** Unknown damper parameters

No.	Damper location $x_d$ (m)		Loss factor $\phi$		Spring stiffness factor $K$ (N.m/rad)	
	LB	UB	LB	UB	LB	UB
<b>C1</b>	3.18	15.89	0.10	0.99	2.83E+05	1.98E+06
<b>C2</b>	3.10	15.50	0.10	0.99	2.71E+05	1.90E+06
<b>C3</b>	3.01	15.06	0.10	0.99	2.67E+05	1.87E+06
<b>C4</b>	2.93	14.65	0.10	0.99	2.49E+05	1.74E+06

Note: LB = lower bound; UB = upper bound.

In the training, validation, and testing using ANNs, the input and output of each cable were prepared in the matrix form as formed in Eq. (5.28a) and Eq. (5.28b), respectively. In details, Input composed of the parameters ( $l, m, f_1, f_2, \dots, f_k$ ); note that frequencies  $f_k$  are the calculated frequencies, not measured ones. Output presented targeted tensions  $H$  (values in Table 5.11). Datasets were separated into 70% for training, 15% for testing and 15 % for validation; the number of neurons in the hidden layer was 15; ran 30 times independently and averaged the results. Figure 5.16 shows the performance (R, MAPE, and RMSE) of training in ANNs versus the number of used frequencies; the maximum number of used frequencies was three because the available measured frequencies was also three. Obviously, the more frequencies are used for training, the higher quality of training process is achieved; For all selected cables,  $R > 0.995$  and  $MAPE < 2\%$  when all three frequencies are combined in the input matrix. In addition to Figure 5.16, the scatters between estimated and targeted tensions with five known features ( $m, l, f_1, f_2, f_3$ ) are depicted in Figure 5.17, showing a good performance of training the datasets.

The successfully trained model was employed to estimate tensions in the cables. Features imported into the well-trained model were cable length  $l$ , mass per unit length  $m$ , and three measured frequencies (in Table 5.10). The output of the trained model was estimated tension. Table 5.13 shows estimated tensions by ANNs, by string theory as well as the comparison with designed tension. Overall, tensions of four selected cables were successfully identified using cable length, mass per unit length and measured frequencies but still taking unknown cable properties and HDR damper parameters into consideration. The discrepancy between estimated tensions and its designed values was relatively small, around 1.5 % on average.

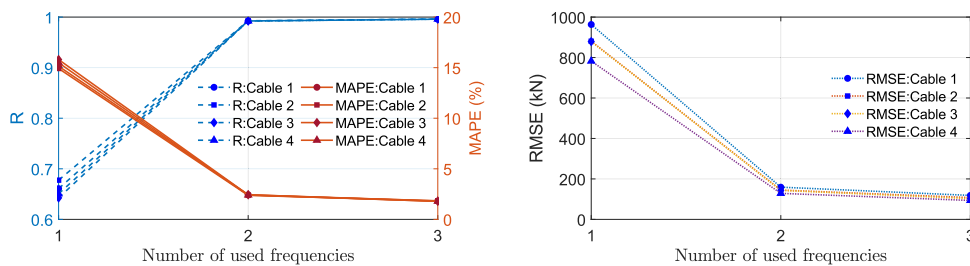


**FIGURE 5. 16.** R, MAPE and RMSE of training in ANNs of Tatara Bridge cables (cable C1, cable C2, cable C3, cable C4).

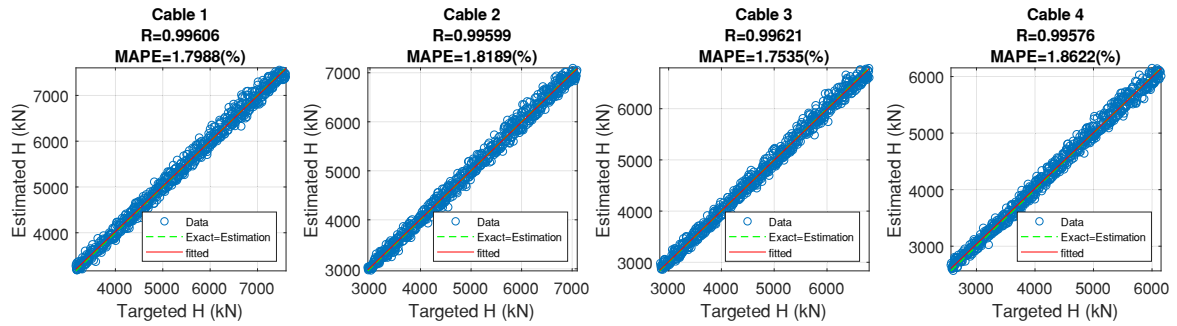


**FIGURE 5. 17.** Scatters between estimated and targeted tensions with five known features ( $l, m, f_1, f_2, f_3$ ).

**TABLE 5. 13.** Estimated tension and the comparison with designed value.

No.	Tension by ANNs		Tension by string theory Eq. (5.33) (kN)	Designed tension $H_0$ (kN)	Difference (%) $\frac{(H - H_0)}{H_0} \times 100$
	Features imported into trained model ( $l; m; f_1; f_2; f_3$ )	Output of trained model $H$ (kN)			
C1	(317.72; 121.80; 0.362; 0.716; 1.070)	6152.22	6334.89	6210.20	-0.93
C2	(309.94; 112.60; 0.376; 0.736; 1.096)	5811.79	5917.10	5712.10	1.75
C3	(301.20; 108.20; 0.381; 0.759; 1.137)	5446.60	5664.89	5380.40	1.23
C4	(292.93; 100.70; 0.391; 0.767; 1.143)	5050.88	5128.12	5008.40	0.85

## 5.7. Summary

In this chapter, a straightforward framework for the vibration-based cable tension estimation method is proposed through the application of Artificial Neural Networks (ANNs). Two cable models, namely cable with and without lateral attachments were introduced, in which rotational restraint stiffness at cable ends was also considered; the finite difference formulation for the eigen analysis of cable vibration was derived to create datasets for training, validation and testing in ANNs. The verifications were implemented for cables with wide ranges of cable bending stiffness and sag effect. The discussions were made on how to select the ranges of values of unknown parameters; the proposed framework was also applied to evaluate tensions in some cables of Tataru Bridge as an engineering application.

The main conclusions of the study are as follows:

- 1) Cable tension was successfully estimated using only three known parameters including cable length, mass per unit length and measured frequencies, and regardless of other unknown factors like cable bending stiffness, axial stiffness, cable inclination, restrained conditions at cable ends and lateral attachments.
- 2) For cable without lateral supports, using at least two measured frequencies could result in high accuracy of estimated tension, including cables with large sag and bending stiffness parameters. Also, while the proposed method successfully estimated tension, the taut-string theory, with the same amount of available information, resulted in unaccepted errors, especially for cables with moderate or large sag/bending stiffness properties.
- 3) For cable with lateral supports, the number of known measured frequencies was at least three to reach acceptable accuracy of estimated tension, including cables with large sag and bending stiffness characteristics.
- 4) Although increasing the number of frequencies in the input matrix caused higher performance of ANNs model, this performance did not significantly increase when the number of used frequencies was more than the minimum number mentioned above.
- 5) The proposed method succeeded in estimating full-scale tensions in the cables of Tatara Bridge by utilizing cable length, mass per unit length and three measured frequencies; The discrepancy between the estimated tensions and the designed values was around 1.5 % on average.

## Appendix: Derivation of stiffness matrix

Stiffness matrix  $[K_1]_{n \times n}$  is obtained from the first two part of Eq. (5.7). Substitution of the finite difference quotations shown in Figure 5.2 into Eq. (5.7) yields

$$EI \frac{(\tilde{v}_{i+2} - 4\tilde{v}_{i+1} + 6\tilde{v}_i - 4\tilde{v}_{i-1} + \tilde{v}_{i-2})}{a_1^4} - H \frac{(\tilde{v}_{i+1} - 2\tilde{v}_i + \tilde{v}_{i-1})}{a_1^2} + \dots = 0 \quad (5.38)$$

It is noted that only the parts before the three-dot sign of Eq. (5.38) are used to establish  $[K_1]_{n \times n}$ . Applying Eq. (5.38) to Note 1 ( $i = 1$ )

$$EI \frac{(\tilde{v}_3 - 4\tilde{v}_2 + 6\tilde{v}_1 - 4\tilde{v}_0 + \tilde{v}_{-1})}{a_1^4} - H \frac{(\tilde{v}_2 - 2\tilde{v}_1 + \tilde{v}_0)}{a_1^2} + \dots = 0 \quad (5.39)$$

Boundary condition at the cable end ( $y = 0$ )

$$\tilde{v}(x)|_0 = 0; \text{ and } K_r \frac{d\tilde{v}(x)}{dx} \Big|_0 = EI \frac{d^2\tilde{v}(x)}{dx^2} \Big|_0 \quad (5.40a, b)$$

Finite difference version of Eq. (5.40)

$$\tilde{v}_0 = 0; \text{ and } K_r \frac{(\tilde{v}_1 - \tilde{v}_{-1})}{2a_1} - EI \frac{(\tilde{v}_1 - 2\tilde{v}_0 + \tilde{v}_{-1})}{a_1^2} = 0 \quad (5.41a, b)$$

Using  $\tilde{v}_0 = 0$ , Eq. (5.41b) results in

$$\tilde{v}_{-1} = \frac{(K_r/2a_1 - EI/a_1^2)}{(K_r/2a_1 + EI/a_1^2)} \tilde{v}_1 \quad (5.42)$$

Making use of Eq. (5.41a), Eq. (5.42) and  $\zeta = l\sqrt{H/EI}$ , Eq. (5.39) becomes

$$\frac{Hl^2}{a_1^4\zeta^2} \{ \tilde{v}_3 - 4\tilde{v}_2 + 6\tilde{v}_1 + \frac{[K_r/2a_1 - Hl^2/(a_1^2\zeta^2)]}{[K_r/2a_1 + Hl^2/(a_1^2\zeta^2)]} \tilde{v}_1 \} - \frac{H}{a_1^2} (\tilde{v}_2 - 2\tilde{v}_1) + \dots = 0 \quad (5.43)$$

Rearrangement of Eq. (5.43) into matrix form gives

$$\frac{H}{a_1^2} \left( \frac{1}{\zeta^2} \right) [A_{1,1} \ A_{1,2} \ \dots \ A_{1,n-1} \ A_{1,n}] \{ \tilde{v}_1 \ \tilde{v}_2 \ \dots \ \tilde{v}_{n-1} \ \tilde{v}_n \}^T + \dots = 0 \quad (5.44)$$

where  $A_{1,1} = n^2\alpha + 2\zeta^2$ ,  $A_{1,2} = -4n^2 - \zeta^2$ ,  $A_{1,3} = n^2$ , and  $A_{1,4} = A_{1,5} = \dots = A_{1,n} = 0$ . They are the elements in the first row of the matrix  $[K_1]_{n \times n}$ . Note that  $\alpha$  in  $A_{1,1}$  is defined as

$$\alpha = \frac{\zeta^2 [K_r/(a_1H)] (a_1/l)^2 - 2}{\zeta^2 [K_r/(a_1H)] (a_1/l)^2 + 2} + 6 \quad (5.45)$$



Applying Eq. (5.38) to Node 2 ( $i = 1$ )

$$EI \frac{(\tilde{v}_4 - 4\tilde{v}_3 + 6\tilde{v}_2 - 4\tilde{v}_1 + \tilde{v}_0)}{a_1^4} - H \frac{(\tilde{v}_3 - 2\tilde{v}_2 + \tilde{v}_1)}{a_1^2} + \dots = 0 \quad (5.46)$$

Replacing  $\tilde{v}_0 = 0$ , Eq. (5.46) becomes

$$EI \frac{(\tilde{v}_4 - 4\tilde{v}_3 + 6\tilde{v}_2 - 4\tilde{v}_1)}{a_1^4} - H \frac{(\tilde{v}_3 - 2\tilde{v}_2 + \tilde{v}_1)}{a_1^2} + \dots = 0 \quad (6.47)$$

Also, rearranging Eq. (5.47) into matrix form as

$$\frac{H}{a_1^2} \left( \frac{1}{\zeta^2} \right) [A_{2,1} \ A_{2,2} \ \dots \ A_{2,n-1} \ A_{2,n}] \{\tilde{v}_1 \ \tilde{v}_2 \ \dots \ \tilde{v}_{n-1} \ \tilde{v}_n\}^T + \dots = 0 \quad (5.48)$$

where  $A_{2,1} = -4n^2 - \zeta^2$ ,  $A_{2,2} = 6n^2 + 2\zeta^2$ ,  $A_{2,3} = -4n^2 - \zeta^2$ ,  $A_{2,4} = n^2$ , and  $A_{2,5} = A_{2,6} = \dots = A_{2,n} = 0$ . They are put into the second row of the matrix  $[K_1]_{n \times n}$ .

By applying Eq. (5.38) to the remaining nodes, the stiffness matrix  $[K_1]_{n \times n}$  are derived as Eq. (5.12) in the main text. It is worth noting that the boundary conditions at the cable end ( $y = l$ ) are as below, which are used when writing Eq. (5.38) at node  $n$ .

$$\tilde{v}(x)|_l = 0; \quad K_r \frac{d\tilde{v}(x)}{dx} \Big|_l = -EI \frac{d^2\tilde{v}(x)}{dx^2} \Big|_l \quad (5.49)$$

## CHAPTER 6. CONCLUSIONS AND FUTURE STUDY

This research focuses on damping and tension of stay cables with dampers. The present study covers various aspects including theoretical development, practical approach, field measurement verification as well as application to full-scale cables of cable stayed bridges. This chapter summarizes main contributions, conclusions and future works.

### 6.1. Conclusions

Five points in the problem statement section (Section 1.2) were addressed through four main chapters in this dissertation (Chapter 2 to Chapter 5). The main conclusions are as follows:

- **Chapter 2:** The Problem 1 in the problem statement section was solved in this chapter. The damping formulation of cables with dampers was proposed which accounts for rotational restraint between cable and damper, damper support stiffness and damper stiffness. Under these factors, the added damping was always lower than its value in non-restraint cases. The reduction of damping is defined by reduction factors. In the design a stay cable with damper, damping can be re-identified by multiplying the designed damping of a conventional case by the reduction factors proposed in this chapter.
- **Chapter 3:** The Problems 2 and 3 in the problem statement section are solved in this chapter. Regarding the Problem 2, the effect of boundary conditions (hinged-hinged, fixed-fixed and rotational restraint ends) on cable damping was studied. It showed that cable bending stiffness triggered a reduction of the damping of cables with fixed-fixed end whereas an inverse observation was found for hinged-hinged end cables. By adjusting supports at cable ends with finite rotational restraint stiffness, the damper works more effectively. About the Problem 3, the universal curve of damping was proposed, which incorporated several parameters like cable bending stiffness, boundary conditions at cable ends (hinged, fixed or restraint ends), damper stiffness, damper support stiffness and negative stiffness into a single damping curve. The universal curve is independent of any influencing parameter. Universal damping curve is a useful tool for the design of cable vibration control with damper effortlessly, especially multi-mode controls.

- **Chapter 4:** The Problem 4 in the problem statement section was solved in this chapter. The procedure and implementation of damping analysis is performed on full-scale cables of Shinminato Bridge. It showed that cable sag caused a notable reduction of the damping ratio for the mode 1 whereas having almost no effect on the mode 2 and a relatively small reduction for the mode 3. Additionally, cable sag triggered larger reduction of damping in fixed-fixed end cables than that of hinged-hinged end cables. Measured damping ratios were compared to theoretical values, and the results showed that the damper effectiveness was greater than 0.7 for all cables, except for mode 2 (0.66) and mode 3 (0.58) of cable C01E. Moreover, the variation of damping ratios and frequencies versus amplitudes was also investigated. While frequencies were almost unchanged over amplitudes, the damping ratios tended to increase first as amplitudes decreased, then damping ratios decreased as amplitudes continuously decreased.
- **Chapter 5:** The last point in the problem statement section was solved in this chapter. The framework for the identification of tension under limited information of cable properties was proposed for the first time. Cable tension was successfully estimated using just three known parameters including cable length, mass per unit length and measured frequencies, and regardless of other unknown factors like cable bending stiffness, axial stiffness, cable inclination, restrained conditions at cable ends and lateral attachments. For cable without lateral supports, using at least two measured frequencies could result in high accuracy of estimated tension, including cables with large sag and bending stiffness parameters. For cable with lateral supports like dampers or cross ties, the number of known measured frequencies was at least three to reach acceptable accuracy of estimated tension.

## 6.2. Future study

The followings highlight some of the issues that can be extended:

- 1) The parameters related to restraints such as rotational restraint stiffness, damper support stiffness, damper stiffness, and negative stiffness are assumed as a spring. Obviously, these restraints depend heavily on actual conditions of cable-damper. For instance, rotational restraint stiffness at damper location depends on shapes, material of bushings and anchoring techniques; damper support stiffness relies on stiffness of support, length of supports,

configuration of support etc. Therefore, future work would emphasize on a parametric study of these restraints to provide a reasonable stiffness range of these restraints.

- 2) Next, the amplitude dependency of measured damping has been observed during full-scale measurement. The theoretical development on this problem is also a future work.

## REFERENCES

1. de Sá Caetano E. *Cable vibrations in cable-stayed bridges*. Vol 9: IABSE; 2007.
2. Gimsing NJ, Georgakis CT. *Cable supported bridges: Concept and design*. John Wiley & Sons; 2011.
3. Mehrabi AB. In-service evaluation of cable-stayed bridges, overview of available methods and findings. *Journal of Bridge Engineering*. 2006;11(6):716-724.
4. Casas JR. A combined method for measuring cable forces: The cable-stayed Alamillo Bridge, Spain. *Structural Engineering International*. 1994;4(4):235-240.
5. Zui H, Shinke T, Namita Y. Practical formulas for estimation of cable tension by vibration method. *Journal of structural engineering*. 1996;122(6):651-656.
6. Mehrabi AB, Tabatabai H, Lotfi HR. Damage detection in structures using precursor transformation method. *Journal of intelligent material systems and structures*. 1998;9(10):808-817.
7. Mehrabi AB, Ligozio CA, Ciolko AT, Wyatt ST. Evaluation, rehabilitation planning, and stay-cable replacement design for the hale boggs bridge in Luling, Louisiana. *Journal of Bridge Engineering*. 2010;15(4):364-372.
8. Cho S, Yim J, Shin SW, Jung H-J, Yun C-B, Wang ML. Comparative field study of cable tension measurement for a cable-stayed bridge. *Journal of Bridge Engineering*. 2013;18(8):748-757.
9. Fujino Y, Kimura K, Tanaka H. *Wind resistant design of bridges in Japan: developments and practices*. Springer Science & Business Media; 2012.
10. Kumarasena S, Jones NP, Irwin P, Taylor P. *Wind-Induced Vibration of Stay Cables [Final Report; August 2007]*. United States. Federal Highway Administration;2007.
11. PTI. Recommendations for stay cable design, testing and installation. In: *Cable-Stayed Bridges Committee Phoenix*; 2007.
12. Pacheco BM, Fujino Y, Sulekh A. Estimation curve for modal damping in stay cables with viscous damper. *Journal of Structural Engineering*. 1993;119(6):1961-1979.
13. Krenk S. Vibrations of a taut cable with an external damper. *J Appl Mech*. 2000;67(4):772-776.

14. Krenk S, Nielsen SR. Vibrations of a shallow cable with a viscous damper. *Proceedings of the Royal Society of London Series A: Mathematical, Physical and Engineering Sciences*. 2002;458(2018):339-357.
15. Irvine HM, Caughey TK. The linear theory of free vibrations of a suspended cable. *Proceedings of the Royal Society of London A Mathematical and Physical Sciences*. 1974;341(1626):299-315.
16. Mehrabi AB, Tabatabai H. Unified finite difference formulation for free vibration of cables. *Journal of Structural Engineering*. 1998;124(11):1313-1322.
17. Hoang N, Fujino Y. Analytical study on bending effects in a stay cable with a damper. *Journal of Engineering mechanics*. 2007;133(11):1241-1246.
18. Fujino Y, Hoang N. Design formulas for damping of a stay cable with a damper. *Journal of structural engineering*. 2008;134(2):269-278.
19. Chen L, Sun L, Nagarajaiah S. Cable with discrete negative stiffness device and viscous damper: passive realization and general characteristics. *Smart Struct Syst*. 2015;15(3):627-643.
20. Zhou P, Li H. Modeling and control performance of a negative stiffness damper for suppressing stay cable vibrations. *Structural Control and Health Monitoring*. 2016;23(4):764-782.
21. Shi X, Zhu S, Li J-Y, Spencer BF. Dynamic behavior of stay cables with passive negative stiffness dampers. *Smart Materials and Structures*. 2016;25(7):075044.
22. Shi X, Zhu S, Spencer Jr BF. Experimental study on passive negative stiffness damper for cable vibration mitigation. *Journal of Engineering Mechanics*. 2017;143(9):04017070.
23. Javanbakht M, Cheng S, Ghrib F. Impact of support stiffness on the performance of negative stiffness dampers for vibration control of stay cables. *Structural Control and Health Monitoring*. 2020;27(10):e2610.
24. Dong Q, Cheng S. Impact of Damper Stiffness and Damper Support Stiffness on the Performance of a Negative Stiffness Damper in Mitigating Cable Vibrations. *Journal of Bridge Engineering*. 2021;26(3):04020131.
25. Ren W-X, Chen G, Hu W-H. Empirical formulas to estimate cable tension by cable fundamental frequency. *Structural Engineering and Mechanics*. 2005;20(3):363-380.
26. Spencer Jr B, Nagarajaiah S. State of the art of structural control. *Journal of structural engineering*. 2003;129(7):845-856.
27. Yamaguchi H, Nagahawatta HD. Damping effects of cable cross ties in cable-stayed bridges. *Journal of Wind Engineering and Industrial Aerodynamics*. 1995;54:35-43.
28. Sun L, Hong D, Chen L. In - plane free vibrations of shallow cables with cross - ties. *Structural Control and Health Monitoring*. 2019;26(10):e2421.

29. Le LX, Katsuchi H, Yamada H. Effect of rotational restraint at damper location on damping of a taut cable with a viscous damper. *Journal of Bridge Engineering*. 2020;25(2):04019139.
30. Le LX, Katsuchi H, Yamada H. Damping of cable with HDR damper accounting for restraint boundary conditions. *Journal of Bridge Engineering*. 2020;25(12):04020105.
31. Chen L, Di F, Xu Y, Sun L, Xu Y, Wang L. Multimode cable vibration control using a viscous - shear damper: Case studies on the Sutong Bridge. *Structural Control and Health Monitoring*. 2020;27(6):e2536.
32. Kim BH, Park T. Estimation of cable tension force using the frequency-based system identification method. *Journal of sound and Vibration*. 2007;304(3-5):660-676.
33. Ma L. A highly precise frequency-based method for estimating the tension of an inclined cable with unknown boundary conditions. *Journal of Sound and Vibration*. 2017;409:65-80.
34. Zarbaf SEHAM, Norouzi M, Allemang RJ, Hunt VJ, Helmicki A. Stay cable tension estimation of cable-stayed bridges using genetic algorithm and particle swarm optimization. *Journal of Bridge Engineering*. 2017;22(10):05017008.
35. Dan D-h, Xia Y, Xu B, Han F, Yan X-f. Multistep and multiparameter identification method for bridge cable systems. *Journal of Bridge Engineering*. 2018;23(1):04017111.
36. Zarbaf SEHAM, Norouzi M, Allemang R, Hunt V, Helmicki A, Venkatesh C. Vibration-based cable condition assessment: a novel application of neural networks. *Engineering Structures*. 2018;177:291-305.
37. Zhou H, Xiang N, Huang X, Sun L, Xing F, Zhou R. Full-scale test of dampers for stay cable vibration mitigation and improvement measures. *Structural monitoring and maintenance*. 2018;5(4):489-506.
38. Tabatabai H, Mehrabi AB. Design of mechanical viscous dampers for stay cables. *Journal of Bridge Engineering*. 2000;5(2):114-123.
39. Krenk S, Høgsberg JR. Damping of cables by a transverse force. *Journal of engineering mechanics*. 2005;131(4):340-348.
40. Xu YL, Zhou H. Damping cable vibration for a cable-stayed bridge using adjustable fluid dampers. *Journal of Sound and Vibration*. 2007;306(1-2):349-360.
41. Huang Z, Jones NP. Damping of taut-cable systems: Effects of linear elastic spring support. *Journal of engineering mechanics*. 2011;137(7):512-518.
42. Fournier JA, Cheng S. Impact of damper stiffness and damper support stiffness on the efficiency of a linear viscous damper in controlling stay cable vibrations. *Journal of Bridge Engineering*. 2014;19(4):04013022.
43. Javanbakht M, Cheng S, Ghrib F. Refined damper design formula for a cable equipped with a positive or negative stiffness damper. *Structural Control and Health Monitoring*. 2018;25(10):e2236.

44. Yoneda M, Shimoda I. Influence of Spring Stiffness on Additional Damping Characteristics of Viscous Shear Damper for Cable Vibration Control and Damping Evaluation Curve for its Design (In Japanese). *Collection of Papers of the Japan Society of Civil Engineers*. 1993(480):77-86.
45. Yamaguchi H. Stayed cable dynamics and its vibration control. *Bridge aerodynamics*. 1998:235-253.
46. Kumarasena S, Jones N, Irwin P, Taylor P. Wind induced vibration of stay cables: FHWA-HRT-05-083. *Washington, DC: US Department of Transportation, Federal Highway Administration*. 2007.
47. Takano H, Ogasawara M, Ito N, Shimosato T, Takeda K, Murakami T. Vibrational damper for cables of the Tsurumi Tsubasa Bridge. *Journal of Wind Engineering and Industrial Aerodynamics*. 1997;69:807-818.
48. Nakamura A, Kasuga A, Arai H. The effects of mechanical dampers on stay cables with high-damping rubber. *Construction and Building Materials*. 1998;12(2-3):115-123.
49. Cu VH, Han B. High-damping rubber damper for taut cable vibration reduction. *Australian Journal of Structural Engineering*. 2015;16(4):283-291.
50. Hoang N, Fujino Y. Combined damping effect of two dampers on a stay cable. *Journal of Bridge Engineering*. 2008;13(3):299-303.
51. Bert CW. Material damping: An introductory review of mathematic measures and experimental technique. *Journal of Sound and Vibration*. 1973;29(2):129-153.
52. Marshall JD, Charney FA. A hybrid passive control device for steel structures, I: Development and analysis. *Journal of Constructional Steel Research*. 2010;66(10):1278-1286.
53. Chung D. Structural composite materials tailored for damping. *Journal of alloys and compounds*. 2003;355(1-2):216-223.
54. Kelly SG. *Mechanical vibrations: theory and applications*. Cengage learning; 2012.
55. Hwang J, Ku S. Analytical modeling of high damping rubber bearings. *Journal of Structural Engineering*. 1997;123(8):1029-1036.
56. Le LX, Siringoringo DM, Katsuchi H, Fujino Y. Stay cable tension estimation of cable - stayed bridge under limited information on cable properties using artificial neural networks. *Structural Control and Health Monitoring*. e3015.
57. Jana D, Nagarajaiah S. Computer vision - based real - time cable tension estimation in Dubrovnik cable - stayed bridge using moving handheld video camera. *Structural Control and Health Monitoring*. 2021;28(5):e2713.
58. Cunha A, Caetano E, Delgado R. Dynamic tests on large cable-stayed bridge. *Journal of Bridge Engineering*. 2001;6(1):54-62.
59. de Sá Caetano E, Bartek R, Magalhães F, Keenan C, Trippick G. Assessment of cable forces at the London 2012 Olympic Stadium roof. *Structural Engineering International*. 2013;23(4):489-500.

60. Humar J. *Dynamics of structures*. CRC press; 2012.
61. Ricciardi G, Saitta F. A continuous vibration analysis model for cables with sag and bending stiffness. *Engineering Structures*. 2008;30(5):1459-1472.
62. Ceballos MA, Prato CA. Determination of the axial force on stay cables accounting for their bending stiffness and rotational end restraints by free vibration tests. *Journal of sound and vibration*. 2008;317(1-2):127-141.
63. Chen C-C, Wu W-H, Chen S-Y, Lai G. A novel tension estimation approach for elastic cables by elimination of complex boundary condition effects employing mode shape functions. *Engineering Structures*. 2018;166:152-166.
64. Irvine M. *Cable structures*. New York: Dover Publications, Inc.; 1992.
65. Ahmad J, Cheng S, Ghrib F. An analytical approach to evaluate damping property of orthogonal cable networks. *Engineering structures*. 2014;75:225-236.
66. Caracoglia L, Jones N. In-plane dynamic behavior of cable networks. Part 1: formulation and basic solutions. *Journal of Sound and Vibration*. 2005;279(3-5):969-991.
67. Di F, Sun L, Chen L. In - plane dynamic behaviors of two - cable networks with a pretensioned cross - tie. *Structural Control and Health Monitoring*. 2021;28(7):e2755.
68. Zahedi S, Tornberg A-K. Delta function approximations in level set methods by distance function extension. *Journal of Computational Physics*. 2010;229(6):2199-2219.
69. Adeli H. Neural networks in civil engineering: 1989–2000. *Computer - Aided Civil and Infrastructure Engineering*. 2001;16(2):126-142.
70. Adeli H, Park HS. A neural dynamics model for structural optimization— theory. *Computers & structures*. 1995;57(3):383-390.
71. Masri S, Chassiakos A, Caughey T. Identification of nonlinear dynamic systems using neural networks. 1993.
72. Gavin HP. The Levenberg-Marquardt algorithm for nonlinear least squares curve-fitting problems. *Department of Civil and Environmental Engineering, Duke University*. 2019:1-19.
73. Kişi Ö, Uncuoğlu E. Comparison of three back-propagation training algorithms for two case studies. 2005.
74. Javanbakht M, Cheng S, Ghrib F. Multimode vibration control of stay cables using optimized negative stiffness damper. *Structural Control and Health Monitoring*. 2020;27(4):e2503.
75. Tabatabai H, Mehrabi A, Morgan B, Lotfi H. Non-destructive bridge evaluation technology: Bridge stay cable condition assessment. *Final report submitted to the FHWA, Construction Technology Laboratories, Inc, Skokie, IL*. 1998.



